Development and preclinical assessment of ROR2-specific CAR-T cells for the treatment of clear cell renal cell carcinoma and multiple myeloma

Entwicklung und präklinische Evaluation ROR2-spezifischer CAR-T Zellen zur Behandlung des klarzelligen Nierenzellkarzinoms und des Multiplen Myeloms

Doctoral thesis for a doctoral degree
at the Graduate School of Life Sciences,
Julius-Maximilians-Universität Würzburg,
Section Infection and Immunity

submitted by

Justus C. Weber

from

Mannheim, Germany

Würzburg, 2022

Submitted on: ……..……..

Office stamp

Members of the Thesis Committee

Chairperson:	Prof. Dr. Markus Sauer
Primary Supervisor:	Prof. Dr. Michael Hudecek
Supervisor (Second):	Prof. Dr. Hermann Einsele
Supervisor (Third):	Prof. Dr. Thomas Herrmann
Supervisor (Fourth):	Prof. Dr. Christoph Rader

Date of Public Defense: ……..……

Date of Receipt of Certificates: ……..

Table of Contents

Summary

Adoptive immunotherapy using chimeric antigen receptor (CAR)-modified T cells is an effective treatment for hematological malignancies that are refractory to conventional chemotherapy. To address a wider variety of cancer entities, there is a need to identify and characterize additional target antigens for CAR-T cell therapy. The two members of the receptor tyrosine kinase-like orphan receptor family, ROR1 and ROR2, have been found to be overexpressed on cancer cells and to correlate with aggressive cancer phenotypes. Recently, ROR1-specific CAR-T cells have entered testing in phase I clinical trials, encouraging us to assess the suitability of ROR2 as a novel target for CAR-T cell therapy. To study the therapeutic potential of targeting ROR2 in solid and hematological malignancies, we selected two representative cancer entities with high unmet medical need: renal cell carcinoma and multiple myeloma.

Our data show that ROR2 is commonly expressed on primary samples and cell lines of clear cell renal cell carcinoma and multiple myeloma. To study the efficacy of ROR2-specific CAR-T cell therapy, we designed two CAR constructs with 10-fold binding affinity differences for the same epitope of ROR2. We found both cell products to exhibit antigen-specific anti-tumor reactivity *in vitro*, including tumor cell lysis, secretion of the effector cytokines interleukin-2 (IL-2) and interferon-gamma (IFNγ), and T cell proliferation. *In vivo* studies revealed ROR2-specific CAR-T cells to confer durable responses, significant survival benefits and long-term persistence of CAR-expressing T cells. Overall, there was a trend towards more potent anti-tumor efficacy upon treatment with T cells that expressed the CAR with higher affinity for ROR2, both *in vitro* and *in vivo*.

We performed a preclinical safety and toxicology assessment comprising analyses of ROR2 expression in healthy human and murine tissues, cross-reactivity, and adoptive T cell transfer in immunodeficient mice. We found ROR2 expression to be conserved in mice, and low-level expression was detectable in the male and female reproductive system as well as parts of the gastrointestinal tract. CAR-T cells targeting human ROR2 were found to elicit similarly potent reactivity upon recognition of murine ROR2. *In vivo* analyses showed transient tissue-specific enrichment and activation of ROR2-specific CAR-T cells in organs

with high blood circulation, such as lung, liver, or spleen, without evidence for clinical toxicity or tissue damage as determined by histological analyses.

Furthermore, we humanized the CAR binding domain of ROR2-specific CAR-T cells to mitigate the risk of adverse immune reactions and concomitant CAR-T cell rejection. Functional analyses confirmed that humanized CARs retained their specificity and functionality against ROR2-positive tumor cells *in vitro*.

In summary, we show that ROR2 is a prevalent target in RCC and MM, which can be addressed effectively with ROR2-specific CAR-T cells in preclinical models. Our preliminary toxicity studies suggest a favorable safety profile for ROR2-specific CAR-T cells. These findings support the potential to develop ROR2-specific CAR-T cells clinically to obtain cell products with broad utility.

Zusammenfassung

Adoptive Immuntherapie mit T-Zellen, die chimäre Antigenrezeptoren (CAR) exprimieren, ist ein effektiver Behandlungsansatz für Chemotherapie-resistente Blutkrebserkrankungen. Die Übertragung dieses Konzepts auf weitere Krebsarten erfordert die Identifikation und Charakterisierung neuer Zielstrukturen für die CAR-T Zelltherapie. ROR1 und ROR2, die beiden Mitglieder der Familie der Rezeptortyrosinkinase-ähnlichen Orphan-Rezeptoren, werden auf einer Vielzahl von Tumoren überexprimiert und korrelieren mit einer schlechten Prognose und höherer Krebs-Invasivität. Kürzlich konnte ROR1 als Zielstruktur für die CAR-T Zelltherapie bestätigt werden und die Effektivität und Sicherheit ROR1-spezifischer CAR-T Zellen wird derzeit im Rahmen klinischer Phase-I Studien näher untersucht. Aus diesem Grund waren wir daran interessiert, das therapeutische Potenzial ROR2-spezifischer Zelltherapie zu untersuchen. Als Modellsysteme hierfür wählten wir das Nierenzellkarzinom und das Multiple Myelom als repräsentative hämatologische und solide Krebserkrankungen mit hohem medizinischem Bedarf aus.

Unsere Daten zeigen, dass ROR2 häufig auf Zelllinien und primären Tumorproben des klarzelligen Nierenzellkarzinoms und des Multiplen Myeloms vorkommt. Um die Effektivität ROR2-spezifischer CAR-T Zellen zu untersuchen, wurden zwei CAR Konstrukte mit zehnfach unterschiedlichen Bindungsaffinitäten für dasselbe Epitop von ROR2 hergestellt. Beide Zellprodukte zeigten hohe, antigen-spezifische Antitumor-Reaktivität *in vitro* – insbesondere im Hinblick auf Tumorzell-Lyse, Sekretion der Zytokine Interleukin-2 (IL-2) und Interferon-gamma (IFNγ) und T-Zell Proliferation. *In vivo* beobachteten wir langanhaltende Antitumor-Effektivität durch ROR2-spezifische CAR-T Zellen, sowie signifikante Überlebensvorteile und langfristige T-Zell Persistenz. Außerdem beobachteten wir, sowohl *in vitro* als auch *in vivo*, einen Trend zu stärkerer Antitumor-Effektivität von T-Zellen, die den CAR mit höherer Affinität für ROR2 exprimierten.

Im Rahmen einer präklinischen Toxikologie-Studie analysierten wir die Expression von ROR2 im gesunden Gewebe, die Kreuz-Reaktivität ROR2-spezifischer CAR-T Zellen und deren Sicherheit durch adoptiven T-Zell Transfer in immun-defiziente Mäuse. Unsere Daten zeigen, dass ROR2 in *H. sapiens* und *M. musculus* gleichermaßen exprimiert wird und ROR2 Expression war insbesondere in den weiblichen und männlichen Reproduktionsorganen und

Teilen des Gastrointestinaltrakts detektierbar. Wir konnten außerdem zeigen, dass CAR-T Zellen, die menschliches ROR2 erkennen, vergleichbare Antitumor-Reaktivität gegen Zellen, die murines ROR2 exprimieren, auslösen. Unsere *in vivo* Analysen zeigten temporäre Anreicherung und Aktivierung ROR2-spezifischer CAR-T Zellen in gut durchbluteten Geweben, wie Lunge, Leber und Milz, in der Abwesenheit klinischer Anzeichen für Toxizität oder histologisch nachweisbarer Gewebsschädigungen.

Um die Risiken immunologischer Nebenwirkungen und die damit einhergehende Abstoßung ROR2-spezifischer CAR-T Zellen zu reduzieren, humanisierten wir die CAR Bindedomäne. Unsere Daten zeigen, dass humanisierte ROR2-spezifische CAR-T Zellen vergleichbare Spezifität und Funktionalität gegen ROR2-positive Tumorzellen *in* vitro aufweisen.

Insgesamt zeigen unsere Daten, dass ROR2 eine häufig auftretende Zielstruktur auf der Oberfläche von RCC und MM Zellen ist und diese in präklinischen Modellen effektiv mittels ROR2-spezifischer CAR-T Zellen adressiert werden kann. Unsere vorläufigen Toxizitätsdaten deuten darauf hin, dass ROR2-spezifische CAR-T Zellen ein vorteilhaftes Sicherheitsprofil aufweisen. Alles in allem unterstützen diese Daten das Potenzial der klinischen Entwicklung ROR2-spezifischer CAR-T Zellen als Zellprodukte mit breit gefächerter Anwendbarkeit.

1 Introduction

1.1 Chimeric antigen receptor-modified T cell immunotherapy

One of the first embodiments of autologous adoptive immunotherapy has been the utilization of tumor-infiltrating lymphocytes for the treatment of metastatic melanoma [1]. The discovery and implementation of gene transfer and editing methods has enabled the development of more complex cell products, such as T cell receptor (TCR)-transgenic and chimeric antigen receptor (CAR)-modified T cells [2].

CARs are synthetic receptors designed to provide T cells with an additional target specificity, enabling them to elicit anti-tumor functionalities, such as antigen-dependent target cell lysis, cytokine secretion and proliferation upon recognition of antigen-positive target cells (Figure 1). In general, target recognition by CAR-T cells occurs in a major histocompatibility complex (MHC)-independent manner by direct recognition of cell surface antigens. Therefore, this additional specificity of CAR-T cells is not controlled by thymic selection and may yield potent self-reactive cell products. This effect is intensified by residual expression of CAR targets on healthy tissues (so called cancer-associated antigens, CAA), which are considerably more common than neoantigens (cancer-specific antigens, CSA). Therefore, careful analysis of target expression and assessment of on-target off-tumor toxicities are commonly required [2].

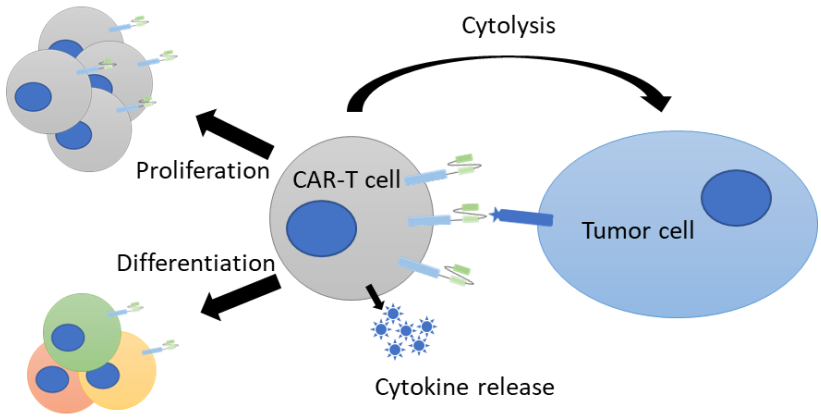

Figure 1 – Overview of antigen-specific CAR-T cell functionalities (adapted from [3]).

In response to antigen recognition, different T cell functionalities are induced, including antigen-specific target cell lysis (cytolysis), secretion of effector cytokines such as IL-2 or IFNγ, T cell proliferation and differentiation.

Chimeric antigen receptor design

CARs are synthetic receptors which combine recognition of cell surface antigens and induction of the TCR signaling pathway into a single protein. CARs are designed in a modular way and consist of an extracellular binding domain and spacer, a transmembrane domain, and a cytoplasmic signaling domain (Figure 2).

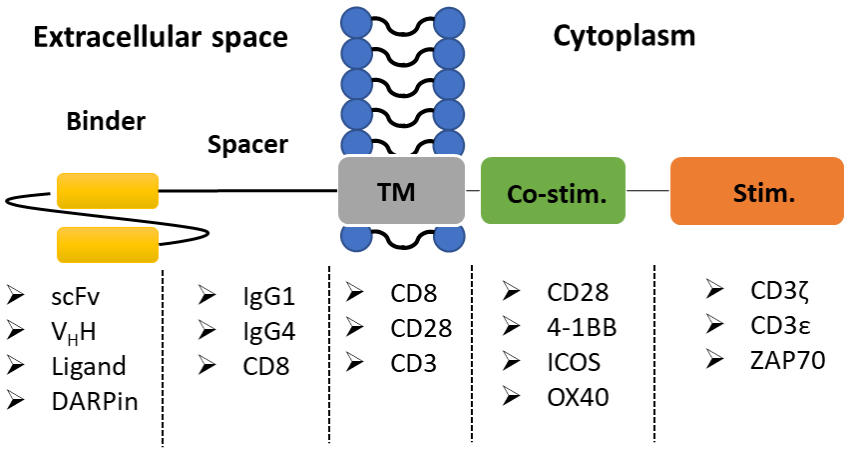

Figure 2 – Chimeric antigen receptor design and exemplary domains (adapted from [4]).

CARs are designed in a modular way to allow for antigen recognition, optimal T cell activation and the concomitant induction of antigen-specific T cell functionalities. Different options used in previous studies are shown for each of the five CAR main modules. scFv: single chain variable fragment, V_HH: Variable heavy chain nanobody, DARPin: Designed ankyrin repeat protein, Co.-stim.: co-stimulatory domain, Stim.: Stimulatory domain.

The binding domain, most commonly a single chain variable fragment (scFv), is responsible for recognition of the respective CAA. However, specificity can also be conferred using alternative binding domains, such as ligands, peptides, toxins, or alternative antibody scaffolds [5-8]. The extracellular spacer domain is responsible for providing flexibility and reach, which are required for optimal target binding and the concomitant formation of a potent immunological synapse between target and CAR-T cell. Due to these requirements, IgG, CD8 and CD28-derived hinge regions have been used most commonly [9, 10]. The transmembrane domain is responsible for signal transduction and commonly originates from proteins such as CD3, CD4, CD8, and CD28 [4, 11]. Recent studies have shown that transmembrane domain selection has an impact on antigen density requirements for potent CAR-T cell activation [12].

Finally, the cytoplasmic domain is responsible for intracellular signaling, T cell activation and the concomitant induction of T cell functionalities. Based on the design of their cytoplasmic domain, three CAR generations can be discriminated: While first generation CAR-T cells only contain an activation domain – most commonly CD3ζ, second and third generation CAR-T cells are equipped with one or more additional co-stimulatory domains which serve as signal enhancers. In general, these domains are derived from co-stimulatory molecules within the TCR signaling complex, such as CD28 or 4-1BB [13, 14]. To further increase the therapeutic potential of cell therapy, different types of armored CAR-T cells are currently being developed, providing concomitant delivery of immuno-supportive or therapeutic molecules, including cytokines, enzymes, or antibodies [15-17].

Differences in signaling between CAR- and TCR-based T cell activation

While CAR-T cell therapy has achieved astonishing clinical effects, profound differences in T cell activation, signaling, and down-stream effects have been observed between TCR- and CAR-modified T cells. Recent studies have observed structural and compositional differences between TCR- and CAR-based immune synapses, which were shown to culminate in dissimilar activation kinetics and signal intensities [18]. In-depth analyses have shown that CARs induce insufficient proximal signaling and phosphorylation of the kinases ZAP-70 and LAT, leading to suboptimal T cell activation and reduced antigen sensitivity. These signaling differences were shown to be over-compensated by CARs through supraphysiological phosphorylation of other kinases involved in the TCR signaling pathway [19, 20]. Importantly, supraphysiological phosphorylation in the activated and basal state has previously been reported to be associated with CAR-T cell exhaustion and a loss of anti-tumor functionality [21]. Several solutions for this characteristic have been proposed, including targeted insertion of CAR constructs into the TCR locus, modifications to the CD3ζ signaling domain, and overexpression of selected transcription factors [22-24].

The impact of antigen density and binding affinity on CAR-T cell performance

Another major difference between TCR- and CAR-modified T cells relates to antigen density requirements: While MHC presentation of 1 to 10 peptides is considered sufficient for target cell lysis in the context of TCR-mediated signal transduction, CAR-modified T cells have been shown to require about 10-fold higher antigen quantities [25, 26]. This characteristic renders CAR-T cells less sensitive to antigen-low tumor cells, which may contribute to antigen-low tumor relapses. To reduce the antigen density requirements of CAR-T cells, several strategies have been implemented, including the utilization of high affinity CAR binding domains or transmembrane domain modifications [6, 12, 27-29].

Binding affinity is another key difference between CARs and TCRs: While the affinity of physiological TCRs is usually in the micromolar range, most CARs contain binding domains with nano- or picomolar affinities [30, 31]. This difference is largely owed to the choice of CAR binding domain, which is commonly an antibody-derived scFv fragment. Antibodies are naturally designed to exhibit high specificity and affinity and undergo additional affinity maturation processes to achieve more potent efficacy. Additionally, techniques to isolate, identify and characterize monoclonal antibodies, are designed to obtain high affinity variants [32-35]. Recent studies have analyzed the impact of binding affinity on CAR-T cell efficacy and have shown that affinity affects antigen requirements. In general, T cells equipped with low-affinity CARs require higher antigen densities to induce equally potent functionalities [6, 27, 28]. While most previous studies have focused on affinity differences within the nanomolar range, one study employed ligand-based ICAM-1-specific CAR-T cells with affinities ranging from the micromolar to nanomolar range, circumventing the antibody pre-selection bias. [6]. In general, CAR-T cells target CAAs which are overexpressed on cancer cells and show basal expression in healthy tissues. Therefore, the utilization of low affinity CAR-T cells has repeatedly been described to yield safer CAR-T cell products, albeit at the risk of insufficient control of antigen-low tumor cells, increasing the risk for antigen-low tumor relapse.

As of July 2022, six CAR-T cell products have been approved by the FDA and 755 clinical trials are ongoing worldwide [36, 37]. While CAR-T cell therapy has been shown to mediate remarkable anti-tumor efficacy, its clinical application is limited to a selection of hematological cancers [38, 39]. However, clinical data obtained from these products has unveiled universal concepts that predict CAR-T cell safety and efficacy and set the basis for the rational design and optimization of CAR-T cell products.

Cytokine release syndrome is a common acute side effect of CAR-T cell therapy

Clinical data has found cytokine release syndrome (CRS) to be the most acute side effect of CAR-T cell therapy. CRS is a systemic inflammation which is generally observed within a few days of CAR-T cell administration and its severity was found to vary based on different factors, such as tumor burden and tissue infiltration. CRS is characterized by high serum levels of interleukin-6 (IL-6), one of the master regulators of proinflammatory signaling. This observation has led to the implementation of IL-6 blockade as the established treatment algorithm to control toxicities in high-grade CRS. Recent studies have shown that the IL-6 responsible for CRS is largely secreted by macrophages, upon activation though IFNγ secreted by CAR-T cells upon tumor recognition [40, 41].

On-target off-tumor toxicity in response to antigen expression on healthy tissues

Another common side effect of CAR-T cell therapy is on-target off-tumor toxicity caused by the recognition of antigen-positive healthy cells. In the context of CD19-specific CAR-T cells, this toxicity manifests in deletion of healthy CD19-positive B cells, leading to B-cell aplasia and concomitant hypogammaglobulinemia. However, this toxicity can be managed clinically by intravenous immunoglobulin supplementation and is thus considered an acceptable toxicity [42]. However, more severe side effects have been observed in clinical trials, such as lung toxicities leading to the death of a patient treated with receptor tyrosine-protein kinase erbB-2 (Her2)-specific CAR-T cells, as well as severe liver toxicities upon treatment with carbonic anhydrase IX (CAIX)-specific CAR-T cells [43, 44]. Furthermore, recent studies have shown that on-target toxicity is also context dependent. A recent analysis showed that

ROR1-specific CAR-T cells show safety and efficacy in preclinical models but may lead to lethal toxicities depending on lymphodepleting chemotherapy regimens [45].

Tumor immune evasion in the context of CAR-T cell therapy

Clinical results obtained from CD19-specific CAR-T cells have unveiled different mechanism contributing to tumor immune evasion. These principles can be grouped into primary (pre-existing) and secondary (acquired) mechanisms. The most common primary mechanisms include the expression or secretion of immunoinhibitory molecules, cancer heterogeneity, and differences in the pathways required for tumor cell eradication [46-48]. In contrast, secondary resistance mechanisms are acquired during cancer progression or treatment. The most common secondary immune evasion mechanism is antigen down-regulation or loss, leading to antigen-low or negative tumor relapse. Importantly, this type of immune evasion has been described for all CAR-T cell products in the clinic and is considered a universal mechanism for cell and immunotherapy. However, different underlying mechanisms for the observed antigen losses have been described, such as alternative splicing, heterozygous deletions, or antigen masking by unintentional CAR transduction of malignant cells [49-53]. Common strategies to circumvent this type of immune evasion are the utilization of CAR-T cell products with low antigen density requirements or capable of addressing multiple antigens in parallel, such as dual, tandem, or switchable CAR approaches [54-57].

Immunogenicity of CAR constructs leads to CAR-T cell rejection

Furthermore, CARs have been shown to be immunogenic, due to the incorporation on non-human binding domains, and the formation of neoepitopes at their artificial domain intersections. While *in vitro* analyses have demonstrated that CAR immunogenicity may lead to CAR-T cell neutralization and eradication, its impact on the clinical efficacy of CAR-T cells remains unclear. A recent study employing CAIX-specific CAR-T cells observed limited CAR-T cell engraftment, which correlated with high plasma concentrations of CAR-specific antibodies and the emergence of a CAR-T cell-specific cellular immune responses [44]. Additionally, another study employing sequential administration of mesothelin-specific mRNA-based CAR-T cells observed severe toxicities in the form of an anaphylactic shock [58].

However, none of these severe or neutralizing responses have been observed in clinical trials evaluating the safety of CD19-specific CAR-T cells, despite the emergence of anti-idiotype antibodies directed against the murine FMC63 scFv fragment representing the CAR binding domain [59]. Notably, a recent study showed persistence of CD19-specific CAR-T cell for over ten years after treatment, underlining that further research is required to assess the impact of immunogenicity on the clinical efficacy and safety of CAR-T cells [60]. Furthermore, a recent study has shown that lymphodepleting chemotherapy, which is commonly used for patient conditioning prior to CAR-T cell administration, has an influence on CAR-T cell persistence and engraftment. These findings have led to the implementation of optimized chemotherapy regimens using cyclophosphamide and fludarabine [61]. Recent analyses have hypothesized that this novel pre-conditioning approach has a major impact on CAR-T cell rejection by humoral and cellular anti-CAR immune responses [44, 59].

Antibody humanization is a common approach to reduce immunogenicity and has been suggest as a viable option for CAR-T cell products as well [62]. Recent studies have reported the development of humanized CD19-specific CAR-T cells and showed similar anti-tumor efficacy *in vitro* as clinically validated cell products [63]. Detailed analyses have shown humanized antibodies to carry residual immunogenic potential, which was identified to largely originate from the complementarity determining region (CDR). Since the CDRs are responsible for conferring antigen specificity and affinity, they cannot be altered – establishing a baseline immunogenicity [64].

In summary, the development of optimized CAR-T cell products requires consideration of multiple factors with intertwined implications for overall CAR-T cell performance. For this reason, we chose a systematic approach to identify a lead candidate for clinical development. To this end, we employed a CAR backbone which has previously been shown to confer clinical efficacy as the basis for our analyses and focused on the impact of CAR binding affinity and scFv humanization on CAR-T cell performance and preclinical safety.

1.2 Receptor tyrosine kinase-like orphan receptor 2 (ROR2)

During the last decades, a major focus in cancer research has been the identification and assessment of novel CSA and CAA. While different biomarkers have been identified, additional requirements must be met to serve as candidate targets for cellular therapy. Recently, the European Society for Blood and Marrow Transplantation (EBMT) has published a list of recommendations to facilitate the selection of targets for cellular therapy. In brief, a potential CAR-T cell target should I) be expressed uniformly on the cell surface of malignant cells and cancer stem cells, II) not be prone to antigen loss, and III) not be expressed on critical healthy tissues [65]. Recently, the two members of the receptor tyrosine kinase-like orphan receptor family, ROR1 and ROR2, have been suggested as biomarkers due to their overexpression on cancer cells and absence on most healthy adult tissues. Previous studies have shown that ROR1 is a suitable target for the treatment of breast cancer, lung cancer, B-cell chronic lymphocytic leukemia, mantle cell lymphoma, and acute myeloid leukemia using CAR-T cells. [5, 66]. Therefore, we hypothesized that its family member, ROR2, is also a viable target for cellular therapy. Importantly, ROR2 is commonly overexpressed in different hematological and solid cancers and has been shown to correlate with tumor invasiveness and the formation of metastases (Figure 3) [67-69].

The physiological role of ROR2

Physiological expression of ROR2 has been observed during embryonic development, where it plays a crucial role for development of the nervous system and limbs [70-73]. However, ROR2 is downregulated during gestation, and has been shown to be virtually absent in most adult human tissues [74]. Residual ROR2 expression has been reported for osteoblasts, a subpopulation of plasma cells and parts of the uterus, where it has been suggested to play a role in embryo implantation [67, 75, 76]. The ROR2 protein structure consists of an extracellular domain containing an IgG-like, a frizzled and a kringle domain, as well as a cytoplasmic tyrosine kinase domain (Figure 4) [77]. Despite its denomination as an orphan receptor, WNT5A has been reported to interact with ROR2 and to induce WNT signaling, leading to cytoskeletal rearrangement, cell polarization, migration, and tissue invasion [71, 78, 79]. ROR2 is highly conserved between species and analogs have been identified in

D. melanogaster, *C. elegans*, and *M. musculus*, where they play similar roles in developmental processes [73, 79, 80]. As of July 2022, no ROR2 isoforms have been reported, indicating the absence of protein variants characterized by intracellular retention or secretion [81, 82]. However, inactivating mutations have been found in ROR2 and were shown to be associated with Robinow syndrome and brachydactyly type B, two hereditary diseases manifesting in limb and skeletal malformations [83]. Importantly, these features are equivalently replicated in ROR2$^{-/-}$ mice, underlining the high evolutionary conservation of ROR2 [84].

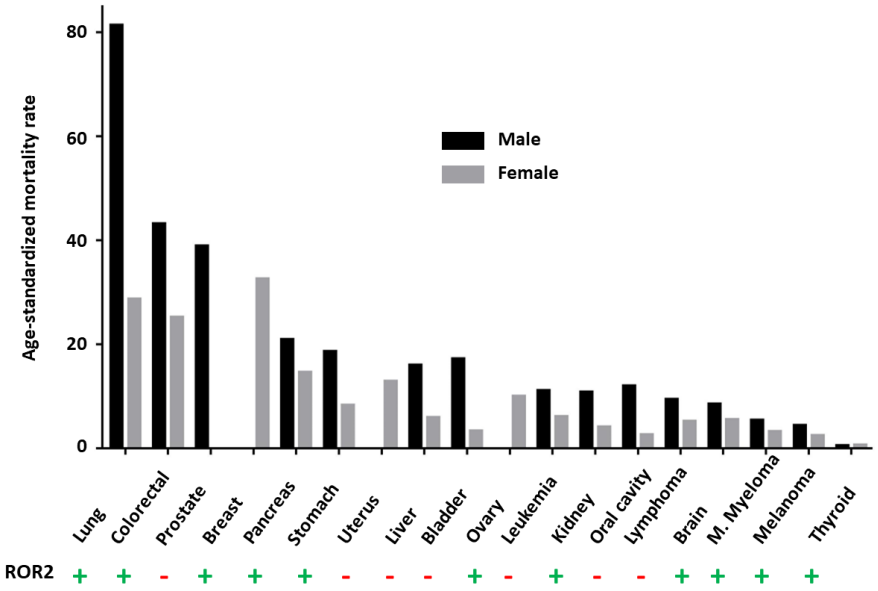

Figure 3 – 2020 age-standardized mortality rates of cancers originating from indicated tissues in Europe and corresponding ROR2 expression status.

Figure is a compilation of publicly available data obtained from [67-69, 85-93]. Data shown is age-standardized mortality in deaths per 100.000 people in 2020 for cancers originating from indicated tissues of people in Europe and ROR2 expression status in these cancers. Age-standardized mortality rates were extracted from [85]. ROR2 expression status was obtained from indicated references [67-69, 86-93]). High ROR2 expression in the respective cancer entity or a subtype thereof is indicated by "+", absent or low ROR2 expression is indicated by "-".

Development of ROR2-specific antibodies

While ROR2 has been suggested as a biomarker, conflicting data regarding its protein expression have been reported. A recent study investigated the reasons for these discrepancies and found the majority of studies to employ unspecific and cross-reactive

antibodies for immunohistochemical analyses [94]. These findings have raised questions regarding the reliability of protein-based ROR2 expression datasets.

Until recently, this absence of suitable reagents was also true for ROR2-specific antibodies with therapeutic potential. In 2017, Peng et al. reported the isolation of a first ROR2-specific antibody from a naïve rabbit library (XBR2-401, K_D= 7nM) [95]. We reasoned that the therapeutic potential of this antibody might benefit from affinity maturation and humanization. Therefore, we employed X-ray crystal structure guided affinity maturation and CDR grafting to obtain an affinity mature clone (X3.12, K_D=0.7 nM) and two humanized variants thereof (hX3.12.5 and hX3.12.6). Subsequent X-ray crystallography revealed the antibodies to recognize the exact same epitope within the ROR2 kringle domain, and their specificity was confirmed using Retrogenix' custom cell microarray technology [62]. Others have also tried to generate ROR2-specific binders for diagnostic and therapeutic applications, including a human ROR2-specific antibody, and an ADC using the conditionally active biologics technology [96, 97].

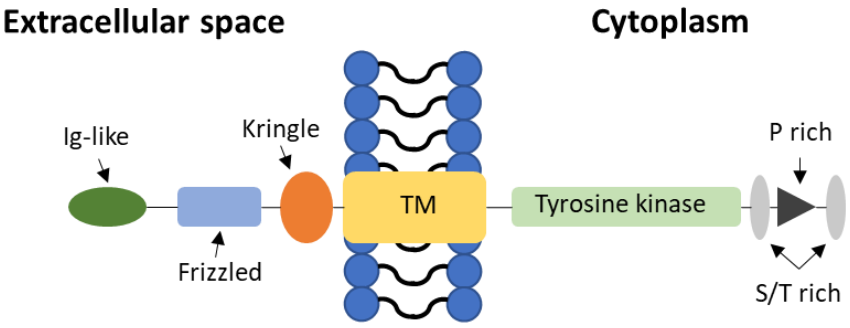

Figure 4 – ROR2 domain structure (adapted from [98]).

ROR2 has a highly conserved extracellular domain structure containing an Ig-like, a Frizzled and a Kringle domain. The cytoplasmic fraction of ROR2 contains a tyrosine kinase domain, as well as two Serine/Threonine-rich (S/T rich) and a Proline rich (P rich) domain. TM: transmembrane domain.

In summary, this previous work supports the evaluation of ROR2 as a candidate target for CAR-T cell therapy, due to its overexpression on cancer cells, its absence in most healthy adult tissues and its role in tumor pathogenesis. Renal cell carcinoma and multiple myeloma were chosen as representative solid and hematological malignancies to study the expression of ROR2 and the anti-tumor efficacy of ROR2-specific CAR-T cell therapy.

1.3 Renal cell carcinoma

Every year, 115.000 patient are diagnosed with kidney cancer and around 49.000 patients succumb to the disease [99, 100]. The most common type of kidney cancer is renal cell carcinoma (RCC), which originates from epithelial cells and can be classified into three subtypes: clear cell (ccRCC), papillary (pRCC), and chromophobe renal cell carcinoma (ChRCC). CcRCC represents the most common subtype and accounts for approximately 80 % of all cases, whereas pRCC and ChRCC represent 10 % and 5 %, respectively [101-103]. Locally advanced or metastatic disease is found in around 30 % of all newly diagnosed RCC cases, and another third has been shown to relapse with locally invasive or metastatic disease [104].

Established RCC therapy

RCC has been shown to be highly resistant to cytotoxic chemotherapy, stimulating the development of novel treatment approaches [105]. While significant progress has been made by targeting common cancer pathways such as the vascular endothelial growth factor receptor (VEGFR) or mammalian target of rapamycin (mTOR) pathways, metastatic RCC is still considered incurable [105, 106]. However, spontaneous tumor regression has been observed in about 1 % of primary and metastatic RCC cases, with the first reports dating back to the 1930's [107, 108]. Detailed analyses have shown that this characteristic can be attribute to the high immunogenicity of RCC, characterized by uniformly high expression of HLA-I molecules in primary and metastatic RCC, and high tumor infiltration of $CD8^+$ T lymphocytes [109-111]. Therefore, different approaches to modulate lymphocyte activity have been tested in RCC, such as cytokine therapy with IL-2 or IFNα, hematopoietic stem cells transplantation (HSCT), treatment with *ex vivo* expanded tumor-infiltrating lymphocytes, as well as immune checkpoint inhibitors [112-118]. While approaches such as cytokine therapy led to an overall response in 15 % to 30 % of patients, complete response rates have been moderate, encouraging the development of more elaborate cell products to cure RCC.

Investigational CAR-T cell therapy for RCC

As of July 2022, two cell surface proteins (CD70 and CAIX) have been suggested as candidate targets for the treatment of RCC using CAR-T cells [119, 120]. However, CAIX-specific first-generation CAR-T cells showed no objective response in clinical trials and were later discontinued due to liver toxicities and limited CAR-T cell persistence [44]. The safety and efficacy of CD70-specific CAR-T cells for the treatment of RCC is currently being evaluated in clinical trials (NCT02830724, NCT04438083) [121]. However, CD70 has been shown to be expressed in subsets of T and B lymphocytes, and overexpression on tumor cells has been shown to induce T cell apoptosis through interaction with CD27 [122, 123]. In consequence, there is a high medical need for the identification of novel RCC-associated cancer antigens and their assessment as candidate targets for CAR-T cell therapy.

Recently, ROR2 has been proposed as a prognostic biomarker for ccRCC, and a correlation between high ROR2 mRNA expression and tumor stage was observed in a retrospective analysis of the TCGA ccRCC dataset. Additionally, a causal relationship between ROR2 and matrix metalloprotease 2 expression was observed and ROR2 overexpression *in vitro* led to increased cell migration and tissue invasion properties [69].

Taken together, these previous works indicate that cell therapy may represent a curative treatment option for ccRCC. However, the lack of suitable candidate targets for CAR-T cell therapy represents a major bottleneck for the development of specific cell therapy approaches. We hypothesize that ROR2 is a candidate target for the treatment of ccRCC due to its role in cancer pathogenesis and can be addressed with ROR2-specific CAR-T cells.

1.4 Multiple myeloma

Multiple myeloma (MM) is a hematological malignancy characterized by clonal expansion of plasma cells in the bone marrow and is typically associated with the secretion of aberrant immunoglobulins. MM is preceded by two pre-malignant stages called monoclonal gammopathy of undetermined significance (MGUS) and smoldering multiple myeloma (SMM). Different subtypes of MM have been identified based on the type of immunoglobulin secreted by MM cancer cells [124, 125]. In 2016, approximately 20.000 patients were newly diagnosed with MM in the United States of America, rendering MM the second most common hematological cancer and accounting for around 1% of all newly diagnosed cancer cases [126].

Established MM therapy

MM is generally susceptible to cytotoxic chemotherapy and the approval of novel therapeutics, such as protease inhibitors and immunomodulators, has led to a continuous increase in median survival. However, MM is still considered to be incurable [127-129]. Different risk factors, including age, gender, ethnicity and cytogenetic aberrations have been shown to affect overall and disease-free survival [130]. Autologous stem cell transplantation (ASCT) represents an essential therapeutic approach, which has been shown to improve complete response rates and increase overall survival by approximately 12 months [131].

Investigational and approved immuno- and cell therapy for the treatment of MM

MM is considered to be generally addressable with immuno- and cell therapy, and different approaches, including monoclonal antibodies, bi-specific T cell engagers, and antibody drug conjugates are part of the established treatment algorithms [132-135]. In 2021, the first CAR-T cell product directed against the B cell maturation antigen (BCMA) was approved for the treatment of MM [38, 136]. However, recent studies have shown that antigen loss may occur upon treatment with BCMA-specific CAR-T cells, leading to antigen negative tumor relapses [52, 137]. In consequence, there is a desire for the identification of additional MM-associated antigens and their assessment as candidate targets for CAR-T cell therapy.

The most clinically advanced candidate targets include SLAMF7, CD38, and CD138 and the safety and efficacy of cell products addressing these antigens is currently being evaluated in clinical trials [126]. However, off-tumor expression has been described for most of these antigens, such as CD38 and SLAMF7 expression on the surface of activated T cells, and CD138 expression on the surface of a subset of healthy plasma cells [138-140]. The impact of off-tumor expression on the safety of the respective cell products remains to be analyzed in clinical trials. Together, these findings underline the need to identify novel MM-associated antigens which can be addressed using CAR-T cells.

ROR2 has been described to be overexpressed in MM on the genomic level and its expression was shown to correlate with disease progression. Additionally, ROR2 has been shown to play a role for the interaction between MM cells and bone marrow niches, and ROR2 knockdown was shown to induce detachment-associated apoptosis of MM cells *in vitro* [67].

In summary, the available reported works show that MM is generally susceptible to cellular therapy using CAR-T cells. However, there is a high medical need to identify additional MM-associated antigens with limited expression on healthy cells, and to assess their suitability as candidate targets for CAR-T cell therapy. We hypothesize that ROR2 represents a candidate target for the treatment of MM, due to its role in cancer pathogenesis and maintenance, and can be targeted using ROR2-specific CAR-T cells.

1.5 Hypothesis and specific aims

CAR-T cell therapy is a novel and disruptive cancer treatment and has mediated clinical efficacy in selected hematological malignancies. There is a high medical need and desire to identify novel CAAs, to assess their suitability as candidate targets for CAR-T cell therapy, and to develop corresponding CAR-T cell products.

Recently, the EBMT has published a guideline for the selection of optimal CAR-T cell targets [65]. Based on these recommendations, we hypothesize that ROR2 is a candidate target for CAR-T cell therapy, due to its overexpression on cancer cells, its role in cancer pathophysiology, as well as its absence in adult human tissues. Furthermore, ROR2 overexpression has been reported for several prevalent hematological and solid cancers, rendering it an interesting target for broadly applicable CAR-T cell therapy approaches.

To test our hypothesis, we selected RCC and MM as representative solid and hematological malignancies and pursued three specific aims:

I) ROR2 target assessment and validation:
   To study the expression of ROR2 on the transcriptomic and protein level in primary samples and cell lines of MM and ccRCC.

II) Functional assessment of ROR2-specific CAR-T cells:
   To generate ROR2-specific CAR-T cells and assess their anti-tumor efficacy against MM and ccRCC *in vitro* and *in vivo*.

III) Preclinical safety assessment of targeting ROR2 with CAR-T cells:
   To quantify ROR2 expression in adult human and murine tissues, and to study the safety of ROR2-specific CAR-T cells in a preclinical toxicity model.

First, we studied the expression of ROR2 in primary samples and cell lines of MM and RCC on the transcriptome and protein level, using quantitative real-time PCR (qPCR), immunohistochemistry, flow cytometry and Western blotting. We generated ROR2-specific CARs with different binding affinities using an established CAR backbone with clinical efficacy containing an optimized IgG3 spacer and 4-1BB co-stimulation. ROR2-specific CAR-T cells

were generated by lentiviral transduction and their specificity and efficacy against ccRCC and MM were assessed *in vitro* and *in vivo*.

Furthermore, we assessed the preclinical safety of targeting ROR2 with CAR-T cells. We analyzed the expression of ROR2 in healthy adult human and murine tissues and studied the cross-reactivity of ROR2-specific CAR-T cells for murine ROR2 to assess whether mice represent a relevant toxicity model. We defined comparable relative gene expression and similarly potent *in vitro* efficacy of ROR2-specific CAR-T cells against cells expressing human or murine ROR2 as prerequisites for toxicity testing *in vivo*. Next, we employed adoptive T cell transfer in tumor-free immunodeficient mice and assessed clinical toxicity using physiological, histological and flow cytometry-based analyses. As objective benchmarks, significant weight or health score changes were selected as surrogates for severe on-target toxicities, and tissue-specific T cell enrichment, activation, and concomitant tissue damage were selected to identify clinical toxicities.

Finally, we were interested in evaluating humanization of the CAR binding domain as a means to mitigate adverse immune reactions and concomitant CAR-T cell rejection. We generated ROR2-specific CAR-T cells with humanized binding domains and assessed their specificity and efficacy *in vitro*.

These experiments will provide a preclinical data catalogue to support the clinical development of ROR2-specific CAR-T cells.

2 Materials

2.1 Human subjects

Peripheral blood and plasma samples were obtained from healthy donors consenting to participate in research protocols approved by the institutional review board of the University Wuerzburg. Primary MM cells, cDNA and tissue slides of consenting patients were kindly provided by the department for translational myeloma research, urology, and pathology of the University Hospital Wuerzburg.

2.2 Animal experiments

All animal experiments were approved by the veterinary department of the Regierung von Unterfranken. Animal experiments were conducted at least once using six- to twelve-week-old female NOD.Cg-Prkdc^{scid} Il2rg^{tm1Wjl}/SzJ (NSG) mice obtained from Charles River.

2.3 Cell lines

Table 1 – List of tumoral cell lines.

Name	Description	Provider
786-O	Primary ccRCC, transduced to express ffLuc-eGFP	ATCC, Manassas, USA
Caki-1	Metastatic ccRCC, transduced to express ffLuc-eGFP	Dr. Kalogirou, Würzburg
Caki-2	Primary pRCC, transduced to express ffLuc-eGFP	Dr. Kalogirou, Würzburg
RCC-4	Primary ccRCC, transduced to express ffLuc-eGFP	Dr. Kalogirou, Würzburg
RCC-53	Primary ccRCC, transduced to express ffLuc-eGFP	Dr. Kalogirou, Würzburg
ACHN	Metastatic pRCC, transduced to express ffLuc-eGFP	Dr. Kalogirou, Würzburg
Jurkat E6.1	Acute T cell leukemia	ATCC, Manassas, USA
Lenti-X™	Subclone of human embryonic kidney cell line HEK293 optimized for lentivirus production	Takara, Kyoto, Japan
U-266	Multiple myeloma, transduced to express ffLuc-eGFP	ATCC, Manassas, USA

OPM-2	Multiple myeloma, transduced to express ffLuc-eGFP	DSMZ, Braunschweig, GER
MDA-MB-231	Breast cancer, transduced to express ffLuc-eGFP & variants transduced to express hROR2 or mROR2	ATCC, Manassas, USA
TM-LCL	EBV-transformed lymphoblastoid B cell	Dr. Riddell, Seattle, USA

2.4 Media and buffers

Table 2 – Complete Dulbecco's modified Eagle's medium (cDMEM).

Component	Volume (final concentration)
DMEM (+4.5 g/l glucose, +25 mM HEPES)	500 ml
Penicillin/Streptomycin (10.000 u/ml)	5 ml (90 u/ml)
Fetal bovine serum (heat-inactivated)	45 ml (8 % v/v)

Final medium was sterile filtered using 0.22 µm PES filtration units.

Table 3 – Complete Roswell Park Memorial Institute medium (cRPMI).

Component	Volume (final concentration)
RPMI-1640 (+ GlutaMax, +25 mM HEPES)	500 ml
Penicillin/Streptomycin (10.000 u/ml)	5 ml (90 u/ml)
Fetal bovine serum (heat-inactivated)	45 ml (8 % v/v)

Final medium was sterile filtered using 0.22 µm PES filtration units.

Table 4 – T cell medium (CTL).

Component	Volume (final concentration)
RPMI-1640 (+ GlutaMax, +25 mM HEPES)	500 ml
Penicillin/Streptomycin (10.000 u/ml)	5 ml (90 u/ml)
β-Mercaptoethanol (50 mM)	0.5 ml (0.09 % v/v)
Human serum (heat-inactivated)	45 ml (8 % v/v)

Final medium was sterile filtered using 0.22 µm PES filtration units.

Table 5 – Freezing medium.

Component	Volume (final concentration)
Fetal bovine serum (heat-inactivated)	45 ml
DMSO (cell culture grade)	5 ml

Table 6 – Flow cytometry wash buffer (FACS Buffer).

Component	Volume (final concentration)
DPBS (Ca^{2+}, Mg^{2+}-free)	500 ml
Fetal bovine serum (heat-inactivated)	2.5 ml (0.5 % v/v)
EDTA (0.5 M)	2 ml (2mM)
Sodium azide (1.5 M)	0.5 ml (1.5 mM)

Table 7 – Magnetic activated cell sorting buffer (MACS Buffer).

Component	Volume (final concentration)
DPBS (Ca^{2+}, Mg^{2+}-free)	500 ml
Fetal bovine serum (heat-inactivated)	2.5 ml (0.5 % v/v)
EDTA (0.5 M)	2 ml (2mM)

Table 8 – PBS/EDTA buffer (PBMC wash Buffer).

Component	Volume (final concentration)
DPBS (Ca^{2+}, Mg^{2+}-free)	500 ml
EDTA (0.5 M)	2 ml (2mM)

Table 9 – SDS-PAGE running buffer.

Component	Volume (final concentration)
10x TRIS/glycine/SDS buffer concentrate (BioRad)	100 ml
dH_2O	900 ml

Table 10 – Western blot transfer buffer.

Component	Volume (final concentration)
5x Transfer buffer concentrate (BioRad)	200 ml
dH_2O	600 ml
96% ethanol	200 ml

Table 11 – Western blot wash buffer (20 mM TBS-T pH7.5).

Component	Volume (final concentration)
TRIS base	2.42 g
NaCl	8.77 g
dH_2O	Fill up to 1 l
Tween-20	1 ml

Table 12 – Western blot blocking buffer.

Component	Volume (final concentration)
20 mM TBS-T pH 7.5	100 ml
BSA	10 g (10% w/v)

Table 13 – Western blot antibody incubation buffer.

Component	Volume (final concentration)
20 mM TBS-T pH 7.5	100 ml
BSA	5 g (5% w/v)

Table 14 – Western blot antibody stripping buffer.

Component	Volume (final concentration)
1 M TRIS pH6.8	3 ml
SDS solution (10% w/v)	10 ml
β-Mercaptoethanol	50 µl
dH_2O	37 ml

Table 15 – Heat-induced epitope retrieval buffer (TRIS -EDTA pH 9).

Component	Volume (final concentration)
TRIS base	1.2 g (10 mM)
EDTA	0.7 g (2.4 mM)
dH_2O	Fill up to 1 l

Table 16 – Immunohistochemistry wash buffer (TBS-T pH 7.6).

Component	Volume (final concentration)
TRIS base	6.055 g
NaCl	8.47 g
H_2O	Fill up to 1 l
Tween-20	1 ml

2.5 Vectors and plasmids

Table 17 – List of vectors and plasmids.

Vector ID	Name	Description
pTN0107	XBR2-401 MiH1 41bb	epHIV7-derived lentiviral vector, EF1α-HTLV fusion promotor, GM-CSF signal peptide, XBR2-401 single chain variable fragment (scFv) in V_H-V_L configuration with a $(G_4S)_3$-linker, IgG3 MiH1 Spacer, CD28 transmembrane (TM) domain, 4-1BB (CD137) co-stimulatory domain, CD3ζ stimulatory domain, T2A-site, truncated epidermal growth factor receptor marker (tEGFR), Woodchuck hepatitis virus posttranscriptional regulatory element (WPRE)
pJWB0001	X3.12 MiH1 41bb	epHIV7-derived lentiviral vector, EF1α-HTLV fusion promotor, GM-CSF signal peptide, X3.12 scFv (V_H-V_L; $(G_4S)_3$-linker), IgG3 MiH1 Spacer, CD28 TM, 4-1BB (CD137) co-stimulatory domain, CD3ζ stimulatory domain, T2A-site, tEGFR, WPRE
pJWB0007	hX3.12.5 MiH1 41bb	epHIV7-derived lentiviral vector, EF1α-HTLV fusion promotor, GM-CSF signal peptide, hX3.12.5 scFv (V_H-V_L; $(G_4S)_3$-linker), IgG3 MiH1 Spacer, CD28 TM, 4-1BB (CD137) co-stimulatory domain, CD3ζ stimulatory domain, T2A-site, tEGFR, WPRE
pJWB0008	hX3.12.6 MiH1 41bb	epHIV7-derived lentiviral vector, EF1α-HTLV fusion promotor, GM-CSF signal peptide, hX3.12.6 scFv (V_H-V_L; $(G_4S)_3$-linker), IgG3 MiH1 Spacer, CD28 TM, 4-1BB (CD137) co-stimulatory domain, CD3ζ stimulatory domain, T2A-site, tEGFR, WPRE
pJ01668	ffLuc-eGFP	epHIV7-derived lentiviral vector, EF1α-HTLV fusion promotor, firefly (*P. pyralis*) luciferase + enhanced green fluorescent protein (eGFP) fusion protein, (WPRE)
pTN0045	hROR2	epHIV7-derived lentiviral vector, EF1α-HTLV fusion promotor, full-length human ROR2, T2A-site, tEGFR, WPRE
pTN0050	mROR2	epHIV7-derived lentiviral vector, EF1α-HTLV fusion promotor, human ROR2 signal peptide, murine ROR2 without signal peptide, T2A-site, tEGFR, WPRE
pCHGP-2	-	Packaging plasmid for lentiviral vector production, CMV promotor, human immunodeficiency virus 1 (HIV-1) gag and pol gene, Rev response element (RRE)
pCMV-Rev2	-	Packaging plasmid for lentiviral vector production, CMV promotor, HIV-1 reverse transcriptase (Rev)
pCMV-G	-	Pseudotyping/ envelop plasmid for lentiviral vector production, CMV promotor, vesicular stomatitis virus glycoprotein (VSV-G)

2.6 Flow cytometry reagents

Table 18 – Flow cytometry antibodies.

Antigen	Clone	Conjugates	Isotype	Supplier
CD3	UCHT-1	Pacific Blue, FITC, PE, PerCp, PerCp-Cy5.5, PE-Cy7, APC, APC-Cy7	Mouse IgG1, κ	Biolegend, San Diego, USA
CD3	REA613	VioGreen, VioBlue, PE-Vio770, APC-Vio770	recombinant human IgG1	Miltenyi Biotec, Bergisch Gladbach, GER
CD4	REA623	Pe-Vio770	recombinant human IgG1	Miltenyi Biotec, Bergisch Gladbach, GER
CD4	SK3	PE, PerCp,	Mouse IgG1, κ	Biolegend, San Diego, USA
CD8	SK1	Pacific Blue, PeCy7, APC	Mouse IgG1, κ	Biolegend, San Diego, USA
CD25	BC96	FITC	Mouse IgG1, κ	Biolegend, San Diego, USA
CD38	HIT2	APC	Mouse IgG1, κ	Biolegend, San Diego, USA
CD45	REA747	VioBlue	recombinant human IgG1	Miltenyi Biotec, Bergisch Gladbach, GER
CD45RA	REA639	VioBlue	recombinant human IgG1	Miltenyi Biotec, Bergisch Gladbach, GER
CD45RO	UCHL1	FITC	Mouse IgG2a, κ	Biolegend, San Diego, USA
CD62L	DREG-56	PerCp-Cy5.5	Mouse IgG1, κ	Biolegend, San Diego, USA
CD69	FN50	APC-Cy7	Mouse IgG1, κ	Biolegend, San Diego, USA
CD138	MI15	BV421	Mouse IgG1, κ	Biolegend, San Diego, USA
CD223	11C3C65	PerCp-Cy5.5	Mouse IgG1, κ	Biolegend, San Diego, USA
CD266	REA 315	PE	recombinant human IgG1	Miltenyi Biotec, Bergisch Gladbach, GER
CD279	PD1.3.1.3	PE	Mouse IgG2b	Miltenyi Biotec, Bergisch Gladbach, GER
CD319	REA150	PE	recombinant human IgG1	Miltenyi Biotec, Bergisch Gladbach, GER
CD366	F38-2E2	APC-Cy7	Mouse IgG1, κ	Biolegend, San Diego, USA
ROR2	X3.12	unconjugated, AF647	human IgG1	Dr. C. Rader
ROR2	FAB20641P	PE	Mouse IgG2a, κ	Biotechne, Minneapolis, USA
tEGFR	Cetuximab	AF647	Human IgG1	BMS, Clinton, USA

Table 19 – Flow cytometry isotype controls.

Isotype for	Clone	Conjugates	Provider
Mouse IgG1, κ	MOPC-21	Pacific Blue, FITC, PE, PerCp, PerCp-Cy5.5, PE-Cy7, APC, APC-Cy7	Biolegend, San Diego, USA
Mouse IgG2b	IS6-11E5.11	PE	Miltenyi Biotec, Bergisch Gladbach, GER
Mouse IgG2a, κ	MOPC-173	FITC, PE, Pe-Cy7	Biolegend, San Diego, USA
recombinant human IgG1	REA293	VioGreen, VioBlue, FITC, PE, PE-Vio770, APC, APC-Bio770	Miltenyi Biotec, Bergisch Gladbach, GER

Table 20 – Other flow cytometry reagents.

Reagent	Conjugates	Supplier
123 count eBeads™ Counting Beads	N.A.	Thermo Fisher Scientific, Waltham, USA
7-AAD	N.A.	Miltenyi Biotec, Bergisch Gladbach, GER
Anti-Human IgG/M/A secondary F(ab')2	FITC	Thermo Fisher Scientific, Waltham, USA
Human TruStain FcX™	N.A.	Biolegend, San Diego, USA
Zombie Aqua™ Fixable Viability Kit	N.A.	Biolegend, San Diego, USA

2.7 Chemical compounds

Table 21 – List of chemical compounds.

Name	Provider
2-Mercaptoethanol	ITW Reagents, Glenview, USA
2-Mercaptoethanol (50 mM)	Thermo Fisher Scientific, Waltham, USA
DEPC-treated water	Thermo Fisher Scientific, Waltham, USA
Dimethyl sulfoxide for cell culture (DMSO)	AppliChem, Darmstadt, GER
D-luciferin, potassium salt	Biosynth, Staad, CH
Ethanol absolute	AppliChem, Darmstadt, GER

Ethylenediaminetetraacetic acid (EDTA) 0.5 M	Thermo Fisher Scientific, Waltham, USA
Ethylenediaminetetraacetic acid disodium salt dihydrate	Carl Roth, Karlsruhe, GER
Hematoxylin solution	Carl Roth, Karlsruhe, GER
Histopaque®-1077	Merck, Darmstadt, GER
Hydrogen peroxide solution (30% w/w)	Merck, Darmstadt, GER
Ionomycin calcium salt	Merck, Darmstadt, GER
PBS-Tween tablets	Merck, Darmstadt, GER
Phorbol 12-myristate 13-acetate (PMA)	Merck, Darmstadt, GER
Polybrene (10 mg/ml)	Merck, Darmstadt, GER
Roticlear®	Carl Roth, Karlsruhe, GER
Sodium azide	AppliChem, Darmstadt, GER
Sodium chloride	Carl Roth, Karlsruhe, GER
Sodium dodecyl sulfate	Carl Roth, Karlsruhe, GER
TRIS Base	Carl Roth, Karlsruhe, GER
Tween-20	ITW Reagents, Glenview, USA
Water for molecular biology	Th. Geyer, Renningen, GER

2.8 Commercial kits and other reagents

Table 22 – List of commercial kits and reagents.

Name	Provider
Alexa Fluor™ 647 Antibody Conjugation Kit	Thermo Fisher Scientific, Waltham, USA
Alsever's solution	Merck, Darmstadt, GER
Antibody dilution buffer	DCS, Hamburg, GER
BD Pharm Lyse	BD Biosciences, Heidelberg, GER
Bulk Beads Zirconia 1.5 mm	Biozym Scientific, Hessisch Oldendorf, GER
CalPhos Mammalian Transfection Kit	Takara, Kyoto, Japan
$CD4^+$ T cell Isolation Kit, human	Miltenyi Biotec, Bergisch Gladbach, GER
$CD8^+$ T cell Isolation Kit, human	Miltenyi Biotec, Bergisch Gladbach, GER
CellTrace™ CFSE Cell Proliferation Kit	Thermo Fisher Scientific, Waltham, USA
Clarity Western ECL Substrate	BioRad, Hercules, USA
Collagenase P	Merck, Darmstadt, GER
DC Protein Assay Kit I	BioRad, Hercules, USA
DMEM (+4.5 g/L glucose, GlutaMAX, phenol red)	Thermo Fisher Scientific, Waltham, USA
DNase I	Roche, Basel, CH
DPBS (calcium-free, magnesium-free)	Thermo Fisher Scientific, Waltham, USA
Dynabeads Human T-Activator CD3/28	Thermo Fisher Scientific, Waltham, USA
ELISA MAX™ Deluxe Human IFNγ	Biolegend, San Diego, USA
ELISA MAX™ Deluxe Human IL-2	Biolegend, San Diego, USA
EZ-Link™ Sulfo NHS-SS Biotinylation Kit	Thermo Fisher Scientific, Waltham, USA
Fetal bovine serum (heat-inactivated)	Thermo Fisher Scientific, Waltham, USA
Goat anti-mouse IgG (H+L)-HRP conjugate	Biorad, Hercules, USA
Goat anti-rabbit IgG (H+L)-HRP conjugate	Biorad, Hercules, USA
Hs_GAPDH_1_SG QuantiTect Primer Assay	Qiagen, Venlo, NL

Hs_ROR2_1_SG QuantiTect Primer Assay	Qiagen, Venlo, NL
Human MTC Panel I	Takara, Kyoto, Japan
Human MTC Panel II	Takara, Kyoto, Japan
Human protein medley (skin, uterus, ovaries, placenta, testis, mamma, cecum, intestine)	Takara, Kyoto, Japan
Human serum	Deutsches Rotes Kreuz Blutspendedienst
Liquid DAB+ Substrate chromogen system	Agilent, Santa Clara, USA
Mini-PROTEAN TGX Precast Gels 10%	BioRad, Hercules, USA
Mm_Gapdh_3_SG QuantiTect Primer Assay (200)	Qiagen, Venlo, NL
Mm_Ror2_1_SG QuantiTect Primer Assay (200)	Qiagen, Venlo, NL
Mouse anti-human β-Actin antibody (clone 4C2)	Merck, Darmstadt
Mouse anti-mouse ROR2 antibody (ab190145)	Abcam, Cambridge, UK
Mouse MTC Panel I	Takara, Kyoto, Japan
Mouse MTC Panel III	Takara, Kyoto, Japan
Multi tissue dissociation kit v1	Miltenyi Biotec, Bergisch Gladbach, GER
Normal goat serum (10%)	Thermo Fisher Scientific, Waltham, USA
NucleoBond Xtra Maxi EF	Macherey & Nagel, Düren, GER
NucleoSpin Gel and PCR Clean-up Kit	Macherey & Nagel, Düren, GER
NucleoSpin Plasmid, Mini kit	Macherey & Nagel, Düren, GER
NuPAGE™ LDS Sample Loading Buffer (4x)	Thermo Fisher Scientific, Waltham, USA
NuPAGE™ Sample Reducing Agent (10X)	Thermo Fisher Scientific, Waltham, USA
Okt3 antibody	Miltenyi Biotec, Bergisch Gladbach, GER
Penicillin/Streptomycin (10.000 U/ml)	Thermo Fisher Scientific, Waltham, USA
Phosphatase Inhibitor Cocktail 2	Merck, Darmstadt, GER
Power SYBR™ Green PCR-Master-Mix	Thermo Fisher Scientific, Waltham, USA
Protease Inhibitor Cocktail	Merck, Darmstadt, GER
Rabbit anti-human ROR2 antibody (ab218105)	Abcam, Cambridge, UK

Recombinant human IL-2	Miltenyi Biotec, Bergisch Gladbach, GER
RIPA Buffer	Merck, Darmstadt, GER
Rneasy(R) Mini Kit	Qiagen, Venlo, NL
RPMI-1640 (25 mM HEPES, GlutaMAX, phenol red)	Thermo Fisher Scientific, Waltham, USA
Super Sensitive Link-Label ICH Detection System	DCS, Hamburg Germany
SuperScript™ IV First-Strand Synthesis System	Thermo Fisher Scientific, Waltham, USA
TMB Stop Buffer	ScyTek Laboratories, Logan, USA
Trans-Blot Turbo RTA Mini 0.2 µm PVDF Transfer Kit	BioRad, Hercules, USA
Trypan blue solution 0.4%	Thermo Fisher Scientific, Waltham, USA
Trypsin EDTA 0.05%, phenol red	Thermo Fisher Scientific, Waltham, USA

2.9 Consumables

Table 23 – List of consumables and plasticware.

Name	Provider
6-, 12-, 24-, 48- and 96-well plate flat-bottom	Corning, Kaiserslautern, GER
96-well plate flat-bottom, white	Corning, Kaiserslautern, GER
96-well plate round-bottom	Corning, Kaiserslautern, GER
BD Microlance 3 (20G x 1 1/2 " - Nr.1, 0,9mm x 40mm)	BD Biosciences, Heidelberg, GER
BD Plastipak 1ml 26GA x 3/8in (0.45 x 10mm) Luer	BD Biosciences, Heidelberg, GER
Cell culture flasks 25 and 75 cm^2 surface area	Corning, Kaiserslautern, GER
Dish Nunclon™ Delta 10 cm	Thermo Fisher Scientific, Waltham, USA
CELLSTAR™ EASYstrainer™ 70 µm	Greiner Bio-One, Frickenhausen, GER
E-Plate 16 for xCELLigence RTCA DP	OMNI Life Science, Bremen, GER
Falcon® round-bottom tubes 5 ml with cell strainer	Thermo Fisher Scientific, Waltham, USA
Filter tips 2.5, 10, 20, 200 and 1000 µl	Sarstedt, Nümbrecht, GER
Filtropur V50 vacuum filtration unit 0.2 µm	Sarstedt, Nümbrecht, GER
Flow cytometry tubes 5 ml	Sarstedt, Nümbrecht, GER
Half-area plate 96-well transparent	Corning, Kaiserslautern, GER
Leucosep™ tube 50 ml	Greiner Bio-One, Frickenhausen, GER
MACS® Cell separation column, LS	Miltenyi Biotec, Bergisch Gladbach, GER
MicroAmp Optical 96-Well Reaction Plates	Thermo Fisher Scientific, Waltham, USA
Omnican 40, 1 ml insulin syringes	B. Braun, Melsungen, GER
Serological pipettes 2, 5, 10, 25 and 50 ml	Greiner Bio-One, Frickenhausen, GER
Sterile syringe filter unit, PVDF, 0.45 µm	Merck, Darmstadt, GER
CELLSTAR® 15- and 50-ml conical tubes (PP)	Greiner Bio-One, Frickenhausen, GER

2.10 Equipment

Table 24 – Technical equipment.

Name	Company
BD FACSCanto™ II flow cytometer	BD Biosciences, Heidelberg, GER
BD FACSAria II fluorescence activated cell sorter	BD Biosciences, Heidelberg, GER
BeadBug bead homogenizer	Benchmark Scientific, Sayreville, USA
Biological safety cabinet Herasafe™ KS	Thermo Fisher Scientific, Waltham, USA
Centrifuge Heraeus™ Megafuge™ 40R	Thermo Fisher Scientific, Waltham, USA
ChemiDoc™ MP Gel imaging system	BioRad Laboratories Inc., Hercules, USA
CO_2 incubators Heracell™ 150i and 240i	Thermo Fisher Scientific, Waltham, USA
DynaMag™-15 magnet	Thermo Fisher Scientific, Waltham, USA
Faxitron CP-160 irradiator	Faxitron Bioptics, Tucson, AZ, USA
IVIS Lumina XRMS *in vivo* imaging system	PerkinElmer, Waltham, USA
Microcentrifuge Fresco 17	Thermo Fisher Scientific, Waltham, USA
Mini-PROTEAN® Tetra Vertical Electrophoresis Cell	BioRad Laboratories Inc., Hercules, USA
Mr. Frosty™ Freezing Container	Thermo Fisher Scientific, Waltham, USA
Tecan HydroSpeed™ plate washer	Tecan, Männedorf, CH
Tecan Infinite® 200 PRO plate reader	Tecan, Männedorf, CH
Orbital Microplate shaker	Thermo Fisher Scientific, Waltham, USA
PCR Mastercycler® ep Gradient S	Eppendorf, Hamburg, GER
Pipette controller accu-jet® pro	Brandtech Scientific Inc. Essex, USA
Pipettes research plus 2.5, 10, 20, 200 and 1000 µl	Eppendorf, Hamburg, GER
Power supply Powerpack™ Basic	BioRad Laboratories Inc., Hercules, USA
Primovert Microscope	ZEISS, Jena, GER
QuadroMACS Separator	Miltenyi Biotec, Bergisch Gladbach, GER
Refrigerator -4 and -20 °C	Liebherr, Bulle, CH

3DHistech Pannoramic Scan, IHC slide scanner	3DHistech, Budapest, Hungary
StepOnePlus Real-Time PCR System	Thermo Fisher Scientific, Waltham, USA
Trans-Blot® Turbo™ Transfer System	BioRad Laboratories Inc., Hercules, USA
Ultracentrifuge Sorvall™ WX80	Thermo Fisher Scientific, Waltham, USA
HeraFreeze HLE Series -80 °C freezer	Thermo Fisher Scientific, Waltham, USA
Water bath	Memmert, Schwabach, GER
xCELLigence RTCA DP	Agilent Technologies, Santa Clara, USA

2.11 Software

Table 25 – Software tools.

Name	Application	Provider
Case viewer	Visualization of immunohistochemistry slide scans	3D Histech, Budapest, Hungary
FlowJo v10.4	Flow cytometry data analysis	Becton, Dickinson and Company, Franklin Lakes, USA
GraphPad Prism 7	Graphical data representation; statistical analyses	GraphPad Software, San Diego, USA
Image Lab 5.1	Analysis and evaluation of agarose gels and western blot data	BioRad Laboratories Inc., Hercules, USA
Living Image 4	Visualization and analysis of animal bioluminescence data	PerkinElmer, Waltham, USA
QuPath 0.3.0	Evaluation of IHC slide scans	Bankhead et al. [141]
RTCA Data Analysis Software 1.0	Data representation, export, and evaluation of xCELLigence datasets	Agilent Technologies, Santa Clara, USA

3 Methods

3.1 Molecular biology methods

3.1.1 Vector design and generation

All constructs used in this study were codon optimized for their expression in human cells and customs syntheses were ordered from GeneArt. Lentiviral constructs were obtained by sub cloning into an epHIV7-derived plasmid containing an EF1α-HTLV fusion promoter and woodchuck hepatitis virus posttranscriptional regulatory element (WPRE) [142]. ROR2-specific second-generation CARs consisting of an IgG3 MiH1 spacer, CD28 transmembrane domain, 4-1BB co-stimulatory domain, and CD3ζ stimulatory domain were generated using scFv versions of the four binders XBR2-401, X3.12, hX3.12.5 and hX3.12.6 [62, 95]. For all binders, the variable heavy chain – variable light chain (V_H – V_L) configuration with a $(G_4S)_3$-linker was chosen (Table 17). All CAR constructs were designed to contain a T2A self-cleaving peptide sequence and the truncated epidermal growth factor receptor (tEGFR) selection marker to enable enrichment and depletion of CAR-positive T cells [143].

3.1.2 RNA isolation, cDNA synthesis and quantitative PCR

1×10^6 cells were harvested, washed with sterile ice-cold PBS and RNA isolation was performed using the RNeasy isolation kit as per the manufacturer's protocol. Subsequently, cDNA synthesis was conducted with the SuperScript™ IV First-Strand Synthesis kit using 200 ng to 1 µg of RNA and the $(dT)_{20}$-primer. Matched tumor and healthy tissue cDNA of consenting RCC patients was kindly provided by Dr. C. Kalogirou. All qPCR analyses were done in technical triplicates for each gene and repeated three times. qPCR reactions were performed using the Power SYBR Green Mastermix and bioinformatically validated qPCR primers, as per the manufacturer's protocols. The final composition of the qPCR reactions is summarized in Table 26 and PCR parameters are shown in Table 27. Melting curve analysis was performed as a quality control and relative gene expression values were calculated using GAPDH as the housekeeping gene and appropriate reference samples employing the Pfaffl's or $2^{-\Delta\Delta Ct}$ method, as described [144, 145].

Table 26 – qPCR reaction composition.

Component	Volume
cDNA	0.25 µl
DEPC-treated water	7.75 µl
QuantiTect primer	2 µl
2× Power SYBR Green Mastermix	10 µl
Final volume per well	20 µl

Table 27 – qPCR cycle parameters.

	Step description	Time	Temperature
	Initial activation	15 min	95 °C
40 cycles of	Denaturation	15 sec	94 °C
	Annealing	30 sec	55 °C
	Extension	30 sec	72 °C
	Melting curve analysis	~ 60 min	Gradient: 40 °C – 95 °C

3.1.3 Protein isolation, quantification, and Western blot analysis

To isolate whole cell protein from cell lines, 2 × 10^6 cells were harvested, washed with ice cold PBS, resuspended in RIPA buffer supplemented with 1 % each of protease and phosphatase inhibitor and lysed by shock freezing in liquid nitrogen. For protein isolation from murine tissues, tissue fragments were obtained from cryopreserved mouse organs and homogenized in 500 µl RIPA buffer supplemented with 1 % each of protease and phosphatase inhibitor using 1.5 mm zirconia beads and a bead bug.

Protein concentrations were determined using a modified version of the Lowry assay (Biorad) , as per the manufacturer's protocol. For Western blot analysis 5 to 10 µg of protein

were run on 10 % SDS polyacrylamide gels under reducing conditions and blotted on PVDF membranes using the TransBlot mini system. Blots were washed once with TBS-T, blocked with 10 % BSA in TBS-T for at least 30 min, followed by another two wash steps in TBS-T. Primary Western blot antibodies were diluted 1:1000 in 5 % BSA in TBS-T and blots were incubated at 4 °C for 20 h on an orbital shaker. On the next day, blots were washed thrice in TBS-T, and bound primary antibody was labeled using a 1:1000 dilution of the appropriate secondary antibody in 5 % BSA in TBS-T for 1 h at room temperature. Blots were washed another three times with TBS-T and antibody binding was determined by enhanced chemiluminescence (ECL) substrate conversion measurement on a ChemiDoc MP imaging system. Antibodies were removed using a one-hour incubation at 65°C in stripping buffer and re-probed for β-Actin, as per the afore-mentioned protocol.

3.1.4 Immunohistochemistry of primary RCC samples

Formalin-fixed, paraffin-embedded RCC sample slides of consenting patients were kindly provided by the department of pathology of the University Hospital Wuerzburg and were analyzed for their ROR2 expression by immunohistochemistry. In brief, slides were de-paraffinized using xylol, and heat induced epitope retrieval (HIER) was performed by bringing room temperature TRIS -EDTA Buffer (pH 9.0) to a boil in a pressure cooker and boiling the slides for 5 min, followed by a 20 min cooling phase. Naturally expressed peroxidases were inactivated by incubation with 1:40 diluted H_2O_2 for 15 min at room temperature, and a 20 min incubation with goat serum was employed to reduce unspecific antibody binding. Subsequently, slides were incubated with rabbit anti-human ROR2 antibody diluted 1:1000 in antibody dilution buffer for 20 h at 4°C. On the next day, primary antibody was washed off, and bound antibody was labeled using the Super Sensitive Link-Label IHC Detection System. ROR2 expression was determined calorimetrically using 3,3’-Diaminobenzidine (DAB) and counterstaining with hematoxylin. Slides were digitalized on a 3D Histech Pannoramic Scan IHC slide scanner, tumor areas were determined by histological analysis and H-scores were calculated using the positive cell quantification feature in QuPath [141].

3.2 Tumor cell line methods

3.2.1 Cultivation of tumor cell lines

Adherent renal cell carcinoma cell lines Caki-1, Caki-2, ACHN, RCC-4, and RCC-53, as well as MDA-MB-231 breast cancer cells were cultivated in cDMEM, and 786-O cells were cultivated in cRPMI. All adherent cell lines were sub-cultivated 2-3 times per week using 0.05 % Trypsin-EDTA to maintain sub-confluent cultures. Suspension cell lines U-266, Jurkat, TM-LCL and OPM-2 were cultivated in cRPMI and maintained at cell densities between 0.2 and 2×10^6 cells/ml.

3.2.2 Lentivirus production and titration

6×10^6 Lenti-X 293T cells were seeded in 10 mm dishes and allowed to adhere for 6 h at 37 °C, 5 % CO_2 in a humidified incubator. Subsequently, transfection was performed with the CalPhos Mammalian Transfection Kit (Takara) as per the manufacturer's protocol using 15 µg of the respective epHIV7-based expression plasmid, 10 µg pCHGP-2, 1 µg pCMV-Rev2, and 2 µg of pCMV-G. An equal volume of 2 × HBSS was added to the solution, incubated for 20 min at room temperature and added dropwise to the plates. On the next day, cells were washed twice with warm, sterile PBS, and fresh cDMEM was added. After another 48 h, the lentiviral supernatants were harvested, and cell debris was removed by centrifugation at 2,200 × g for 15 min at 8 °C and subsequent sterile filtration using 0.45 µm PES-membrane filters. Viral particles were concentrated by density ultracentrifugation at 138,510 × g for 2 h at 4 °C using a 20 % sucrose layer. The resulting pellet was dissolved in TBS-T buffer and the viral titer was determined by Jurkat cell titration. To this end, 2.5×10^5 Jurkat cells were seeded in 250 µl of cRPMI in 48-well plates, mixed with 5 µg/ml polybrene and incubated with different volumes of viral particles. After 4 h, 750 µl cRPMI were added to each well and the transduction efficiency was determined by flow cytometry analysis after another 48 h. The virus titer was calculated from samples that yielded a gene transfer rate between 20 % and 40 % using the formula:

$$Virus\ titer\ \left[\frac{TU}{\mu l}\right] = \frac{cell\ count\ at\ time\ of\ transduction\ x\ fraction\ of\ positive\ cells}{Volume\ added\ [\mu l]}$$

3.2.3 Lentiviral transduction of tumor cell lines

Firefly luciferase-expressing cell line variant were generated by lentiviral transduction with a vector encoding for a ffLuc-eGFP fusion protein under control of an EF1α-HTLV fusion promotor. In brief, 0.5 × 10^6 cells were resuspended in 1 ml complete medium supplemented with 5 µg/ml polybrene and transductions were performed using lentiviral supernatants at a multiplicity of infection (MOI) of 5. If needed, ffLuc-eGFP-positive cells were enriched by fluorescence activated cell sorting (FACS) on a FACS Aria II cell sorter.
MDA-MB-231 ffLuc variants overexpressing human or murine ROR2 were generated according to the same protocol using lentiviral vectors encoding for the respective protein under control of an EF1α-HTLV fusion promotor.

3.2.4 Flow cytometry analysis of tumoral cell lines

2 × 10^5 tumor cells were collected, washed once with ice-cold FACS buffer, and stained with antibodies against ROR2, SLAMF7 (CD319), BCMA (CD269) or appropriate isotype control. FMO controls were used where no isotypes were available. 7-AAD was included to discriminate between live and dead cells. When using human antibodies, FC-receptors were blocked before FACS staining using FcX true stain as per the manufacturer's protocol.

3.3 Generation of CAR-modified T cells

3.3.1 Isolation of human T cells

Peripheral blood mononuclear cells (PBMC) were isolated from the blood of healthy donors by density gradient centrifugation. In brief, blood samples were diluted 1:4 in sterile, room-temperature PBS and carefully layered over 15 ml of Histopaque in Leucosep tubes. After centrifugation at 300 × g for 20 min at room temperature without brakes, the PBMC layer was harvested with a pipette and washed twice with ice-cold PBS/EDTA buffer. Subsequently, bulk $CD4^+$ and $CD8^+$ T cells were isolated by negative selection using the respective T cell isolation kits as per the manufacturer's protocol. The enrichment was performed using LS-columns loaded with no more than 100 × 10^6 cells per column.

3.3.2 Lentiviral transduction of human T cells

T cells were seeded in 48-Well plates at a density between 0.25 and 0.5 × 10^6 cells per ml in CTL medium supplemented with 50 u/ml rhIL-2 and CD3/CD28-Dynabeads at a cell:bead-ratio of 1:1 for initial activation. After 16 h, polybrene was added to a final concentration of 5 µg/ml and transductions were performed by spinoculation at 800 × g for 45 min with slow breaks at 32 °C using lentiviral supernatants at a MOI of 3. After another 4-hour incubation at 37 °C, samples were adjusted to 1 ml using CTL supplemented with 50 u/ml rhIL-2. T cells were fed or passaged to bigger wells or flasks every two to three days, based on cell density. On Day 6 after T cell isolation, CD3/CD28-Dynabeads were removed.

3.3.3 Flow cytometry analysis of CAR-modified T cells

Flow cytometry analysis of CAR-modified T cells was routinely performed on day 7 after T cell isolation to confirm purity and gene transfer rate by checking for CD3, CD4, CD8, and tEGFR, as well as 7-AAD to discriminate between live and dead cells. The analysis was repeated three to four days before functional assays to ensure data reproducibility.

In brief, 2 × 10^5 cells were washed with ice-cold FACS buffer at 300 × g, 4 °C for 4 min, stained with the appropriate antibody master mix for 30 min at 4 °C in the dark. Unbound antibody was removed by washing twice with FACS buffer and 1 µl of 7-AAD was added before analysis to discriminate living and dead cells.

3.3.4 Enrichment and expansion of CAR-positive T cells

CAR-positive T cells were enriched by positive MACS selection using in-house biotinylated cetuximab and anti-biotin microbeads. In brief, T cells were adjusted to 1 × 10^7 cells per ml in MACS buffer supplemented with 10 µl of biotinylated cetuximab per ml. Cells were incubated for 15 min at 4°C, washed once with a 10-fold excess of sterile MACS buffer (300 × g, 4 °C, 6 min) and resuspended in a mix of 80 µl MACS buffer and 20 µl anti-biotin beads per 1 × 10^7 cells. After another incubation for 15 min at 4°C, cells were washed again, and CAR-positive cells were isolated by positive selection using LS-columns as per the manufacturer's protocol.

Enriched T cells were expanded by polyclonal stimulation as described previously [146]. In brief, T cells were co-cultivated with irradiated TM-LCL feeder cells and allogeneic PBMCs at a ratio of 1:100:600 (T cells : TM-LCL : PBMC) in 20 ml CTL supplemented with 6 µl Okt-3 antibody. After 24 h, rhIL-2 was added to achieve a final concentration of 50 u/ml. On day 4, cells were washed to remove cell debris and subsequently cultivated in fresh CTL supplemented with 50 u/ml rhIL-2 for another 6 to 10 days before cells were used for functional assays.

3.4 Functional characterization of CAR-modified T cells *in vitro*

3.4.1 Luminescence-based cytotoxicity assay

To determine antigen-specific tumor cell lysis, 5 × 10^3 ffLuc-transduced tumor cells were co-cultured with $CD8^+$ CAR-transduced or untransduced (UTD) T cells at effector:target (E:T)-ratios of 5:1, 1:1 or 1:5 in 200 µl of cRPMI medium supplemented with 150 ng/ml D-Luciferin [147]. The bioluminescence signal was measured on a Tecan Infinite 200 PRO plate reader after 2, 4, 6 and 24 h, and the specific lysis at each respective E:T-ratio and timepoint was calculated using the formula:

$$Spec.Lysis\ (\%) = 1 - \left(\frac{mean\ BLI\ of\ tumor\ cells\ treated\ with\ CAR\ T\ cells}{mean\ BLI\ of\ tumor\ cells\ treated\ with\ UTD\ T\ cells}\right)$$

3.4.2 Impendence-based cytotoxicity (xCELLigence)

For impendence-based cytotoxicity assays, 1.5 x 10^4 786-O ffLuc cells were seeded into E-Plate16 in 100 µl of cRPMI and allowed to adhere for 4 h. Subsequently, $CD8^+$ CAR-transduced or UTD T cells were added to a final E:T-ratio of 1:5 in a total volume of 200 µl of cRPMI. Cell indices were determined on a xCELLigence RTCA DP analyzer in 15 Min intervals at 37 °C, 5 % CO_2 in a humidified incubator. To determine CAR-T cell efficacy, the time to half maximal lysis was determined based on normalized cell index values.

3.4.3 Cytokine secretion assay

5 × 10^4 T cells were co-cultivated with 1.25 × 10^4 tumor cells in 200 µl of cRPMI and supernatants were collected after 24 h. Secretion of the effector cytokines IL-2 and IFNγ was determined by enzyme-linked immunosorbent assay (ELISA) as per the manufacturer's protocols using 1:2 diluted supernatants for $CD8^+$ co-cultures and 1:4 diluted supernatants for $CD4^+$ co-cultures. The concentration of IL-2 and IFNγ was extrapolated from their respective standard curves by 5-parameter logistic curve-fitting (GraphPad Prism 7).

3.4.4 T cell proliferation assay

T cells were labeled with 0.1 µM Carboxyfluoresceinsuccinimidylester (CFSE) as per the manufacturer's protocol and residual dye was quenched using heat-inactivated FBS. Subsequently, $CD4^+$ and $CD8^+$ T cells of each respective condition were mixed 1:1 and co-cultivated with irradiated target cells at a total E:T-ratio of 1:1 for 72 h. In some instances, an E:T ratio of 4:1 was chosen. On the day of analysis, triplicate wells were pooled, labeled with antibodies directed against CD4, CD8 and tEGFR and the proliferation of 7-AAD-negative, living T cells was determined by flow cytometry on a FACS Canto II. Proliferation and expansion indices were calculated with FlowJo v10.4 [148].

3.4.5 Flow cytometry-based cytotoxicity assay of primary MM samples

CD138-enriched primary MM cells of consenting MM patients were kindly provided by the department for translational myeloma research at the university hospital Würzburg. MM cells were labeled with 0.1 µM CFSE as per the manufacturer's protocol and co-cultivated with allogeneic $CD8^+$ T cells at an E:T-ratio of 10:1 for 16 h. Samples were collected, washed once with FACS buffer, and stained for CD8, CD38 and CD138 at 4 °C for 30 min in the dark. Samples were washed twice and resuspended in 100 µl FACS buffer supplemented with 1 µl of 7-AAD and 5 µl Counting Beads. Absolute cell numbers were determined as per the manufacturer's protocol and used to calculate specific lysis.

3.4.6 CAR-Jurkat-based humoral immunogenicity assay

CAR-expressing Jurkat cells were generated by lentiviral transduction as per the primary T cell protocol (chapter 3.3.2). CAR-positive Jurkats were enriched by MACS using in-house biotinylated cetuximab and anti-biotin microbeads. For flow cytometry analysis, 1×10^6 CAR-Jurkats were collected, washed with FACS buffer, and incubated with TruStain FcX for 10 min at room temperature. Subsequently, primary staining with pre-existing anti-CAR antibodies was performed using 10% healthy donor human plasma in PBS for 30 min at 4 °C in the dark. Unbound antibody was removed by washing thrice with FACS buffer, and secondary mAb staining was performed using a 1:1000 dilution of anti-human IgG/M/A F(ab')2-FITC in FACS buffer for 30 min at 4°C in the dark. Unbound secondary antibody was removed by washing thrice with FACS buffer, and flow cytometry analysis of living CAR-Jurkat was performed on BD FACS Canto II.

3.5 Functional characterization of CAR-modified T cells *in vivo*

3.5.1 786-O/NSG xenograft model

To study the efficacy of ROR2-specific CAR-T cells *in vivo*, NOD.Cg-Prkdc^{scid} Il2rg^{tm1Wjl}/SzJ (NSG) mice were subcutaneously injected with 3 × 10^6 786-O ffLuc cells, and tumor engraftment was monitored weekly by bioluminescence imaging (BLI) [149, 150]. 14 days after tumor engraftment, mice were randomized and treated with a single dose of 5 × 10^6 CAR-transduced or UTD T cells (CD4:CD8-ratio = 1:1). Tumor development was continuously monitored by BLI. Additionally, T cell expansion kinetics were monitored by flow cytometry analysis of blood samples obtained on days 7, 14, 21, 28, and 35 after T cell injection using antibodies against CD3, CD4, CD8, tEGFR, and PD-1, as well as the ZombieAqua fixable live/dead marker. At the individual experimental endpoint of each animal, long-term T cell persistence was determined by flow cytometry analysis of single-cell suspensions derived from the spleen, bone marrow and tumor of the mice, obtained during post-mortem examination. Tumors were cut into small pieces and incubated in pre-warmed cRPMI medium supplemented with 0.1 mg/ml DNase I and 0.4 mg/ml Collagenase P for 1 h at 37 °C with intermittent vortexing. All samples were passed through 70 µm cell strainers to generate single-cell suspensions and analyzed by flow cytometry analyzed for T cell frequencies (CD3, CD4, CD8, tEGFR, and PD-1), T cell subsets (CD3, CD4, CD8, CD45RA, CD45RO and CD62L), as well as T cell exhaustion (CD45, PD-1, TIM3 and LAG3).

3.5.2 U-266/NSG xenograft model

To study the efficacy of CAR_{enh} T cells against MM *in vivo*, NSG mice were engrafted with 1 × 10^7 U-266 ffLuc cells by intravenous injection [151]. Tumor engraftment and animal well-being were monitored as described previously. After 35 days, mice were randomized and treated with a single dose of 5 × 10^6 CAR_{enh} or UTD T cells (CD4:CD8 ratio = 1:1). Tumor development was monitored by weekly BLI analysis. Additionally, T cell expansion was confirmed by flow cytometry analysis of blood samples obtained via tail vein puncture on day 7 after T cell injection. Additionally, T cell long-term persistence was analyzed from single-cell suspensions obtained from spleen and bone marrow at the respective experimental endpoints of each animal by flow cytometry using antibodies against CD3, CD4,

CD8, tEGFR and PD-1. Live/dead cell discrimination was performed using the ZombieAqua fixable cell viability marker.

3.5.3 In vivo toxicity model

NSG mice were engrafted with 1×10^7 CAR_{enh} or UTD T cells (n = 5 mice per group) [12]. Animal weight and health scores were monitored daily as surrogates for severe on-target off-tumor toxicities. Mice were sacrificed on day 7, all organs were isolated during post-mortem examination and single-cell suspensions were generated using the multi tissue dissociation kit v1 (Miltenyi) and 70 µm cell strainers as per the manufacturer's protocols. The resulting single-cell suspensions were analyzed by flow cytometry using antibodies against CD45, CD4, CD8, CD25, CD69, PD-1, and tEGFR, as well as ZombieAqua for the discrimination of live/dead cells. T cell frequencies, as well as activation and exhaustion statuses were determined using FlowJo v10.4.

In a similar but independent study, mice were sacrificed on day 7 and day 147, and tissue specific lymphocyte infiltration and tissue damages were assessed by hematoxylin-eosin stain of formalin-fixed, paraffin-embedded tissue slides (in collaboration with AG Rosenfeldt, University Hospital Würzburg, Germany).

3.6 Statistical analyses

All graphs and statistical analyses in this thesis were generated using GraphPad Prism 7. Data shown for *in vitro* analyses is mean ± SEM for samples obtained from n ≥ 3 independent healthy donors, unless state otherwise. Statistical significance was calculated by two-way ANOVA and Tukey's multiple comparison test at a family-wise significance level of 0.05. Regular two-way ANOVA with Tukey's multiple comparison test at a significance level of 0.05 were used for samples obtained from animal experiments. Differences in overall survival were analyzed using the Mantel-Cox log-rank test. For the statistical analysis of H-score differences unpaired, two-tailed Student's T-test at a significance level of 0.05 was used. P values are denoted in graphical representations using the following abbreviations: $p > 0.05$, not significant (n.s.); $p < 0.05$, *; $p < 0.01$, **; $p < 0.001$, ***; $p < 0.0001$, ****.

4 Results

4.1 Efficacy of ROR2-specific CAR-T cells against renal cell carcinoma

4.1.1 ROR2 is a prevalent target in ccRCC

To evaluate ROR2 as a candidate target for the treatment of RCC, we assessed ROR2 expression in tumor samples and matched healthy tissue of a representative RCC patient cohort using qPCR (n = 30, Table 28). We found the GAPDH housekeeping gene to generally yield C_t-values between 16 and 20, and 93 % of samples (28/30) were considered evaluable on this basis. Employing a C_t-threshold of 35 cycles, ROR2 expression was detectable in 86 % of tumor samples (24/28). Relative ROR2 expression was determined by normalization to matched healthy tissues and revealed ROR2 overexpression in 67 % (2/3) of pRCC and 53 % (10/19) of ccRCC cases. In contrast, downregulation of ROR2 was observed in ChRCC samples (Figure 5 A).

To determine the expression of ROR2 on the protein level, immunohistochemical analysis of a matched cohort of pRCC and ccRCC patients was performed (n = 21, Table 29). The data showed significantly higher ROR2 protein expression in ccRCC than pRCC samples (Figure 5 B & C). In general, pRCC samples showed low and inhomogeneous expression (median H-score 14.22), whereas ccRCC samples were characterized by higher and more consistent expression across the tumor area (median H-score 109.4).

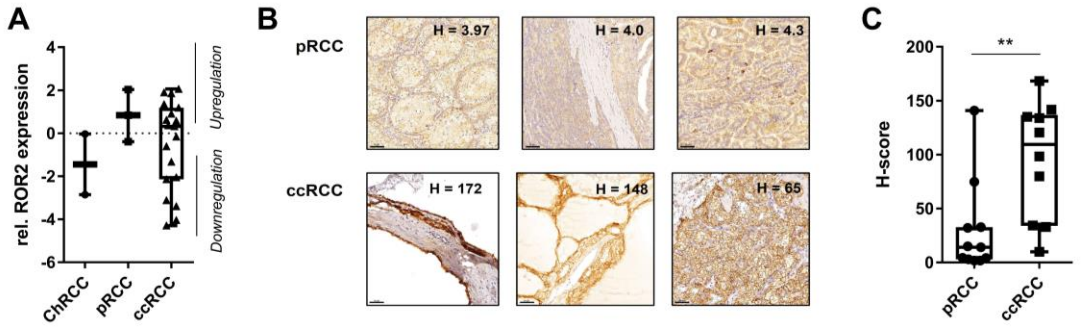

Figure 5 – ROR2 is commonly overexpressed in clear cell renal cell carcinoma patient samples.

(A) Relative ROR2 expression in matched tumor and healthy tissues, as determined by qPCR analysis of chromophobe (ChRCC), papillary (pRCC), and clear cell RCC (ccRCC) samples (n = 24). Data shown was calculated using Pfaffl's method (housekeeping gene: GAPDH; Reference samples: matched healthy tissue). (B) Representative IHC images of ROR2 expression in pRCC and ccRCC samples (H: H-score, scale bar = 50 µm), and (C) H-scores for all patient samples (n = 21). Statistics are based on two-tailed Student's T-Test.

Table 28 – RCC patient characteristics (qPCR analysis).

Characteristic	all patients (n = 30)
Median age (range) – years	64 (46 – 87)
Male – no. (%)	22 (73 %)
RCC subtype – no. (%)	
Chromophobe RCC	3 (10 %)
Papillary RCC	3 (10 %)
Clear cell RCC	24 (80 %)
Tumor grade – no. (%)	
1	2 (7 %)
2	15 (50 %)
3	10 (33 %)
4	3 (10 %)

Table 29 – RCC patient characteristics (IHC analysis).

Characteristic	all patients (n = 21)
Median age (range) – years	65 (23 – 84)
Male – no. (%)	13 (62 %)
RCC subtype – no. (%)	
Papillary RCC	11 (52 %)
Clear cell RCC	10 (48 %)
Tumor grade – no. (%)	
1	5 (24 %)
2	15 (71 %)
3	1 (5 %)
4	0 (0 %)

Next, we were interested in determining whether ROR2 expression was retained in RCC cell lines. qPCR analysis was employed to study ROR2 expression on the transcriptome level of four ccRCC (786-O, RCC-4, RCC-53, and Caki-1) and two pRCC cell lines (Caki-2 and ACHN). We found GAPDH to consistently yield C_t-values in the range of 16 to 19 cycles and found 83 % of samples (5/6) to express ROR2, as determined by a C_t-threshold of 35 cycles. For ccRCC, 786-O, RCC-4 and RCC-53 cells were determined to be ROR2 positive, whereas Caki-1 cells were found not to express ROR2. Additionally, we found both pRCC cell lines, Caki-2 and ACHN, to express ROR2 (Figure 6 A).

To assess the degree of heterogeneity in ROR2 antigen expression, flow cytometry analysis was employed. We found uniform ROR2 expression on the surface of 786-O, RCC-4, and RCC-53 (ccRCC), as well as Caki-2 and ACHN cells (pRCC). Median fluorescence intensity (MFI)-differences were used to group cell lines based on their ROR2 protein expression. We classified 786-O (dMFI = 1,083) and Caki-2 (dMFI = 1,021) cells as ROR2^{high}, RCC-4 (dMFI = 633) as ROR2^{med} and RCC-53 (dMFI = 228) and ACHN (dMFI = 348) as ROR2^{low}. Caki-1 cells were determined to be ROR2-negative despite antibody background binding (dMFI = 93) based on our qPCR analysis (Figure 6 B).

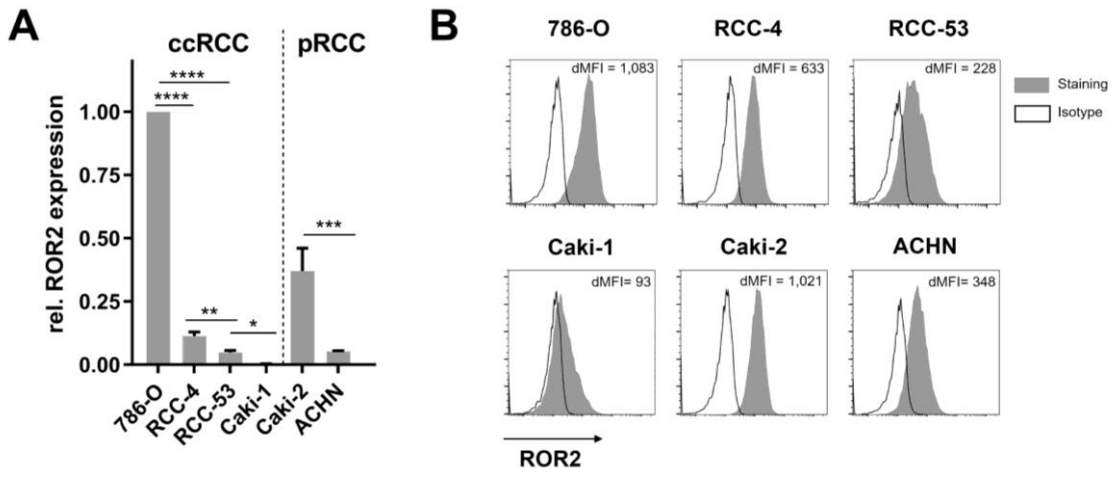

Figure 6 – ROR2 is uniformly expressed on the surface of RCC cell lines.

(A) qPCR-based gene expression and (B) flow cytometry analysis of ROR2 expression on RCC cell lines. qPCR data shown was calculated using the $2^{-\Delta\Delta Ct}$ method with GAPDH as the house keeping gene and normalized to 786-O cells. For flow cytometry analyses, the difference between median fluorescence intensities of stained (gray) and FMO (plain) samples is shown as dMFI. Statistics in (A) were calculated by one-way ANOVA and Tukey's multiple comparisons test.

4.1.2 ROR2-specific CAR-T cells confer potent anti-tumor reactivity against ccRCC in vitro

To evaluate the susceptibility of RCC to ROR2-specific CAR-T cells, we focused on ccRCC due to its significantly higher expression of ROR2 protein in primary samples (chapter 4.1.1). We generated two second-generation CAR constructs, one with lower (CAR_{wt}, XBR2-401 binding domain, K_D = 7 nM) and one with higher affinity (CAR_{enh}, X3.12 binding domain, 0.7 nM) for the same epitope of ROR2 (Figure 7 A) [62]. CAR-modified T cells were generated by lentiviral transduction of healthy donor T cells and CAR-positive T cells were obtained by tEGFR enrichment. We found stable CAR expression on the surface of T cells transduced with either construct by flow cytometry using the tEGFR marker as a surrogate (Figure 7 B) [143].

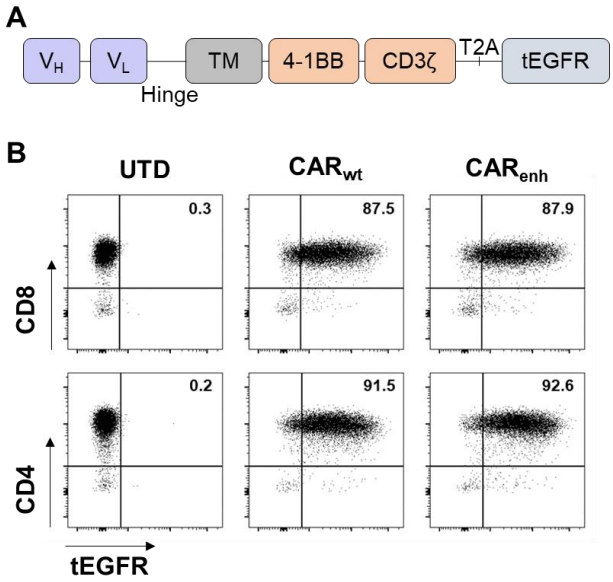

Figure 7 – ROR2-specific CARs show stable expression on the surface of healthy donor T cells.
(A) Schematic representation of ROR2-specific CAR constructs used in this study. (B) Representative, flow cytometry dot plots of CD4 or CD8 and tEGFR as a surrogate marker for CAR expression on the surface of untransduced (UTD) and CAR-transduced T cells after MACS enrichment and expansion.

To study the function of ROR2 CAR-T cells, we first analyzed antigen-dependent tumor cell lysis upon 24-hour co-cultivation of $CD8^+$ ROR2 CAR or untransduced (UTD) T cells with ccRCC cell lines in defined effector:target (E:T)-ratios (Figure 8 A). Both cell products revealed potent antigen-specific tumor cell lysis of ROR2-positive 786-O, RCC-4 and RCC-53 cells, but not ROR2-negative Caki-1 cells, in a dose (E:T-ratio)-dependent manner, with a trend towards more potent cytolysis by CAR_{enh} than CAR_{wt} T cells. A correlation between CAR-T cell

efficacy and ROR2 MFI was observed, as depicted by complete eradication of ROR2^{high} 786-O cells and ROR2^{med} RCC-4 cells within 24 hours at an E:T-ratio of 5:1, whereas only around 70 % of ROR2^{low} RCC-53 cells were lysed under the same conditions. These data suggest CAR-T cell performance to correlate with antigen quantities.

To study the cytolysis conferred by ROR2 CAR-T cells in more detail, tumor cell lysis kinetics were determined by real-time analysis using the xCELLigence platform. 786-O cells were allowed to adhere in E-Plate16, co-cultivated with CAR-transduced or UTD T cells at an E:T-ratio of 1:5, and tumor cell lysis kinetics were acquired by impendence measurement in 15-minute intervals. In line with our previous analysis, we observed potent lysis of 786-O cells by CAR_{wt} and CAR_{enh} T cells, but not UTD T cells. Comparative analysis of normalized cell index values revealed both CAR-T cell products to exhibit comparable lysis kinetics with a trend towards more rapid tumor control by CAR_{enh} than CAR_{wt} T cells (Figure 8 B). This observation was confirmed by comparison of the time to half-maximal lysis as a surrogate for CAR-T cell efficacy, which was found to be 42.6 ± 25.5 h for CAR_{wt} and 32.25 ± 12.4 h for CAR_{enh} T cells (Figure 8 C). However, this trend did not reach statistical significance.

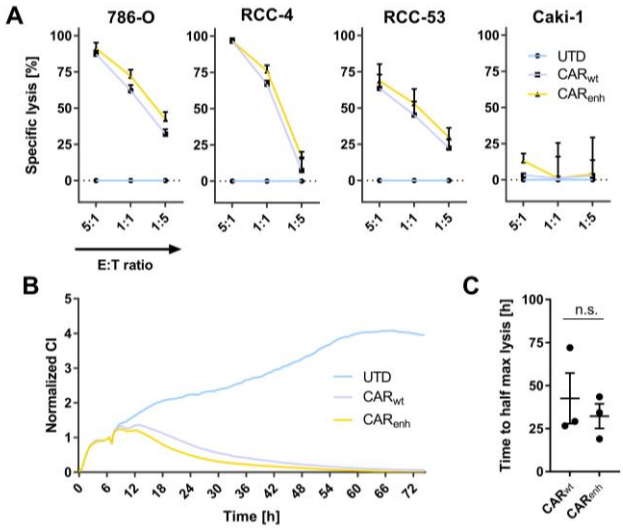

Figure 8 – ROR2-specific CAR-T cells exhibit potent antigen-specific lysis of ccRCC cell lines *in vitro*.

(A) Specific lysis of ffLuc-transduced ccRCC cell lines upon 24-hour co-cultivation with CD8$^+$ ROR2-CAR or UTD T cells at indicated E:T-ratios. Data shown is mean ± SEM for n = 3 independent donors. (B) Representative real-time cytotoxicity assay using the xCELLigence platform. Data shown is the mean normalized cell index of 786-O cells co-cultivated with ROR2-CAR or UTD T cells at an E:T-ratio of 1:5. (C) The time to half-maximal lysis was calculated from cytotoxicity kinetics obtained from impendence-based killing assay of n = 3 independent donors. Statistics are based on two-tailed paired Student's T test.

Next, we assessed the secretion of effector cytokines by ROR2-specific CAR-T cells in response to antigen-specific stimulation. $CD4^+$ and $CD8^+$ ROR2-CAR or UTD T cells were co-cultured with ccRCC cell lines for 24 hours and the concentrations of IL-2 and IFNγ in the supernatant were quantified by enzyme-linked immunosorbent assay (ELISA).

We observed high cytokine concentrations in the supernatants of $CD4^+$ and $CD8^+$ CAR-T cells in response to antigen-specific stimulation with ROR2-positive 786-O, RCC-4, and RCC-53 cells, but not ROR2-negative Caki-1 cells. In line with our lysis assessments, a correlation between ROR2 MFI as a surrogate for antigen quantity and cytokine secretion was observed. $ROR2^{high}$ 786-O cells induced the highest levels of IL-2 and IFNγ secretion, whereas release of both cytokines was markedly reduced upon stimulation with $ROR2^{med}$ RCC-4 and $ROR2^{low}$ RCC-53 cells. In line with their physiological role, $CD4^+$ T cells were found to generally secrete higher cytokine quantities than $CD8^+$ T cells expressing the same CAR (Figure 9).

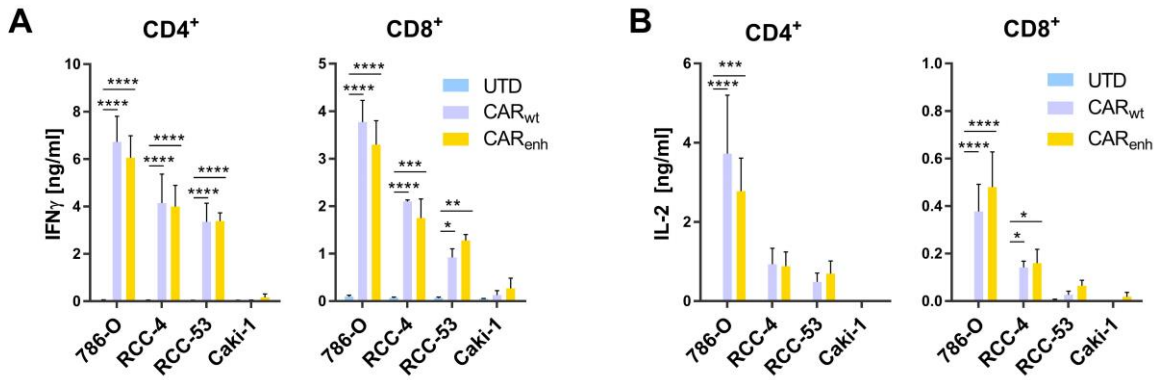

Figure 9 – ROR2-specific CAR-T cells elicit potent cytokine secretion upon stimulation with ROR2-positive ccRCC cell lines *in vitro*.

The concentration of the effector cytokines IFNγ (A) and IL-2 (B) in the supernatant of $CD4^+$ or $CD8^+$ ROR2-specific CAR or UTD T cells upon 24-hour co-cultivation with indicated ccRCC cell lines at an E:T-ratio of 4:1 was determined by ELISA. Data shown is mean ± SEM for n = 3 independent donors. Statistics are based on two-way ANOVA and Tukey's multiple comparisons test.

Next, we assessed the proliferation of ROR2-specific CAR-T cells in response to antigen-specific stimulation. $CD4^+$ and $CD8^+$ T cells were labeled independently with CFSE and mixed in a 1:1 ratio, commonly used in clinical grade CAR-T cell products [61]. Subsequently, T cells were co-cultivated with ccRCC cell lines at a total E:T-ratio of 1:1 for 72 hours (Figure 10). Flow cytometry analysis revealed potent T cell proliferation of CAR_{wt} and CAR_{enh} T cell products upon simulation with ROR2-positive ccRCC cell lines but not ROR2-negative Caki-1 cells. UTD T cells did not show T cell proliferation in response to ROR2 expression on ccRCC cell lines. The data showed a similar correlation between ROR2 MFI values as a surrogate for target quantities and T cell proliferation as our previous analyses, with $ROR2^{high}$ 786-O cells inducing a 3 to 4.5-fold expansion, as compared to a 2 to 3-fold expansion by $ROR2^{low}$ RCC-53 cells in the same time interval. Additionally, we found $CD8^+$ T cells to proliferate more efficiently than $CD4^+$ T cells in this co-culture setting, leading to an enrichment of $CD8^+$ T cells at the assay endpoint. There was a consistent trend towards more potent proliferation of CAR_{enh} than CAR_{wt} T cells in response to antigen specific stimulation, but no statistically significant difference between the two cell products was observed.

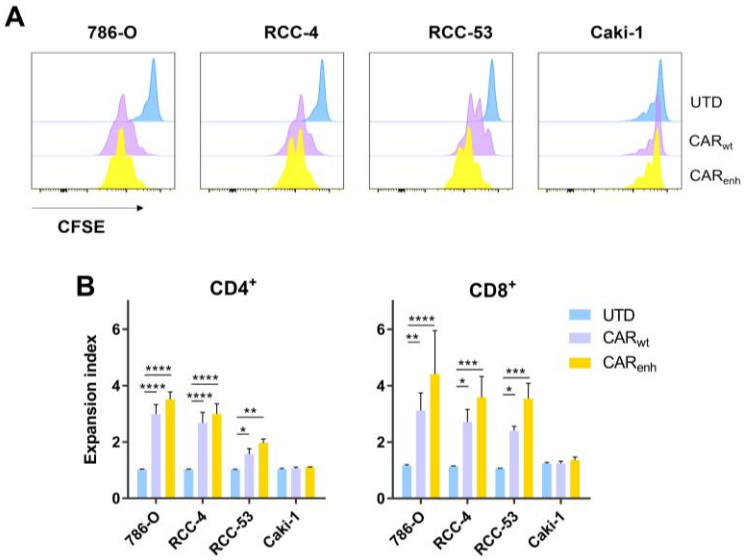

Figure 10 – ROR2-specific CAR-T cells elicit potent T cell proliferation upon stimulation with ROR2-positive ccRCC cell lines *in vitro*.

A) Representative flow cytometry histograms of $CD8^+$ T cells and (B) expansion indices of 1:1-mixtures of $CD4^+$ and $CD8^+$ ROR2-specific CAR- or UTD T cells upon co-cultivation with indicated RCC cell lines for 72 hours. Data shown in (B) is mean ± SEM for n = 3 independent donors. Statistics are based on two-way ANOVA and Tukey's multiple comparisons test.

4.1.3 ROR2-specific CAR-T cells are effective against ccRCC in a 786-O xenograft model

To assess the anti-tumor efficacy of ROR2-specific CAR-T cells *in vivo*, a murine xenograft model was employed. Immunodeficient NSG mice were inoculated with 3 × 10^6 786-O ffLuc cells by subcutaneous injection, and tumor development was monitored by bioluminescence imaging. We observed development of a solid tumor mass at the injection site within 14 days after tumor cell inoculation in all mice. On day 14, mice were randomized based on their BLI signal and treated with a single dose of 5 × 10^6 UTD, CAR_{wt}, or CAR_{enh} T cells, containing equal proportions of $CD4^+$ and $CD8^+$ T cells (Figure 11 A). Prior to injection, CAR expression was re-confirmed by flow cytometry analysis to ensure comparable CAR-T cell frequencies and expression levels between the groups. (Figure 11 B & C)

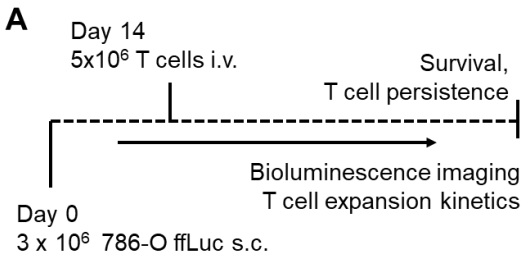

B

	UTD	CAR_{wt}	CAR_{enh}
CD4	*102*	*26.700*	*25.948*
CD8	*117*	*19.761*	*20.210*

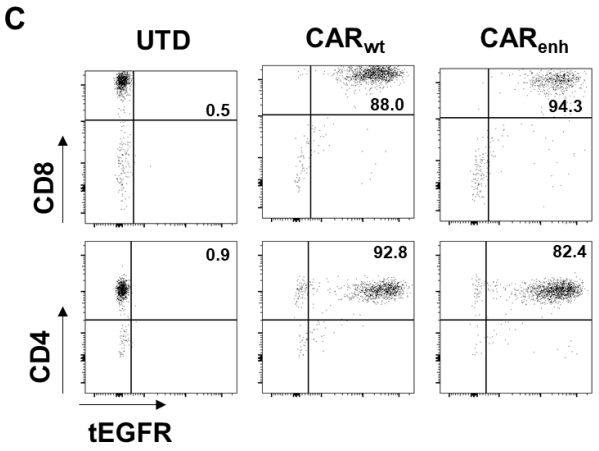

Figure 11 – Experimental design to study the anti-tumor efficacy of ROR2-specific CAR-T cells against ccRCC *in vivo*.

(A) Schematic representation of the 786-O/NSG xenograft model used to study the efficacy of ROR2 CAR-T cells against ccRCC *in vivo*. (B) Median fluorescence intensity (MFI) values of tEGFR expression as a surrogate for CAR expression levels in the final cell products used to treat mice as shown in (A). (C) Flow cytometry dot plots of CD4 or CD8 and tEGFR as a surrogate for CAR expression on the surface cells used to assemble the final T cell products. Frequencies of $CD4^+$ or $CD8^+$ CAR-positive T cells are shown.

Treatment with either of the two ROR2-specific CAR-T cell products, but not UTD T cells, induced rapid tumor regression and significantly prolonged overall survival (Figure 12 A & B). The overall response rate was 100 % (5/5 in both CAR-treated groups). Treatment with ROR2-specific CAR-T cells increased the median overall survival by 61 % to 84 days, as compared to 52 days for UTD-treated mice (Figure 12 C).

BLI analysis revealed mice treated with ROR2-specific CAR-T cells to reach their peak of response on day 7 after T cell inoculation, whereas no objective response was observed in mice treated with UTD T cells (Figure 12 A). Comparative BLI analysis between the day of T cell inoculation and the peak of response was used to delineate differences between the *in vivo* efficacy of CAR_{wt} and CAR_{enh} T cells. The data showed CAR_{enh} T cells to elicit superior anti-tumor functionality and to induce significantly deeper remission than CAR_{wt} T cells (Figure 12 D). However, local tumor relapse was observed in all CAR-treated mice.

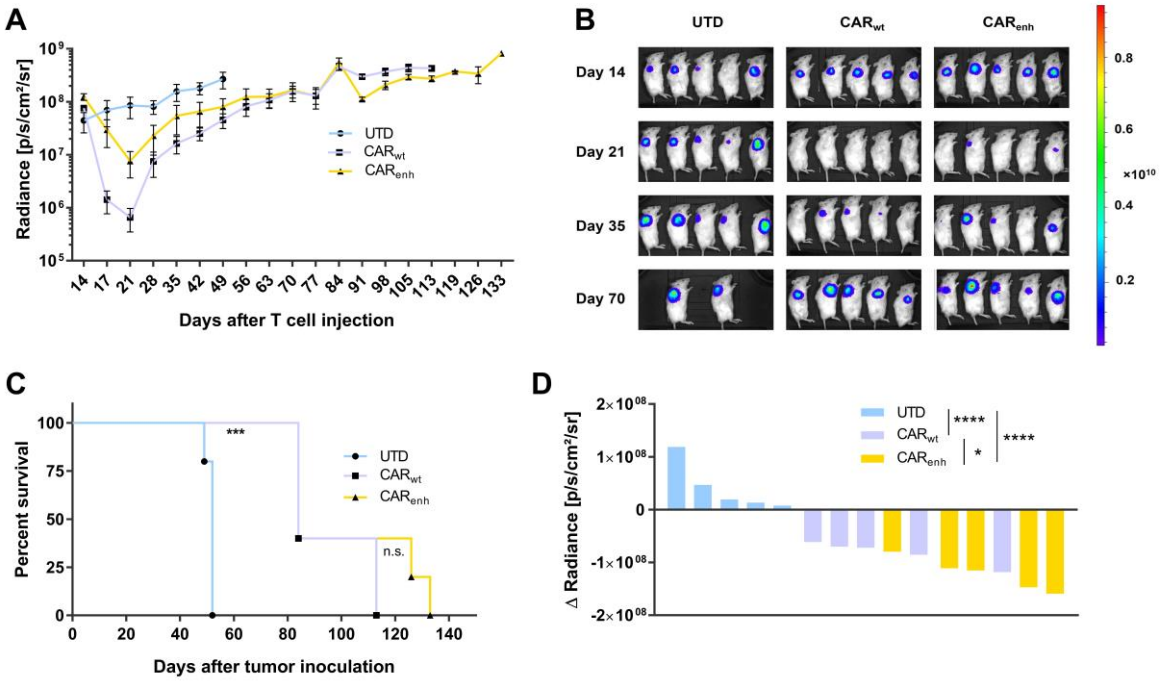

Figure 12 – ROR2-specific CAR-T cells exhibit potent anti-tumor efficacy against ccRCC *in vivo*.
(A) BLI curve and (B) representative bioluminescence images of mice treated as shown in Figure 11 A. (C) Kaplan-Meyer curve (percent survival) of mice treated as described in Figure 11 A. Statistics are based on Mantel-Cox log-rank test. (D) Depth of remission as determined by the difference in radiance between day 21 and day 14 after tumor inoculation. Statistics are based on two-way ANOVA and Tukey's multiple comparisons test.

To study the efficacy of ROR2-specific CAR-T cells *in vivo* in more detail, blood samples were analyzed by flow cytometry to monitor T cell expansion and contraction kinetics. We found CAR-T cells to be most frequent during the peak of response on day 7 after T cell inoculation. During this peak of expansion, significantly higher frequencies of CAR_{enh} T cells than CAR_{wt} or

UTD T cells were found in circulation, coinciding with deeper remission and more potent anti-tumor efficacy of mice treated with CAR_{enh} T cells. CAR_{enh} T cells remained detectable in 2 out of 5 mice until day 21 after T cell inoculation, whereas CAR_{wt} and UTD T cells approached detection limits (Figure 13 A). Next, long-term CAR-T cell persistence was studied by flow cytometry analysis of spleen, bone marrow, and residual tumor at the individual experimental endpoint of each animal. Despite different analysis timepoints, T cells were found in at least one of these tissues in every animal, indicating T cell engraftment and persistence. We observed no difference in the frequency of long-term persisting T cells in mice treated with CAR_{wt}, CAR_{enh}, and UTD T cells in any of the tissues. Importantly, considerable T cell quantities, representing between 1 % and 10 % of all living cells, were detectable within residual tumor (Figure 13 B).

To explore the reasons for local tumor relapse despite T cell persistence, we assessed the ROR2 status of the tumor, as well as T cell differentiation and exhaustion. Flow cytometry analysis revealed no significant differences in cell surface ROR2 protein expression between tumor samples obtained from mice treated with ROR2-specific CAR-T cells or UTD T cells (Figure 13 C). Phenotype analysis showed CAR_{enh} T cells to be differentiated towards the T effector cell subset (T_{Eff}), whereas CAR_{wt} and UTD T cells showed higher frequencies of memory phenotypes, such as effector memory (T_{EM}) and central memory (T_{CM}) T cells (Figure 13 D). To assess T cell inhibition, expression of the exhaustion markers PD-1, TIM3, and LAG3 was analyzed by flow cytometry. We found neither CAR_{wt} nor CAR_{enh} T cells to display a phenotype typically associated with exhausted T cells, as defined by PD-1, TIM3, LAG3 triple-positivity (Figure 13 E). However, exhaustion marker single- and double-positive subpopulations were detectable in tumors obtained from mice treated with CAR_{wt} or CAR_{enh} T cells.

In summary, these data suggest that antigen loss is not the reason for tumor relapse, as shown by comparable ROR2 MFI values, as well as the persistence of non-exhausted T_{Eff} and T_{EM} cells within the tumor microenvironment. Furthermore, the presence of increased T_{Eff} frequencies in CAR_{enh}-treated as compared to CAR_{wt}-treated mice at the individual experimental endpoints indicates a prolonged anti-tumor efficacy.

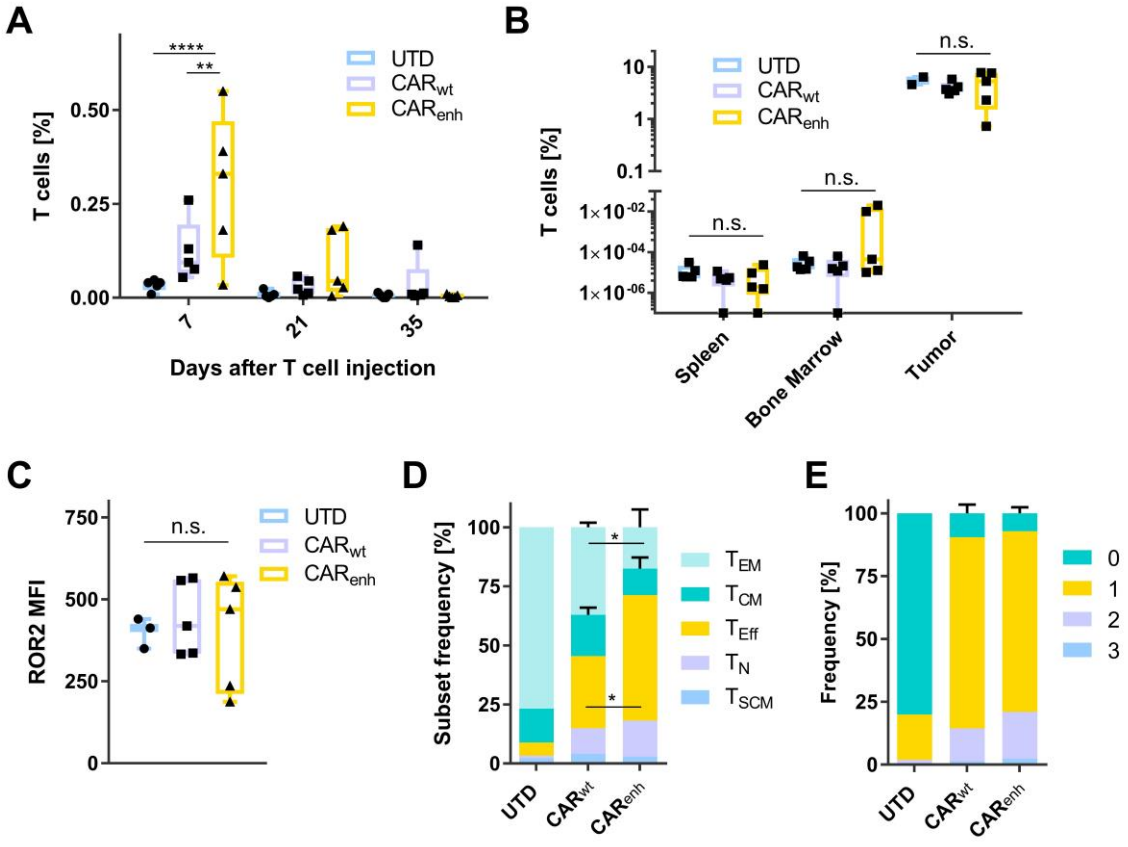

Figure 13 – CAR_{enh} T cells exhibit potent expansion, and persistent anti-tumor efficacy *in vivo*.

(A) Frequency of human T cells as a fraction of living, single-cell lymphocytes in blood samples obtained from mice treated as shown in Figure 11 A on indicated days after T cell injection. (B) Frequency of living, single-cell human T cells in spleen, bone marrow and tumor at the experimental endpoint of each respective animal. (C) ROR2 median fluorescence intensity of living single tumor cells isolated from the primary injection site at the experimental endpoints of mice treated as indicated in Figure 11 A. (D) T cell subset frequencies as a fraction of live, single human T cells obtained from the tumor microenvironment. (T_{EM}: Effector memory T cells, T_{CM}: Central memory T cells, T_{Eff}: Effector T cells, T_N: Naïve T cells, T_{SCM}: Stem cell memory T cells.) (D) Frequency of live, single human T cells obtained from the tumor microenvironment at the respective experimental endpoint of each animal expressing the indicated number of exhaustion markers PD-1, LAG3, and TIM3. Statistics are based on two-way ANOVA with Tukey's multiple comparison test.

4.1.4 Interim conclusion

Here, we studied the expression of ROR2 in primary samples and cell lines of RCC. Employing a transcriptomic and protein-based analyses, we show that ROR2 is commonly and uniformly expressed on the surface of RCC cells.

ROR2-specific CAR-T cells with different binding affinities for the same epitope of ROR2 were generated and their functionality was assessed *in vitro* and *in vivo*. *In vitro* analyses revealed CAR_{wt} and CAR_{enh} T cells to elicit potent antigen-specific functionalities including tumor cell lysis, cytokine secretion and T cell proliferation, against the ROR2-positive ccRCC tumor cell lines 786-O, RCC-4, and RCC-53 but not against ROR2-negative Caki-1 cells. Additionally, we observed a correlation between ROR2 MFI values as a surrogate for antigen quantities and CAR-T cell efficacy. Furthermore, the data showed a trend towards more potent *in vitro* efficacy by CAR_{enh} than CAR_{wt} T cells, including increased antigen-specific tumor cell lysis, secretion of higher cytokine concentrations in response to $ROR2^{low}$ RCC-53 cells, and superior T cell proliferation.

Finally, the *in vivo* efficacy of ROR2-specific CAR-T cells was studied using a subcutaneous 786-O/NSG xenograft model. We observed rapid tumor regression and significantly increased overall survival of mice treated with ROR2-specific CAR-T cells as compared to UTD T cells. Furthermore, a trend towards more prolonged survival was observed for mice treated with CAR_{enh} , as compared to CAR_{wt} T cells. CAR_{enh} T cells were found to induce significantly deeper remission, accompanied by higher expansion and prolonged T cell persistence *in vivo* than CAR_{wt} or UTD T cells. Finally, CAR_{enh} T cells were found to exhibit a long-term T_{Eff} phenotype indicative of an ongoing anti-tumor response until the experimental endpoints.

In summary, these data show that ROR2 is commonly expressed on RCC cells and can be targeted with ROR2-specific CAR-T cells *in vitro* and *in vivo*.

4.2 Efficacy of CAR_{enh} T cells against multiple myeloma

4.2.1 CAR_{enh} T cells confer potent anti-myeloma efficacy in vitro

To evaluate the reactivity of ROR2-specific CAR-T cells against MM, we selected the cell lines U-266 and OPM-2 and evaluated their ROR2 expression on the transcriptome and protein levels. Using qPCR we found U-266 to be ROR2-positive, whereas OPM-2 cells showed no ROR2 expression (Figure 14 A). Subsequent flow cytometry analysis revealed U-266 cells to express uniformly high levels of ROR2 protein on the cell surface, while OPM-2 cells were confirmed to be ROR2-negative (Figure 14 B).

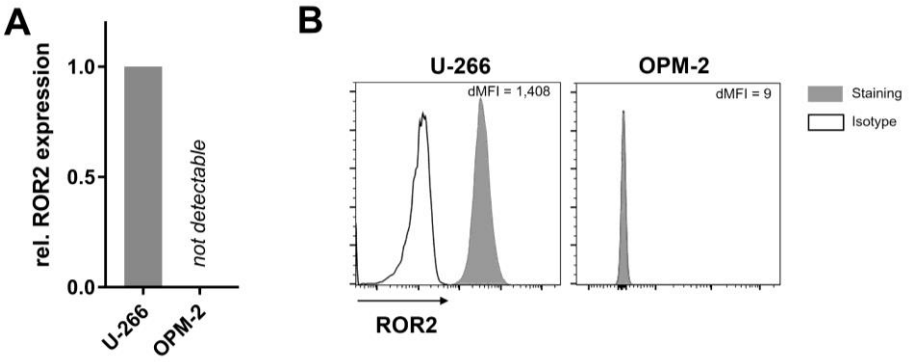

Figure 14 – ROR2 is uniformly expressed on the surface of U-266 cells.
(A) ROR2 gene expression analysis of MM cell lines U-266 and OPM-2, as determined by qPCR. Data shown was determined using the $2^{-\Delta\Delta Ct}$ method with GAPDH as the housekeeping gene. Data was normalized to U-266 cells and is a representative of n = 3 independent analyses. (B) Representative flow cytometry histograms of ROR2 expression on U-266 and OPM-2 cells. The difference between median fluorescence intensities of stained (gray) and FMO (clear) samples is shown as dMFI.

Next, we were interested in assessing the anti-tumor efficacy of ROR2-specific CAR-T cells against MM cells *in vitro*. Due to its superior *in* vivo performance (chapter 4.1), we focused on CAR_{enh} T cells for these analyses. First, we studied antigen-dependent lysis of MM cell lines upon co-cultivation with CAR_{enh} or UTD T cells. We found CAR_{enh} T cells to exhibit high-level specific lysis of U-266 cells in a dose-dependent manner within 24 hours, whereas no lysis of ROR2-negative OPM-2 cells was observed (Figure 15 A).

In light of these data, we also sought to assess the recognition of primary MM cells by CAR_{enh} T cells. To this end, flow cytometry-based analyses were employed to study antigen-dependent cytolysis of patient-derived MM cells upon co-cultivation with allogeneic $CD8^+$ CAR_{enh} or UTD T cells (n = 15 independent MM samples, Table 30). We observed potent antigen-specific tumor cell lysis in 93 % (14/15) of patient-derived tumor samples with a median specific lysis of 91.94 % within 16 hours at an E:T-ratio of 10:1. Partial responses (≤ 75 % specific lysis) were observed in 27 % (4/15) of samples (Figure 15 B & C).

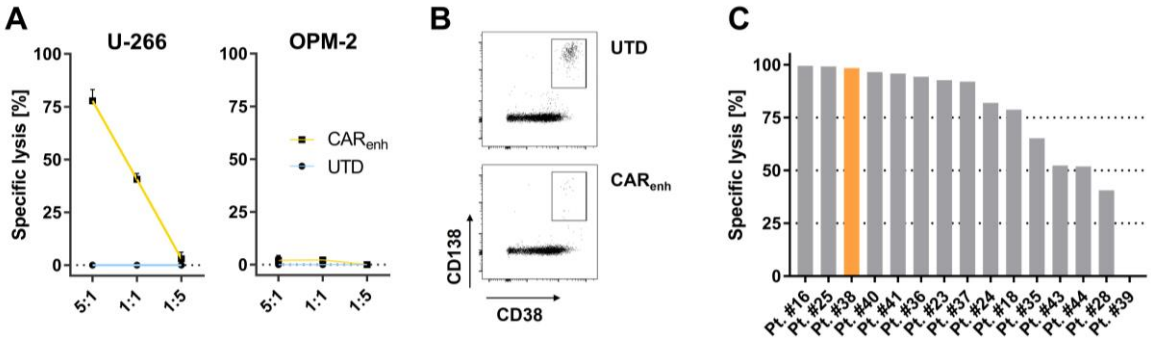

Figure 15 – CAR_{enh} T cells exhibit antigen-specific lysis of ROR2-positive MM cell lines and patient-derived MM samples *in vitro*.

(A) Specific tumor cell lysis of indicated ffLuc-transduced MM cell lines upon 24-hour co-cultivation with $CD8^+$ CAR_{enh} or UTD T cells at indicated E:T-ratios. Data shown is mean ± SEM for n = 3 independent donors. (B) Representative flow cytometry dot plot of cytotoxicity analyses using patient-derived MM cells and allogeneic $CD8^+$ CAR_{enh} or UTD T cells. Data shown is a representative of data obtained from n = 15 independent patient-derived samples. (C) Specific lysis of patient-derived $CD138^+/CD38^+$ MM cells upon co-cultivation with allogeneic $CD8^+$ or CAR_{enh} or UTD T cells at an E:T-ratio of 10:1 for 16 hours (n = 15). The donor shown in panel (B) is highlighted in orange.

Table 30 – MM patient characteristics (cytolysis analysis).

Characteristic	all patients (n = 15)
Median age (range) – years	68 (40-78)
Male – no. (%)	8 (53 %)
Tumor stage at diagnosis – no. (%)	
IA	3 (20 %)
IIIA	9 (60 %)
IIIB	3 (20 %)
Myeloma subtype – no. (%)	
IgG	7 (47 %)
IgA	5 (33 %)
Light chain	3 (20 %)
Cytogenetic profile – no. (%)	
High-risk	6 (40 %)
Standard risk	9 (60 %)
Remission state – no. (%)	
Newly diagnosed	3 (20 %)
Stable disease	1 (7 %)
Refractory	1 (7 %)
Progressive disease	10 (67 %)
Previous therapy regimens	
Median no. (range)	2.5 (0-8)

Next, we were interested in studying the secretion of effector cytokines by CAR_{enh} T cells in response to antigen-specific stimulation with MM cells. $CD4^+$ and $CD8^+$ CAR_{enh} or UTD T cells were individually co-cultivated with U-266 or OPM-2 cells at an E:T-ratio of 4:1 for 24 hours and the concentration of IL-2 and IFNγ in the co-culture supernatants were quantified by ELISA. We observed potent cytokine secretion by both $CD4^+$ and $CD8^+$ CAR_{enh} T cells but not UTD T cells upon stimulation with ROR2-positive U-266 cells. OPM-2 cells did not induce cytokine secretion by CAR_{enh} or UTD T cells. $CD4^+$ CAR_{enh} T cells were found to secrete higher quantities of both cytokines than corresponding $CD8^+$ T cells upon stimulation with U-266 cells, yielding IFNγ concentrations up to 1,700 pg/ml and IL-2 levels up to 900 pg/ml within 24 hours (Figure 16). In contrast, $CD8^+$ CAR_{enh} T cells showed significantly lower secretion of either cytokine in response to stimulation with U-266 cells.

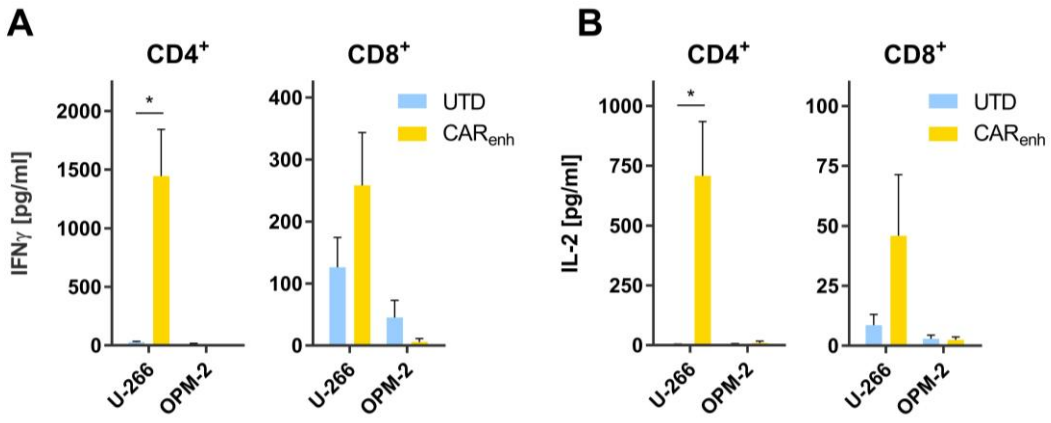

Figure 16 – CAR_{enh} T cells elicit potent cytokine secretion upon stimulation with ROR2-positive MM cell lines *in vitro*.

$CD4^+$ and $CD8^+$ CAR_{enh} or UTD T cells were individually co-cultivated with indicated MM cell lines at an E:T-ratio of 4:1 for 24 hours. Secretion of the effector cytokines IFNγ (A) or IL-2 (B) in co-culture supernatants was determined by ELISA. Data shown is mean ± SEM for n = 3 independent donors. Statistics are based on two-way ANOVA and Tukey's multiple comparison test.

Finally, we were interested in assessing proliferation of CAR_{enh} T cells in response to antigen-specific stimulation with MM cells. $CD4^+$ and $CD8^+$ CAR_{enh} and UTD T cells were labeled individually with CFSE, mixed in a 1:1 ratio, and co-cultivated with U-266 or OPM-2 cells at a total E:T-ratio of 1:1 for 72 hours (Figure 17). We found CAR_{enh} T cells to exhibit potent T cell proliferation upon stimulation with ROR2-positive U-266, but not ROR2-negative OPM-2 cells. UTD T cells showed no significant proliferation in response to either cell line. Additionally, $CD4^+$ and $CD8^+$ CAR_{enh} T cells were found to proliferate to a similar extent, as shown by mean expansion indices of 2.28 for $CD4^+$ and 2.19 for $CD8^+$ CAR_{enh} T cells.

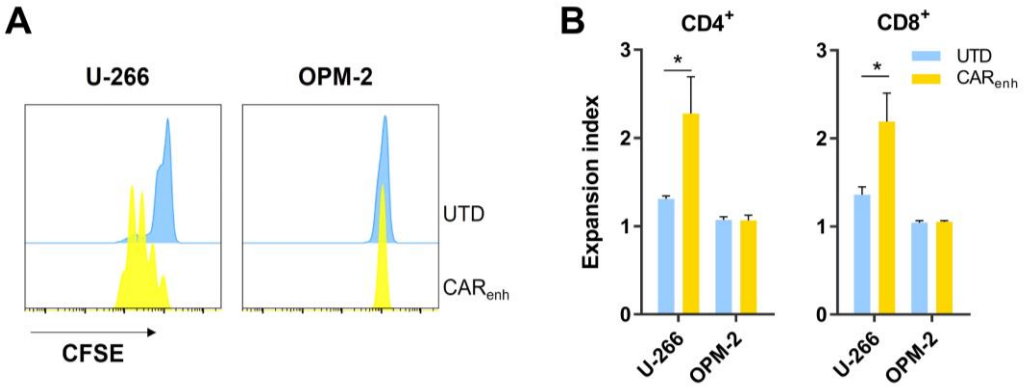

Figure 17 – CAR_{enh} T cells elicit potent T cell proliferation upon stimulation with ROR2-positive U-266 cells.
(A) Representative flow cytometry histograms of CFSE dye dilution by T cell proliferation upon 72-hour co-cultivation of CAR_{enh} or UTD T cells (equal proportions of $CD4^+$ and $CD8^+$ T cells) with indicated tumor cells. Data shown was gated on $CD8^+$ T cells and is a representative of data obtained from n = 3 independent donors. (B) Expansion indices of $CD4^+$ and $CD8^+$ CAR_{enh} or UTD T cells upon 72-hour simulation with indicated tumor cells. Data shown is mean ± SEM for n = 3 independent donors. Statistics are based on two-way ANOVA and Tukey's multiple comparison test.

4.2.2 CAR_{enh} T cells eradicate MM in a subset of mice using a U-266/NSG xenograft model

To assess the anti-tumor efficacy of CAR_{enh} T cells against MM *in vivo*, a U-266/NSG xenograft model was employed (Figure 18). To this end, NSG mice were inoculated with 1×10^7 U-266 ffLuc cells by intravenous (tail vein) injection and tumor engraftment was monitored by bioluminescence imaging.

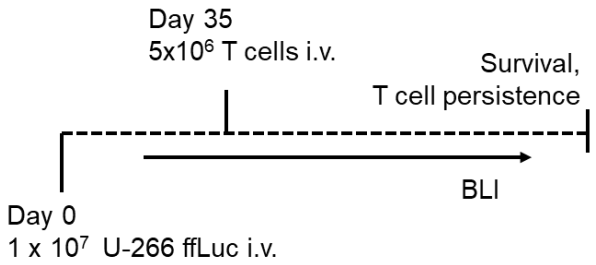

Figure 18 – Experimental design to study the anti-tumor efficacy of CAR_{enh} T cells against MM *in vivo.*
NSG mice were intravenously inoculated with 1 × 10^7 U-266 ffLuc cells, and tumor burden was monitored by weekly bioluminescence imaging. Mice were randomized on day 35 and treated with a single dose of CAR_{enh} or UTD T cells containing equal proportions of $CD4^+$ and $CD8^+$ T cells.

MM engraftment was achieved in 80 % (24/30) of mice within 35 days. BLI analysis revealed U-266 engraftment to recapitulate clinical manifestations of human MM with preferential engraftment in the bone marrow, as well as extramedullary disease comprising involvement of the lung, lymph nodes and central nervous system (Figure 19 A). To accommodate for engraftment variability, mice were matched based on their BLI signal and disease distribution on day 35, randomized into two groups, and treated with a single dose of 5 × 10^6 (CD4:CD8 ratio = 1:1) CAR_{enh} or UTD T cells. CAR expression analysis of the final cell product was performed prior to T cell inoculation, and we found both $CD4^+$ and $CD8^+$ CAR_{enh} T cells to be above 95% CAR-positive (Figure 19 B). Treatment with CAR_{enh} T cells but not UTD T cells induced rapid tumor control and significantly improved overall survival (Figure 19 C & D). BLI analysis revealed the peak of response to be reached on day 7 after T cell inoculation. Simultaneously, we observed an overall objective response in 83 % (10/12) of CAR_{enh}-treated mice, as indicated by a significantly reduced tumor burden in CAR_{enh}- as compared to UTD-treated mice (Figure 19 E).

Furthermore, complete responses were observed in 25 % (3/12) of mice treated with CAR_{enh} T cells. Interestingly, all mice exhibiting complete responses were found to suffer from temporary tumor relapses between day 30 and day 90 after CAR_{enh} T cell inoculation. The BLI data shows a wave-like pattern in this period, indicating two sequential tumor relapses which were rapidly being control. All three mice achieved complete response around day 120 after CAR_{enh} T cell inoculation and remained in remission until the end of the experiment on day 286.

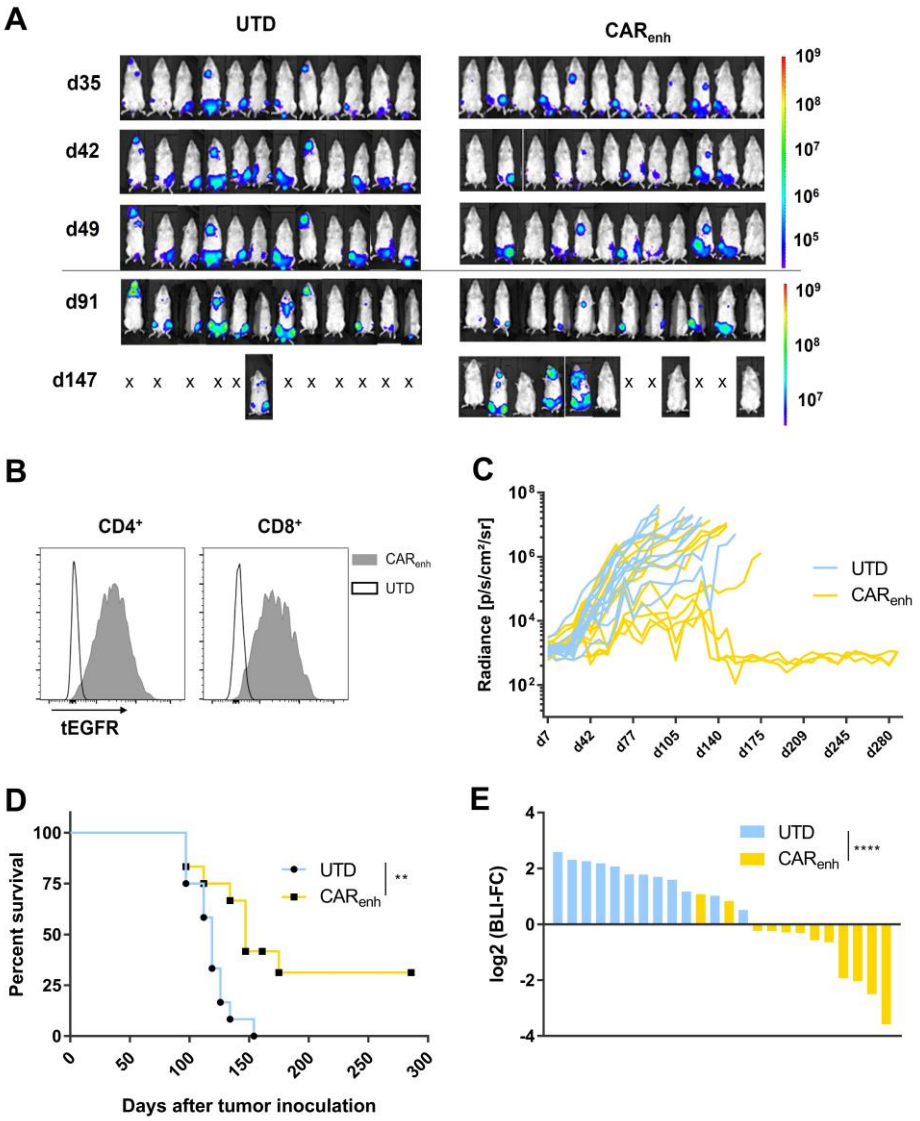

Figure 19 – CAR$_{enh}$ T cells exhibit potent anti-tumor efficacy in a U-266/NSG xenograft model.

(A) BLI images obtained at indicated timepoints after tumor inoculation of mice treated as described in Figure 18. (B) Flow cytometry histograms of tEGFR expression on the surface of CAR$_{enh}$ (gray) and UTD T cells (blank) as a surrogate for CAR expression in the final T cell product. (C) Average radiance over time for mice treated as described in Figure 18. (D) Kaplan-Meyer curve (overall survival) of mice treated as described in Figure 18. Statistics were calculated using the Mantel-Cox log-rank test. (E) Objective treatment response on day 7 after T cell inoculation, as determined by BLI. Data shown is the log2 of the BLI fold change between day 42 and day 35. Statistics are based on two-tailed unpaired Student's T-Test.

To assess T cell performance, blood samples were obtained at the peak of response on day 7 and analyzed by flow cytometry. T cells were detectable in samples obtained both CAR_{enh} and UTD-treated mice and represented between 0.01 % and 0.05 % of all lymphocytes in circulation. Significantly lower frequencies of CAR_{enh} than UTD T cells were detectable in circulation on day 7, despite the absence of an objective response in UTD-treated mice (Figure 20 A).

Finally, we were interested in assessing T cell persistence in mice treated with CAR_{enh} or UTD T cells at their respective experimental endpoints. Human T cells were detectable in the bone marrow of all mice, revealing T cell engraftment and persistence. However, T cells were less consistently found in the blood and spleen at the experimental endpoints, independent of the treatment group (Figure 20 B). No significant difference in T cell persistence was observed between mice treated with CAR_{enh} or UTD T cells. Additionally, we found no difference in long-term T cell persistence between mice with partial and complete responses upon treatment with CAR_{enh} T cells.

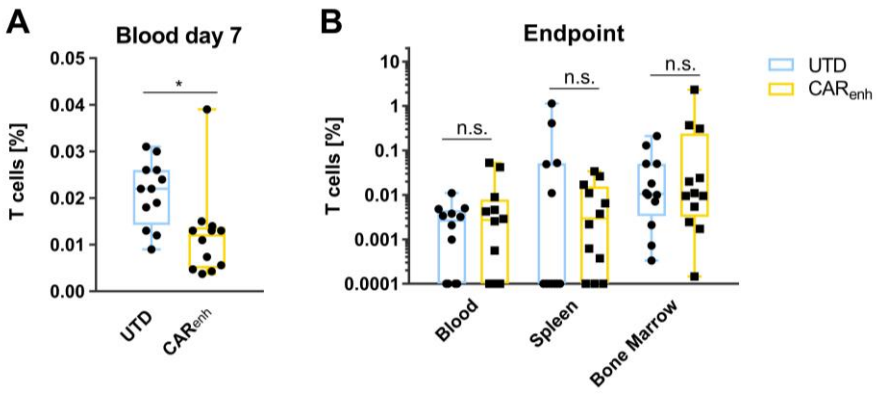

Figure 20 – CAR_{enh} T cells exhibit long-term persistence in a U-266/NSG xenograft model.

(A) Frequency of living human T cells in circulation on day 7 after T cell inoculation, as a fraction of total living lymphocytes. (B) Frequency of living human T cells in indicated tissues at the respective experimental endpoint of each animal, as a fraction of total living lymphocytes. Statistics are based on two-way ANOVA and Tukey's multiple comparison test.

4.2.3 Interim conclusion

Here, we studied the anti-tumor functionality of ROR2-specific CAR_{enh} T cells for the treatment of MM.

We confirmed the expression of ROR2 in two representative MM cell lines, U-266 and OPM-2, by qPCR and flow cytometry. The data show that U-266 cells uniformly express ROR2, whereas OPM-2 were found to be ROR2-negative. *In vitro* analyses revealed CAR_{enh} T cells to elicit potent antigen-specific lysis of U-266, but not OPM-2 cells. These findings could be replicated in patient-derived MM cells and were independent of tumor stage and remission status. We also showed that ROR2-specific CAR_{enh} T cells exhibit potent cytokine secretion and T cell proliferation in response to antigen-specific stimulation with ROR2-positive U-266 cells, but not OPM-2 cells.

Finally, the *in vivo* efficacy of CAR_{enh} T cells was studied using a U-266/NSG xenograft model. We found intravenous U-266 inoculation to establish clinically relevant manifestations of MM, as characterized by bone marrow infiltration and extramedullary disease, within 35 days of tumor inoculation. CAR_{enh} T cell treatment induced rapid tumor control, and significantly increased overall survival. We observed an objective overall response rate of 83 % and complete remission was achieved in 25 % (3/12) of CAR_{enh}-treated mice.

Taken together, these data show that ROR2 is commonly expressed on the surface of MM cells and can be targeted with ROR2-specific CAR_{enh} T cells *in vitro* and *in vivo*.

4.3 Preclinical safety assessment of ROR2-specific CAR-T cells

4.3.1 ROR2 expression is conserved in M. musculus

First, the expression of ROR2 in healthy adult tissues was determined, to rule out widespread high-level expression of ROR2, to identify candidate organs for on-target off-tumor toxicities upon treatment with ROR2-specific CAR-T cells, and to assess whether mice represent a suitable toxicology model. Gene expression analysis was performed by qPCR using commercially available human and murine pooled tissue panels (Figure 21). All samples yielded C_t values between 16 and 19 for the GAPDH housekeeping gene. In *H. sapiens*, ROR2 gene expression was detectable in the male and female reproductive system, as well as in the intestine and colon. In contrast, brain, heart, liver, kidney, skeletal muscle, and leukocytes were found to be ROR2 negative, using a C_t threshold of 35 cycles. For *M. musculus*, ROR2 gene expression was similarly detectable in tissues derived from the male or female reproductive system, as well as parts of the gastrointestinal tract. Additionally, low-level mROR2 expression was observed in the spleen, lung, and liver. No ROR2 transcripts were found in skeletal muscle, as determined by C_t thresholding (35 cycles). Overall, these data show that ROR2 transcripts are detectable in similar tissues of *H. sapiens* and *M. musculus*, where they share comparable gene expression relative to GAPDH.

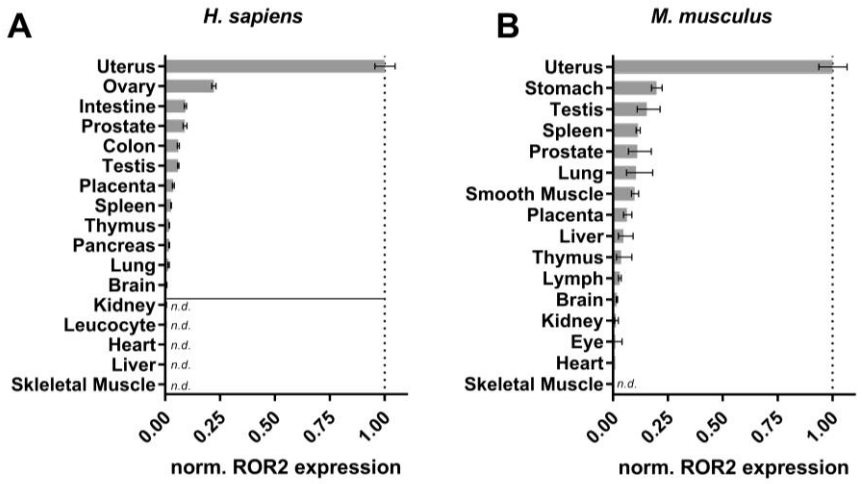

Figure 21 – ROR2 gene expression is detectable in selected healthy adult human and murine tissues.
qPCR analysis of ROR2 expression in indicated human (A) and murine (B) tissues. Data shown represents mean expression fold-changes with upper and lower limits for n = 3 independent experiments, as determined using the $2^{-\Delta\Delta Ct}$ method, with GAPDH as the housekeeping gene and data obtained for the highest expressing tissue (human or murine uterus, respectively) as the reference sample (n.d.: not detectable).

Next, the expression of ROR2 protein was assessed by Western blot analysis of healthy tissues of *H. sapiens* and *M. musculus*. For the analysis of human ROR2, we focused those tissues with the highest relative ROR2 gene expression (Figure 21) and a selection of negative controls using commercially available pooled tissue lysates. We detected low-level ROR2 protein expression in the uterus, ovaries, placenta, and testis, but not in mamma, cecum, intestine, and skin (Figure 22 A). For the assessment of murine ROR2, we generated tissue-specific whole cell lysates from cryopreserved NSG mouse organs. Western blot analysis revealed ROR2 protein expression to be detectable in the uterus and ovaries. No specific band was observed in tissues obtained from the gastrointestinal tract, despite low-level ROR2 gene expression, as determined by qPCR analysis. Furthermore, unspecific bands (approx. 150 kDa) were detected in lysates obtained from liver and kidney, which did not match the molecular size of ROR2 (Figure 22 B).

These data recapitulate our previous findings on the transcriptome level and show ROR2 protein to be detectable in tissues obtained from the reproductive system of *H. sapiens* and *M. musculus*.

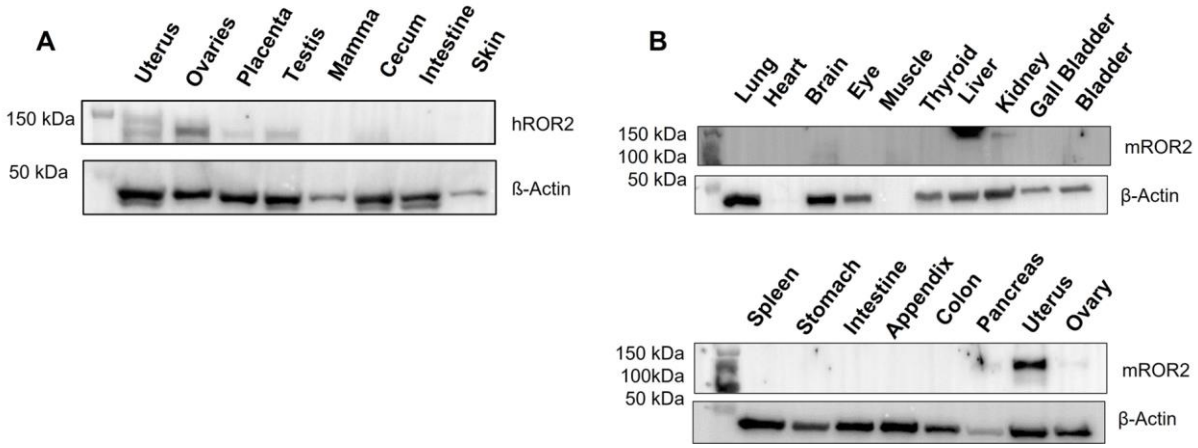

Figure 22 – ROR2 protein expression is detectable in selected healthy adult human and murine tissues.
ROR2 protein expression was analyzed using Western blotting of indicated human (A) and murine (B) tissues. β-actin was utilized as a loading control.

4.3.2 hROR2-specific CAR_{enh} T cells cross-react with murine ROR2 in vitro

Next, we were interested in determining whether hROR2-specific CAR_{enh} T cells show cross-reactivity for murine ROR2. We generated MDA-MB-231 variants (wildtype: ROR2-negative) ectopically expressing human or murine ROR2 by lentiviral transduction and confirmed expression by flow cytometry (Figure 23 A). Subsequently, antigen-specific tumor cell lysis of the MDA-MB-231 variants by CAR_{enh} T cells was assessed. We found CAR_{enh} T cells to elicit similarly potent antigen-specific lysis of MDA-MB-231 cell expressing human or murine ROR2, but not wildtype MDA-MB-231 cells (Figure 23 B). These data suggest that CAR_{enh} T cells show cross-reactivity against murine ROR2.

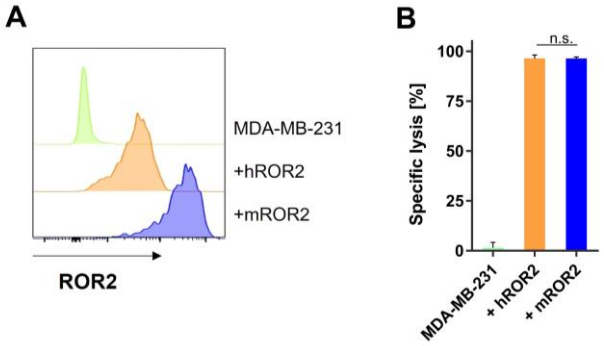

Figure 23 – hROR2-specific CAR_{enh} T cells exhibit antigen-specific lysis of cells expressing human or murine ROR2 *in vitro*.

(A) Flow cytometry histograms of MDA-MB-231 wildtype cells (ROR2 negative) and MDA-MB-231 cells overexpressing human (+hROR2) or murine ROR2 (+mROR2). (B) Specific tumor cell lysis of indicated MDA-MB-231 variants upon 24-hour co-cultivation with CAR_{enh} or UTD T cells at an E:T-ratio of 5:1. Data shown is mean ± SEM for n = 3 independent donors. Statistics are based on two-way ANOVA and Tukey's multiple comparison test.

Next, we were interested in assessing differences in cytokine secretion and T cell proliferation in response to stimulation with cells expressing human or murine ROR2. We observed potent secretion of the effector cytokines IL-2 and IFNγ by both $CD4^+$ and $CD8^+$ CAR_{enh} T cells upon 24-hour co-cultivation with MDA-MB-231 cells expressing human or murine ROR2, but not wildtype MDA-MB-231 cells (Figure 24 A). Additionally, we found cytokine secretion levels to be comparable between samples stimulated with cells expressing human or murine ROR2. T cell proliferation analysis revealed similarly potent antigen-dependent T cell expansion upon 72-hour stimulation of CAR_{enh} T cells with

MDA-MB-231 cells expressing hROR2 or mROR2, but not wildtype MDA-MB-231 cells. This effect was similarly pronounced in $CD4^+$ and $CD8^+$ CAR_{enh} T cells (Figure 24 B & C). These data show that CAR_{enh} T cells recognize cells expressing human or murine ROR2 and induce similarly potent T cell functionalities.

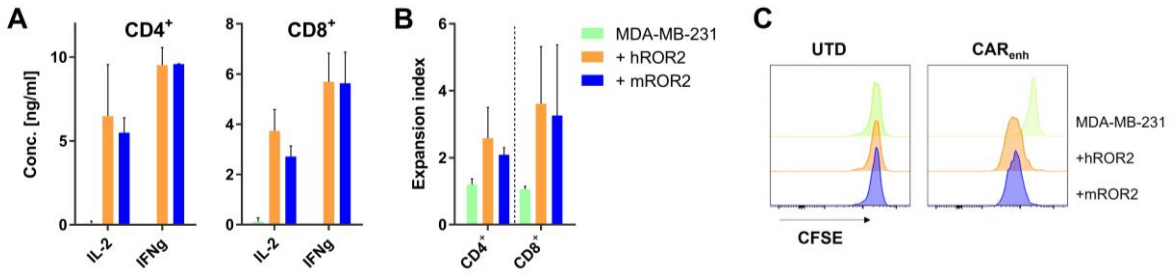

Figure 24 – hROR2-specific CAR_{enh} T cells elicit cytokine secretion and proliferation in response to stimulation with cells expressing hROR2 or mROR2 *in vitro*.

(A) Secretion of the effector cytokines IL-2 or IFNγ in the supernatant of CAR_{enh} or UTD T cells co-cultivated with indicated MDA-MB-231 variants for 24-hours at an E:T-ratio of 4:1, as determined by ELISA. (B) Expansion indices of $CD4^+$ and $CD8^+$ CAR_{enh} T cells upon co-cultivation with indicated MDA-MB-231 variants for 72 hours at an E:T ratio of 4:1. (C) Representative flow cytometry histograms for CAR_{enh} or UTD T cells co-cultivated with MDA-MB-231 wildtype, hROR2 or mROR2 cells for 72-hours at an E:T-ratio of 4:1. Data shown in (A) and (B) is mean ± SD for n ≥ 2 independent donors.

4.3.3 ROR2-specific CAR-T cells do not induce clinical toxicity in mice

We have shown that ROR2 shows a comparable expression pattern in *H. sapiens* and *M. musculus* and revealed that CAR_{enh} T cells elicit potent antigen-specific functionalities upon recognition of human or murine ROR2 *in vitro*. Therefore, we reasoned that *M. musculus* represents a relevant toxicology model to obtain informative data about on-target off-tumor effects elicited by ROR2-specific CAR-T cells. To assess the preclinical safety of ROR2-specific CAR-T cells, tumor-free NSG mice were inoculated with 1×10^7 CAR_{enh} or UTD T cells by intravenous injection (Figure 25 A). Animal well-being and body weight were monitored to assess clinical toxicities. We observed no significant differences in weight and health score development between the two groups, and no mice succumbed to the treatment (Figure 25 B & C). These observations suggest the absence of severe side-effects induced by CAR_{enh} T cell therapy, in this toxicology model.

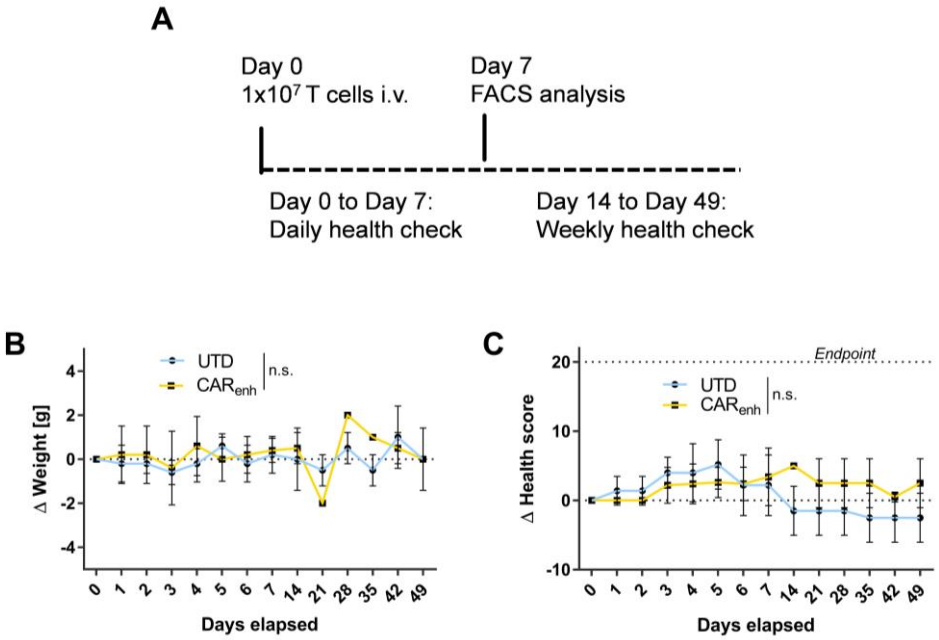

Figure 25 – CAR_{enh} T cells do not show clinical signs of toxicity *in vivo*.
(A) Schematic representation of the murine toxicology model employed to study on-target off-tumor toxicities induced by CAR_{enh} T cells *in vivo*. (B) Weight and (C) health score development relative to the day before T cell inoculation (Day 0) over time of mice treated as shown in (A). Statistics are based on two-way ANOVA and Tukey's multiple comparison test.

Additionally, T cell enrichment and activation were assessed by flow cytometry analysis of tissues-specific single-cell suspensions obtained at the peak of expansion. We found both CAR_{enh} and UTD T cells to be detectable in tissues with high blood circulation, such as lung, heart, and liver on day 7. There was a trend towards increased frequencies of CAR_{enh} T cells as compared to UTD T cells in the liver and lung, and significant enrichment was detectable in the spleen. No enrichment of CAR_{enh} T cells was found in tissues previously determined to be ROR2-positive, such as uterus, ovaries or any tissue obtained from the gastrointestinal tract (Figure 26 A). Next, we were interested in assessing whether there was evidence for T cell activation in distinct murine tissues using flow cytometry analysis of CD69 and PD-1 as surrogates (Figure 26 B & C). We observed a trend towards overall higher expression of CD69 in CAR_{enh} than UTD T cells across tissues and found significant expression differences in kidney, liver, and spleen. A similar trend was observed for PD-1 expression on the surface of CAR_{enh} T cells, which was most pronounced on cells obtained from liver, lung, and spleen. However, no statistically significant upregulation was observed.

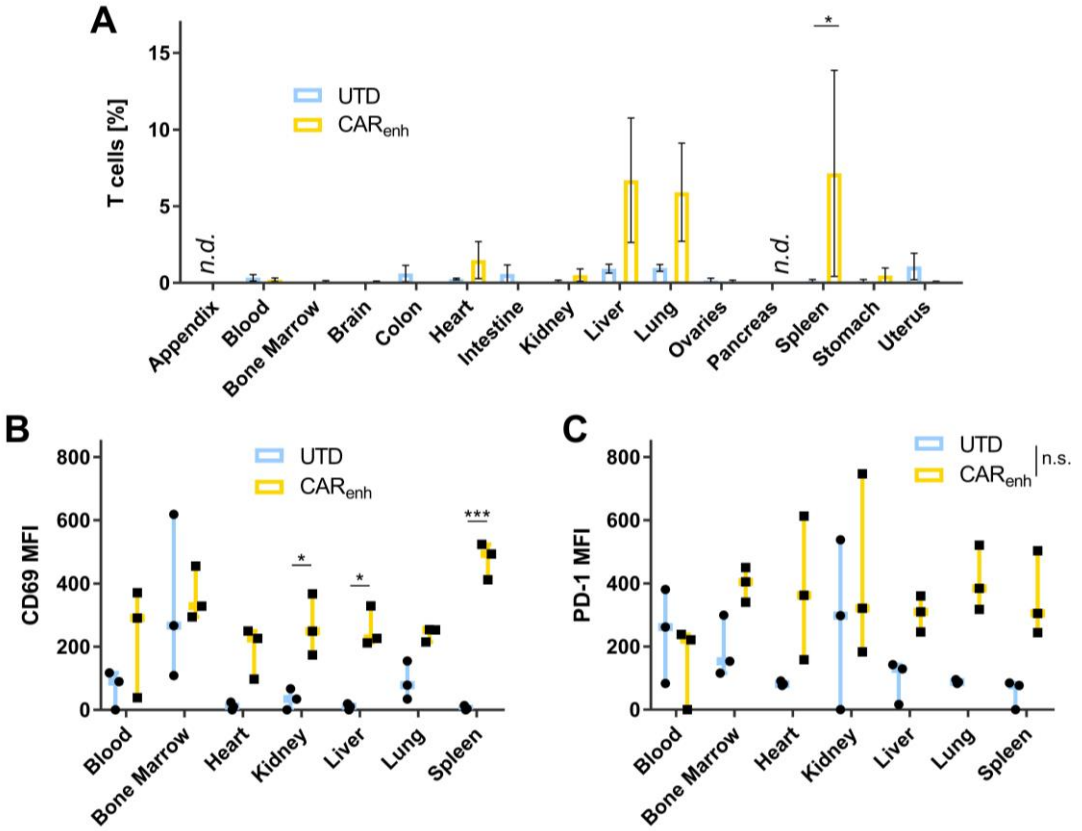

Figure 26 – CAR_{enh} T cells show tissue specific enrichment and T cell activation.

(A) Frequency of living human T cells as a fraction of total living single cells in indicated tissues obtained from mice treated with UTD or CAR_{enh} T cells on day 8 after T cell inoculation. Expression of CD69 (B) and PD-1 (C) on living human T cells obtained from indicated tissues with detectable T cell infiltration. Statistics are based on two-way ANOVA and Tukey's multiple comparison test. n.d.: not detectable.

To study on-target off-tumor toxicity in more detail, tissue-specific T cell infiltration and tissue damage was assessed by histological analysis in a similar but independent experiment (Figure 27). For this analysis, organs were isolated during the peak of T cell expansion on day 7 after CAR-T cell treatment and after T cell contraction on day 147 and analyzed by hematoxylin-eosin stain of formalin-fixed, paraffin-embedded tissue slides. The data showed no signs for tissue-specific T cell enrichment, except for temporary accumulation of ROR2-specific CAR-T cells in the lung. We found no indication for damages in any murine tissue and lung infiltration was found to have resolved without long-term effects by the second analysis timepoint.

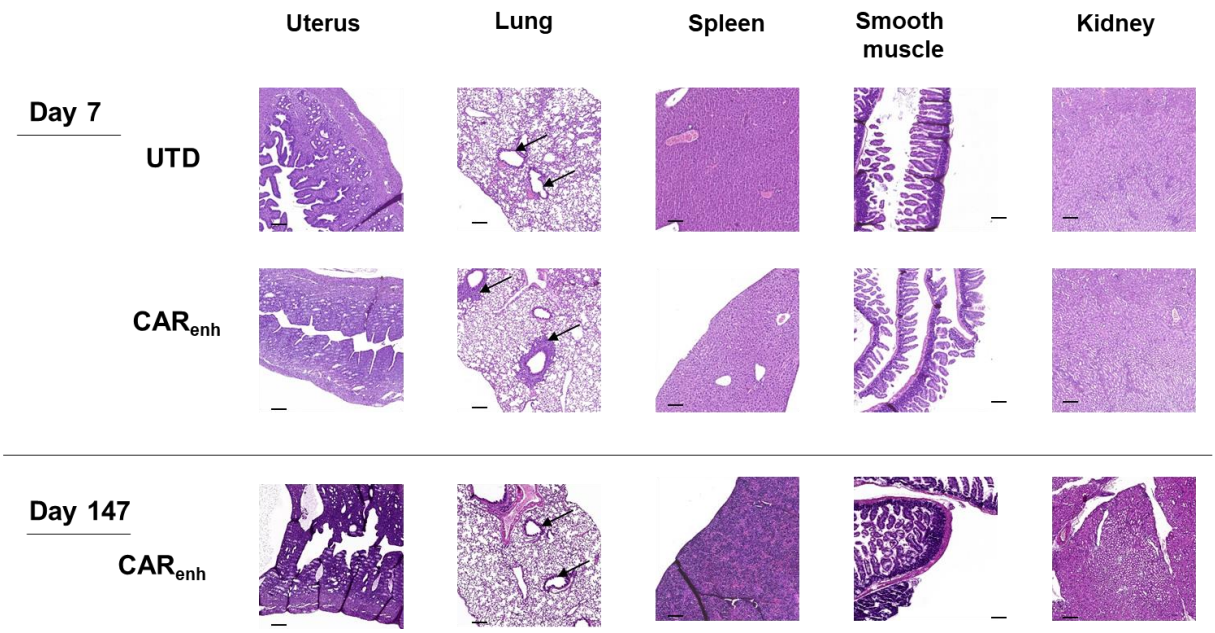

Figure 27 – CAR_{enh} T cells show temporary enrichment in the lung in the absence of tissue damage.
Representative HE stains for indicated tissues obtained on day 7 or day 147 from mice treated with CAR_{enh} or UTD T cells (n = 3 per group) as shown in Figure 25. Organs shown were selected based on their ROR2 gene expression levels (Figure 21). Scale bar represents 200 µm. Arrows point at areas of local lymphocyte infiltration.

4.3.4 ROR2-specific CAR-T cells retain specificity and reactivity after humanization

Next, we were interested in assessing the anti-tumor efficacy of ROR2-specific CAR-T cells with humanized binding domains. For this purpose, we employed CAR constructs with binding domains derived from the hX3.12.5 (CAR_{hu1}) and hX3.12.6 (CAR_{hu2}) antibodies, which have been generated by grafting the X3.12 CDRs (CAR_{enh}) into human antibody frameworks. All three antibodies have been shown to recognize the same ROR2 epitope, avoiding the need to adapt CAR spacer lengths to account for different epitope locations. CAR-T cells were generated by lentiviral transduction of healthy donor T cells and flow cytometry analysis revealed stable expression of all three CARs (Figure 28 A). For functional analyses, 786-O and U-266 cells were selected as representative ROR2-positive tumor cell lines and OPM-2 was chosen as a ROR2-negative control. First, we assessed antigen-specific tumor cell lysis by co-cultivation of ROR2-specific CAR- or UTD T cells with tumor cell lines (Figure 28 B). We observed high-level specific lysis of ROR2-positive U-266 and 786-O but not OPM-2 cells by all three ROR2-specific CAR-T cells. There was a trend towards reduced specific lysis of U-266 cells by CAR_{hu1} as compared to CAR_{enh} and CAR_{hu2} T cells. Additionally, we found significantly lower antigen-specific lysis of 786-O cells by CAR_{hu1} as compared to both CAR_{enh} and CAR_{hu2} T cells upon 24-hour co-cultivation at E:T-ratios of 1:1 and 1:5. No statistically significant difference in specific lysis of 786-O and U-266 cells were observed between CAR_{enh} and CAR_{hu2} T cells

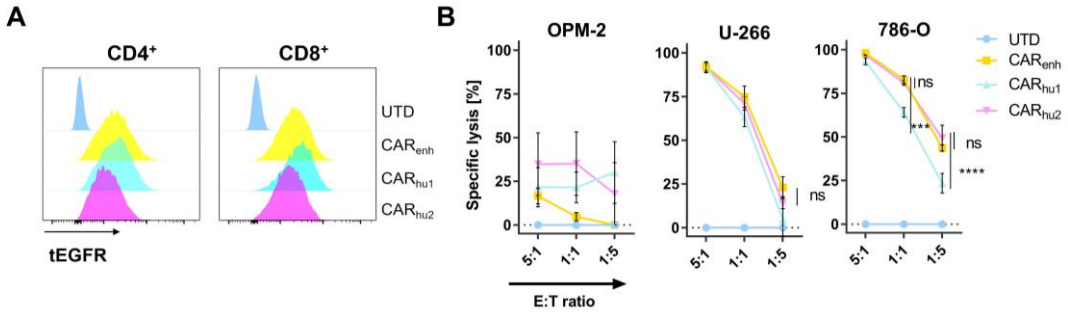

Figure 28 – ROR2-specific CAR-T cells with humanized binding domains exhibit antigen-specific lysis of ROR2-positive tumor cell lines *in vitro*.

(A) Representative flow cytometry histograms showing tEGFR expression as a surrogate for CAR expression on the surface of indicated $CD4^+$ and $CD8^+$ ROR2-specific CAR-T cells after enrichment and expansion. (B) Specific lysis of indicated tumor cells upon 24-hour co-cultivation with ROR2-specific CAR or UTD T cells at indicated E:T-ratios. Data shown is mean ± SEM for n = 3 independent donors. Statistics are based on two-way ANOVA and Tukey's multiple comparisons test.

To assess the secretion of effector cytokines by humanized ROR2-specific CAR-T cells in response to antigen-specific stimulation, $CD4^+$ and $CD8^+$ T cells were individually co-cultivated with ROR2-positive or negative tumor cell lines for 24 hours and cytokine concentrations in the co-culture supernatants were determined by ELISA (Figure 29). We observed high-level secretion of the effector cytokines IL-2 and IFNγ for all three constructs upon stimulation with ROR2-positive 786-O or U-266 cells, but not ROR2-negative OPM-2 cells. There was a trend towards lower cytokine secretion by CAR_{hu1} T cells upon stimulation with 786-O or U-266 cells than CAR_{enh} and CAR_{hu2} T cells. Significantly lower concentrations of IFNγ were observed in co-cultures between 786-O and $CD4^+$-T cells CAR_{hu1} T cells, as compared to CAR_{enh} and CAR_{hu2} T cells.

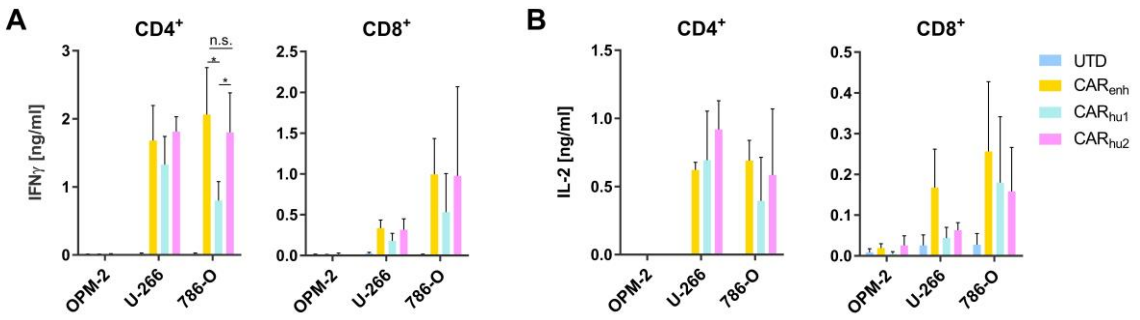

Figure 29 – ROR2-specific CAR-T cells with humanized binding domains elicit potent cytokine secretion upon stimulation with ROR2-positive tumor cell lines *in vitro*.

Secretion of the effector cytokines IFNγ (A) and IL-2 (B) upon 24-hour stimulation of indicated CAR-transduced or UTD T cells with indicated tumor cells lines at an E:T-ratio of 4:1, as determined by ELISA. Data shown is mean ± SEM for n = 3 independent donors. Statistics are based on two-way ANOVA and Tukey's multiple comparisons test.

Furthermore, we were interested in assessing the proliferation of humanized ROR2-specific CAR-T cells in response to antigen-specific stimulation (Figure 30). We found all three constructs to exhibit potent T cell proliferation in response to stimulation with the ROR2-positive tumor cell lines U-266 and 786-O, but not ROR2-negative OPM-2 cells. There was a consistent trend of lower proliferation in response to ROR2-specific stimulation by CAR_{hu1} T cells, as compared to CAR_{enh} or CAR_{hu2} T cells in both, $CD4^+$ and $CD8^+$ T cells. Additionally, we found stimulation with 786-O cells to induce significantly lower proliferation of CAR_{hu1} than both CAR_{enh} and CAR_{hu2} T cells. For $CD4^+$ T cells, we found no difference in T cell proliferation between CAR_{enh} and CAR_{hu2} T cells.

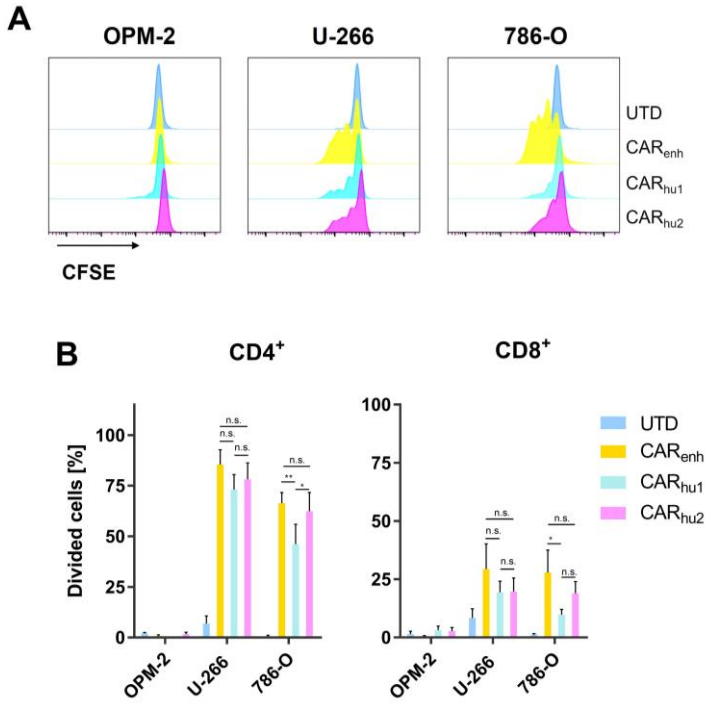

Figure 30 – ROR2-specific CAR-T cells with humanized binding domains elicit potent T cell proliferation upon stimulation with ROR2-positive tumor cell lines.

(A) Representative flow cytometry histograms of CFSE dye dilution by antigen-dependent T cell proliferation of indicated $CD4^+$ T cells upon co-cultivation with indicated tumor cell lines for 72-hours at an E:T-ratio of 4:1. (B) Fraction of cells that underwent at least one cell division upon stimulation with indicated tumor cell lines at an E:T-ratio of 4:1 for 72 hours. Data shown is mean ± SEM for n = 3 independent donors. Statistics are based on two-way ANOVA and Tukey's multiple comparisons test.

Finally, we were interested in assessing whether binding domain humanization had an impact on CAR immunogenicity, and in particular on the recognition by naturally occurring anti-idiotype antibodies. For this analysis, we generated CAR-Jurkat cells by lentiviral transduction, and enriched CAR-positive Jurkat cells using the tEGFR marker. CAR-Jurkat cells were used for flow cytometry analysis to assess the presence of naturally occurring anti-CAR antibodies in the plasma of healthy donors (Figure 31). We observed significantly higher MFI values for CAR_{wt}-Jurkats, as compared to tEGFR-transduced control Jurkat cells. In contrast, CAR_{enh}, CAR_{hu1}, and CAR_{hu2} Jurkats showed similar MFI values as tEGFR-transduced Jurkats, suggesting a reduced propensity for background antibody binding. No statistically significant difference in MFI between CAR_{enh}, CAR_{hu1}, CAR_{hu2}, and tEGFR-transduced Jurkats was observed.

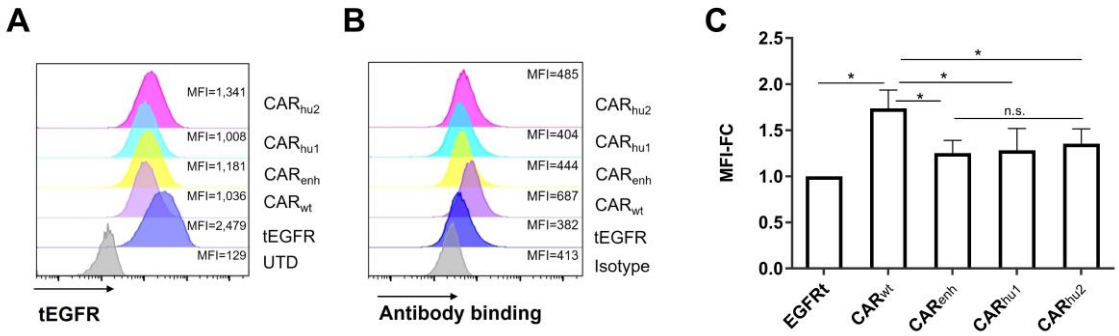

Figure 31 –Jurkat cells expressing humanized ROR2-specific CARs or CAR_{enh} show a reduced propensity for background binding of pre-existing anti-CAR antibodies in vitro.

(A) Flow cytometry histograms of tEGFR expression on the surface of CAR-Jurkats as a surrogate for CAR expression. Median fluorescence intensities are shown as MFI. (B) Representative flow cytometry histograms for the detection of naturally occurring antibodies directed against ROR2-specific CARs on the surface of CAR-positive Jurkat cells. Median fluorescence intensities are shown as MFI. Data shown is a representative of n = 5 independent donors. (C) Binding of pre-existing anti-CAR antibodies in health donor plasma using CAR-Jurkat cells. Data shown represents the MFI-foldchange between stained and isotype controls of indicated CAR-Jurkat variants. Data shown is mean ± SEM for n = 5 independent donors. Statistics are based on two-way ANOVA and Tukey's multiple comparisons test.

4.3.5 Interim conclusion

Here, we studied two key aspects of CAR-T cell safety: on-target off-tumor toxicities and CAR immunogenicity.

We analyzed ROR2 expression on the transcriptome and protein level in *H. sapiens* and *M. musculus* and found ROR2 expression to be conserved in mice. We also assessed the cross-reactivity of hROR2-specific CAR_{enh} T cells for murine ROR2 *in vitro* and observed similarly potent anti-tumor efficacy in response to stimulation with cells expressing human or murine ROR2. Next, we studied the preclinically safety of ROR2-specific CAR-T cells using a murine toxicology model. We observed tissue specific enrichment of CAR_{enh} T cells in the spleen, liver, and lung with significant upregulation of CD69 in the spleen. However, no clinical toxicity in the form of weight loss, health score changes or death was observed upon CAR_{enh} T cell therapy. Additionally, histological analysis showed no signs of tissue damage in response to CAR_{enh} T cell treatment.

Next, we generated humanized ROR2-specific CAR-T cells and determined their functionality *in vitro*. We observed both humanized CAR-T cells to elicit potent antigen-specific T cell functionality upon stimulation with ROR2-positive but not ROR2-negative tumor cells. In-depth analysis revealed CAR_{enh} and CAR_{hu2} T cells to elicit similarly potent anti-tumor effects, whereas the efficacy of CAR_{hu1} T cells was significantly decreased. Finally, we analyzed the humoral immunogenicity of ROR2-specific CAR-T cells *in vitro* using flow cytometry analysis of CAR-Jurkat cells. We found CAR_{enh}, CAR_{hu1}, and CAR_{hu2} Jurkat cells to show a reduced propensity for antibody binding as compared to CAR_{wt} Jurkats.

In summary, these data provide first insights into the safety of targeting ROR2 with CAR-T cells and show an acceptable safety profile for CAR_{enh} T cells in our preclinical models.

5 Discussion

Adoptive immunotherapy using CAR-modified T cells has mediated remarkable clinical responses in selected hematological malignancies. These results have fueled the interest in developing CAR-T cell products for other cancer entities, requiring the identification and assessment of novel candidate targets for CAR-T cell therapy and the concomitant development of cell products. We hypothesized that ROR2 is a candidate target for CAR-T cell therapy, due to its overexpression on cancer cells and correlation with poor prognosis. To test this hypothesis, we I) studied the expression of ROR2 in ccRCC and MM, II) developed and functionally characterized ROR2-specific CAR-T cells *in vitro* and *in vivo*, and III) employed preclinical toxicology models to gain first insights into the safety of targeting ROR2.

5.1 ROR2 expression in ccRCC and MM

First, we were interested in studying the expression of ROR2 in RCC. To this end, ROR2 gene expression was analyzed in a representative renal cancer patient collective using qPCR. We observed ROR2 expression in 86 % (24/28) of evaluable samples and ROR2 overexpression as compared to matched normal tissue was found in 67 % (2/3) of pRCC and 53 % (10/19) of ccRCC patient samples. To confirm the expression of ROR2 on the protein level, IHC analysis of a matched pRCC and ccRCC patients was employed. We found ROR2 protein to be expressed in 71 % of all RCC cases and observed significant overexpression in ccRCC as compared to pRCC samples. These findings are in line with a previous study, which analyzed the TCGA ccRCC RNAseq dataset and found ROR2 to be overexpressed in ccRCC and to correlate with poor prognosis and a more invasive tumor phenotype [69, 152]. In light of the higher frequency of ccRCC than pRCC and the higher ROR2 protein expression level in IHC analyses, we decided to focus on ccRCC as a proof of concept. However, our data suggest that a subset of pRCC cases is also characterized by ROR2 overexpression.

Next, we analyzed the expression of ROR2 in RCC cell lines using qPCR and flow cytometry and found 75 % (3/4) of ccRCC and 100 % (2/2) pRCC cell lines to be ROR2-positive. Flow cytometry analysis confirmed ROR2-positive cell lines to show homogenous ROR2 protein

expression and MFI thresholding was employed to cluster cell lines based on antigen quantities. Our data suggest that 786-O are ROR2^{high}, whereas RCC-4 and RCC-53 are ROR2^{med} and ROR2^{low}, respectively. These data are in line with previous studies, which individually confirmed 786-O and RCC-4 cells to express ROR2 [62, 69, 153]. However, out data represents the first comparative analyses of ROR2 expression across ccRCC cell lines.

Next, we focused on assessing the expression of ROR2 in MM. We focused on two representative MM cell lines, U-266 and OPM-2, and determined their ROR2 expression on the protein and transcriptomic level. Using qPCR and flow cytometry, we found U-266 to uniformly express ROR2, whereas OPM-2 cells were shown to be ROR2-negative. Of note, these data were supplemented by flow cytometry analyses of patient-derived MM cells in collaboration with the department for translational myeloma research. The analysis showed ROR2 to be uniformly expressed on the surface of approx. 70 % of patient samples (n = 24, data not shown). These findings are in line with a recent study, which showed U-266 cells to be ROR2-positive and reported ROR2 overexpression on the transcriptomic level in MM [67].

While ROR2 expression has previously been assessed, recent studies have reported conflicting data with regards to its expression. A recent study found these discrepancies to be cause by the utilization of unspecific antibodies for immunohistochemical analyses [94]. This observation has led to a predominance of transcriptome analyses to assess the expression of ROR2, using methods such as qPCR and RNAseq [67, 69]. However, it is commonly accepted that RNA expression does not infer protein expression levels, due to a variety of post-transcriptional and post-translational processes [154, 155]. These previous works underline the relevance of confirming cell surface expression of candidate targets for CAR-T cell therapy.

In summary, these data show that uniform expression of ROR2 protein is commonly found on the cell surface of ccRCC and MM cell lines and patient samples. ROR2 was detectable in around 70 % of RCC and MM patient samples, establishing relevant patient collective sizes for cell therapy using ROR2-specific CAR-T cells.

5.2 Efficacy of ROR2-specific CAR-T cells against ccRCC and MM

To assess the efficacy of ROR2-specific CAR-T cells for the treatment of ccRCC and MM, we generated two second-generation ROR2-specific CARs based on the antibodies XBR2-401 (CAR_{wt}, K_D = 7 nM) and its affinity matured variant X3.12 (CAR_{enh}, K_D = 0.7 nM). Importantly, both binders have been shown to recognize the same epitope within the kringle domain of ROR2 by X-ray crystallography, allowing us to study the impact of binding affinity on CAR-T cell performance without the need to adapt spacer lengths to different epitope locations [62, 95].

Efficacy of ROR2-specific CAR-T cells against ccRCC

First, we were interested in studying the efficacy of ROR2-specific CAR-T cells for the treatment of ccRCC. We found both CAR_{wt} and CAR_{enh} T cells to elicit potent antigen-specific functionalities *in vitro* upon co-cultivation with ccRCC cell lines. These findings are in line with previous studies assessing the antigen-specificity of the binders employed in CAR_{wt} and CAR_{enh} T cells [62, 95]. Furthermore, we observed a correlation between ROR2 MFI values, as a surrogate for cell surface antigen expression, and the potency of anti-tumor functionalities, including tumor cell lysis, cytokine secretion and proliferation. While MFI-based expression assignment does not represent a quantitative protein expression tool, similar correlations have previously been made for a variety of cancer antigens, such as CD19 and ALK and antigen density has been suggested as a key factor determining CAR-T cell efficacy [29, 156, 157]. Quantitative approaches to determine antigen quantities and densities, such as *d*STORM analysis, have recently been reported as a tool to establish causal relationships between antigen expression levels and CAR-T cell efficacy [26].

To assess the impact of binding affinity on CAR-T cell performance, we employed two CAR constructs with higher and lower affinity in this study. We found both cell products to exhibit specific anti-tumor efficacy *in vitro*, with a trend towards a more potent anti-tumor response by T cells expressing the CAR with higher affinity (CAR_{enh}). This observation is in line with previous studies, which have found that CAR-T cells employing high affinity binders are less sensitive to target expression levels. However, most previous studies have neglected to adapt their CAR constructs to differences in epitope location, which has previously been

shown to affect CAR-T cell potency [9]. One study investigated EGFR-specific CAR-T cells based on the antibodies, cetuximab and nimotuzumab, with different binding affinities for overlapping, but not identical three-dimensional epitopes of EGFR. The authors found low affinity nimotuzumab-derived CAR-T cells to be more sensitive to target expression levels and to spare antigen-low cells. Since CAR-T cells generally address overexpressed CAAs, this characteristic may manifest in an improved safety profile [27]. Another study compared Her2-specific CAR-T cells recognizing the same epitope, as determined by molecular modelling, with different binding affinities down to the sub-nanomolar range. The authors observed a similar correlation between binding affinity and antigen density requirements, but this effect was similarly low as the differences we reported, when comparing CAR-T cells with nanomolar and sub-nanomolar affinities [28]. Finally, a third study employing ligand-based ICAM-1 specific CAR-T cells revealed a similar correlation between binding affinity and antigen-density requirements, leading to lower on-target off-tumor toxicities by recognition of naturally occurring low-level ICAM-1 expression [6].

Finally, we compared the *in vivo* efficacy of CAR_{wt} and CAR_{enh} T cells for the treatment of ccRCC. While both cell products exerted potent anti-tumor efficacy, we observed a trend towards deeper remission and increased T cell expansion in mice treated with CAR_{enh} than with CAR_{wt} T cells. These findings are further supported by an increased frequency of T_{Eff} cells in the tumor microenvironment of CAR_{enh}-treated mice at the experimental endpoint. In this regard our data recapitulate clinical findings, showing a high abundance of active $CD8^+$ T cells in ccRCC tumor samples [110, 111].

So far, only a limited number of CAR-T cell products have been developed and evaluated for the treatment of RCC, such as CAIX and CD70-specific CAR-T cells. While CD70-specific CAR-T cells are currently being tested in clinical trials (NCT02830724, NCT04438083), CAIX-specific CAR-T cell trials have been discontinued due to engraftment failure and severe liver toxicities [44, 158]. Additionally, other approaches, such as dendritic cell vaccines or tumor-specific T cells, have been evaluated for RCC. Common targets addressed in these studies include 5T4, MUC-1, and WT-1 [159-162]. However, none of these approaches managed to significantly improve overall survival (reviewed in [106]).

Efficacy of ROR2-specific CAR-T cells against MM

Next, we were interested in studying the anti-MM efficacy of ROR2-specific CAR-T cells. Based our previous results, we decided to focus on CAR_{enh} T cells, and observed potent antigen-specific anti-tumor efficacy against MM cells *in vitro* and *in vivo*.

CAR_{enh} T cells were found to elicit potent lysis of MM cell lines as well as patient-derived MM cells and showed high-level T cell proliferation and secretion of effector cytokines in response to antigen-specific stimulation. Furthermore, CAR_{enh} T cells conferred rapid tumor control and significantly improved overall survival in a U-266/NSG xenograft model. 25 % (3/12) of CAR_{enh}-treated mice showed complete responses and remained tumor-free until the end of the experiment on day 286.

Recently, BCMA-specific CAR-T cells have been approved for the treatment of MM by the FDA [136, 163]. However, BCMA is a challenging target, which has been described to be susceptible to γ-secretases cleavage and concomitant BCMA shedding, affecting antigen densities. A recent study has shown that BCMA solubilization can be prevented with γ-secretase inhibitors [53]. However, the respective clinical trial (NCT03502577) has been suspended for financial reasons. Furthermore, antigen-loss has recently also been reported upon treatment with BCMA-specific CAR-T cells [52]. Antigen escape is considered a universal tumor immune escape mechanism and has been shown to occur in most immuno- and cell therapy approaches, including BCMA-specific and CD19-specific CAR-T cells [48, 49, 51]. Assessing antigen loss in response to ROR2-specific CAR-T cell treatment has been beyond the scope of this study. Nonetheless, we did not observe the emergence of antigen-low or -negative tumor cell variants; neither during *in vitro*, nor *in vivo* analyses of ccRCC or MM. However, careful analysis of antigen loss may be required in future studies.

Furthermore, alternative targets for the treatment of MM with CAR-T cells have been proposed, such as CD38, SLAMF7, and GPRC5D [138, 164, 165]. However, all of these targets have been reported to show low-level expression in healthy tissues, such as SLAMF7 and CD38 expression on activated lymphocytes, and GPRC5D expression on healthy plasma cells and a variety of other tissues. [138, 165, 166]. While a certain background expression of CAAs can be acceptable, the safety and efficacy of CAR-T cell products addressing these

targets need to be verified and is currently being evaluated in clinical trials (GPRC5D: NCT05431608, SLAMF7: NCT04499339, CD38: NCT03464916).

Collectively, we show that ROR2-positive tumor cells are effectively recognized by ROR2-specific CAR-T cells, leading to antigen-specific tumor cell lysis, cytokine secretion and proliferation *in vitro*. We also show that ROR2-specific CAR-T cells induce significant tumor regression and survival benefits, as well as long-term T cell persistence *in vivo*.

5.3 Preclinical safety assessment of ROR2-specific CAR-T cells

Preclinical analyses play a key role for the development and functional assessment of CAR- T cell products. However, the development of predictive preclinical safety models represents an ongoing challenge, due to the quantity of intertwined factors influencing CAR-T cell safety and efficacy in clinical settings. However, preclinical assessment can provide first insights into the safety and efficacy of CAR-T cell products, which may influence strategic decisions during clinical trials. Here, we employ preclinical *in vitro* and *in vivo* models to assess the safety of targeting ROR2. For these analyses, we focused on three core aspects I) off-target toxicity, II) on-target toxicity, and III) humoral CAR immunogenicity.

Off-target toxicity

In this study, we determined the off-target activity of ROR2-specific CAR-T cells by comparing the T cell functionalities of CAR- and UTD T cells in response to stimulation with ROR2-positive or -negative tumor cell lines. While background reactivity was generally observed, we found no difference in T cell efficacy between CAR- and UTD T cells in response to antigen-negative tumor cell lines. It is likely that these background effects are caused by HLA-mismatching, which has previously been reported to play a role in the context of graft-versus-host disease [167].

In general, off-target toxicity can largely be controlled by adequate binder selection. In this case, we had previously determined the affinity and specificity of the binders employed to generate ROR2-specific CAR-T cells by surface plasmon resonance, X-ray crystal structure analysis and Retrogenix' custom cell microarray analysis [62]. While off-target toxicities due

to recognition of additional antigens have not been reported for CAR-T cells, a recent study showed severe cardiovascular off-target toxicity by MAGE-A3-specific TCR-transgenic T cells, caused by off-target recognition of titin on cardiovascular cells [168]. Additionally, recognition of IgG1-based CAR spacers by Fcγ receptors has been shown to induce reciprocal toxicity between CAR-T cells and innate immune cells [169].

These findings underline that off-target toxicities are generally possible in the context of CAR-T cell therapy and need to be considered during preclinical assessment.

On-target off-tumor toxicity

In contrast, on-target toxicities are a common side-effect of cellular therapy caused by the recognition of healthy antigen-positive cells by CAR-transduced T cells. This type of toxicity is largely owed to the predominant utilization of CAA-specific as compared to neoantigen-specific CAR-T cells and depends on target selection and expression [65, 170]. It is known that the prevalence of antigen-positive healthy cells and the tissues in which they occur have an impact on the severity of on-target toxicities. For example, B cell aplasia is commonly observed upon treatment with CD19-specific CAR-T cells, due to antigen expression on normal B cells [171]. This toxicity manifests in subsequent hypogammaglobulinemia and leads to an increased risk of infection, requiring intravenous immunoglobulin supplementation. Due to the severity of the respective cancer, and the ease of clinical management for this toxicity, B cell aplasia is considered an acceptable toxicity and has even been established as an indirect proof for the persistence of CD19-specific CAR-T cells [172, 173]. In contrast, more severe toxicities have been reported upon treatment with CAR-T cells directed against Her2 and CAIX, such as liver toxicities and death [43, 44].

These previous works underline the relevance of studying on-target off-tumor toxicities in preclinical models. However, recent studies have shown that on-target off-tumor toxicity is not only dictated by target expression but is also context dependent. For example, a recent study found cross-reactive ROR1-specific CAR-T cells to be safe in mice but observed lethal toxicities as a result of certain lymphodepleting chemotherapy approaches in a dose-dependent manner [45].

Expression of ROR2 in *H. sapiens* and *M. musculus*

To assess the expression of ROR2, we performed gene and protein expression analyses of healthy adult human and murine tissues. We found ROR2 expression to be detectable in tissues obtained from the male and female reproductive system, as well as parts of the gastrointestinal tract in both species. These findings are in line with previous reports showing low-level expression of ROR2 in colon [174], stomach [175], and uterus [76]. Additionally, we observed ROR2 to show similar relative gene expression levels in those tissues in both, *H. sapiens* and *M. musculus*. Other studies have also reported residual ROR2 expression in plasma cells [67, 176], osteoblasts [75], and the thyroid [74].

In summary, we have shown that ROR2 expression is conserved between human and murine tissues. These findings are in line with previous reports concerning the expression of ROR family receptors on the genomic level [79]. Our data is further supported by a recent study showing that ROR2$^{-/-}$ mice recapitulated the morphological characteristic of brachydactyly type B and Robinow syndrome, suggesting similar physiological roles for ROR2 in both species [84].

Safety of targeting ROR2 in mice

Next, we assessed the cross-reactivity of ROR2-specific CAR-T cells and showed that CAR_{enh} T cells elicit similarly potent antigen-dependent functionality against cells expressing human and murine ROR2 *in vitro*. While a variety of cross-reactive CAR-T cell products have been used to study toxicities in murine models, comparable reactivity has rarely been shown. For example, a recent study using GPC-2-specific CAR-T cells reported differences in cytokine secretion upon stimulation with cell lines expressing defined GPC-2 quantities [12].

Based on our data, we hypothesized that adoptive T cell transfer in tumor-free, immunodeficient mice represents a suitable model to assess the preclinical safety of ROR2-specific CAR-T cells *in vivo*. To study on-target off-tumor effects of ROR2-specific CAR_{enh} T cells, we monitored weight and health scores to identify clinical signs of toxicity, and analyzed tissue-specific T cell enrichment, activation and tissue damage by flow cytometry and histological analysis. We observed T cell enrichment in tissues with high blood

circulation, such as spleen, liver, lung, and kidney. Histological analysis confirmed temporary enrichment of CAR_{enh} T cells in the lung in the absence tissue damage and long-term toxicity. These findings are further supported by the absence of significant weight and health score changes, serving as surrogates for severe toxicity. Murine toxicology models are commonly used to study on-target off-tumor effects preclinically *in vivo*. Most recently, such models have been employed to study the safety of CAR-T cells targeting GPRC5D and GPC-2 [12, 165]. Common objectively measurable parameters include body weight, temperature, and health scores, as well as histological analysis of toxicity-relevant tissues. Clinical data suggests that the frequency and severity of on-target off-tumor effects correlates with CAR-T cell dose levels [177]. In our model, mice were injected with 1×10^7 T cells, which corresponds to around 4×10^8 CAR-positive T cells per kg body weight. While similar T cell doses are commonly used in pre-clinical safety models, clinical anti-tumor efficacy is usually achieved with 100-fold lower CAR-T cell doses [12, 165, 177, 178]. While *in vivo* models represent the gold standard for preclinical safety assessment, complementary *ex vivo* analyses such as organ-on-a-chip models and real-time live-cell fluorescence microscopy are being developed [179, 180].

In summary, these data suggest an acceptable safety profile for ROR2-specific CAR-T cells in our preclinical models.

Humanization of ROR2-specific CAR-T cells

Another common side-effect of CAR-T cell therapy are cellular and humoral immune responses directed against autologous CAR-T cell products. It has been shown that these immune responses can lead to CAR-T cell neutralization or eradication *in vitro* (reviewed in [59]), as well as serious adverse events in clinical trials [58]. In clinical settings, cellular immunogenicity is rarely detected, whereas anti-CAR antibodies are commonly found in the plasma of patients treated with CAR-T cells.

Here, we sought to study the impact of humanized binding domains on CAR-T cell functionality and humoral immunogenicity. For this purpose, we employed two humanized binding domains derived from the X3.12 antibody (CAR_{enh}), which have been shown to recognize the same epitope in the kringle domain of ROR2 as X3.12. Functional analysis

revealed CAR_{enh} and CAR_{hu2} (based on the hX3.12.6 antibody) to elicit comparable anti-tumor efficacy *in vitro*, whereas CAR_{hu1} T cells (based on the hX3.12.5 antibody) showed reduced anti-tumor efficacy upon stimulation with ROR2-positive tumor cell lines. These findings are in line with the initial characterization of the hX3.12.5 and hX3.12.6 antibodies in preclinical analyses [62]. Furthermore, similar results have been obtained during the development of CD19-specific CAR-T cells with humanized binders and suggest that the utilization of optimized humanized binding domains yields highly functional CAR-T cell products [63, 181].

We observed functional differences with regards to cytolysis, cytokine secretion and T cell proliferation between CAR_{hu1} and both CAR_{enh} and CAR_{hu2} T cells in response to stimulation with the 786-O and U-266 cells. Similar trends have previously been observed and a recent study identified functional T cell avidity to play a key role in this regard [182]. The analysis also identified that tumor mutations in non-target proteins, such as the IFNγ receptor, may have a distinct impact on functional CAR-T cell avidity and tumor control. This particular aspect was found to affect the therapeutic implications for hematological and solid tumors in different ways and has been found to contribute to tumor immune escape [47].

To assess the humoral immunogenicity of ROR2-specific CAR-T cells, CAR-transduced Jurkat cells were generated and the prevalence of naturally occurring anti-CAR antibodies was studied using healthy donor plasma [183]. We observed a significant MFI increase between $CAR_{wt,}$ but not CAR_{enh}-transduced Jurkats, as compared to control Jurkats suggesting humoral immunogenicity of the CAR_{wt} receptor. Interestingly, these two receptors only differ in a short amino acid sequence within the HCDR3 loop, which is preserved in the humanized versions CAR_{hu1} and CAR_{hu2}. We did not observe significant differences in MFI between CAR_{enh}, CAR_{hu1}, and CAR_{hu2} Jurkats, further supporting our hypothesis that neoepitopes within the HCDR3 loop of the CAR_{wt} receptor are responsible for this MFI change and its concomitant immunogenicity. These findings are in line with a previous study assessing the cellular immunogenicity of humanized antibodies, which found residual immunogenic potential within the CDR regions [64].

In summary, we have shown that the use of optimal humanized binders yields potent CAR-T cell products with a reduced propensity for antibody binding.

5.4 Summary, and future perspectives

In this study, we have shown that ROR2 is a suitable target for cancer therapy using CAR-modified T cells. The data show potent antigen-dependent anti-tumor efficacy of ROR2-specific CAR-T cells against ccRCC and MM *in vitro* and *in vivo*. Furthermore, preclinical safety assessment in a murine toxicology model suggests that ROR2-specific CAR-T cells show an acceptable safety profile. Collectively, these data suggest that ROR2-specific CAR-T cells may broaden the therapeutic applicability of CAR-T cells, provided that clinical safety and efficacy can be shown in clinical trials.

Previous studies have analyzed the expression of ROR2 on the transcriptome level in different cancer entities and imply broad clinical applicability of ROR2-specific CAR-T cells beyond the two representative entities used in this study [68, 86, 87, 89-93, 184]. However, detailed analyses to identify the exact subsets of eligible patients may be required. Due to the preferential overexpression of ROR2 in solid tumors, it may be relevant to combine ROR2-specific CAR-T cells with additional approaches to boost CAR-T cell performance. Potential starting points may involve the additional overexpression of chemokine receptors, transcription factors, immuno-supportive cytokines, or enzymes [15, 17, 24, 185, 186]. Additionally, it may be relevant to explore combination therapy approaches involving small molecule drugs to render tumor cells more susceptible to lysis or to boost antigen expression levels [187, 188]. These options may also involve the *in-situ* activation of cytotoxic chemotherapeutic compounds [189].

Importantly, ROR1 and ROR2 co-expression has been observed in a few cases, and both targets are believed to be predominantly expressed in different cancer subsets [98, 190]. Therefore, the availability of ROR1 and ROR2-specific CAR-T cell products may significantly broaden the therapeutic applicability of CAR-T cells. So far, ROR1 and ROR2 co-expression has only been observed in neuroblastoma and CLL [176, 191]. The availability of both targets in these entities may allow for the generation or ROR1/ROR2 bi-specific CAR-T cells to circumvent antigen-loss, or the incorporation of additional safety measures using logic operations, such as synthetic Notch receptors [192, 193].

Furthermore, ROR2 has the potential to address tumors with a complex tumor microenvironment, due to its upregulation on activated tumor-associated fibroblasts within the tumor stroma, such as in pancreatic ductal adenocarcinoma and ovarian cancer [88, 90, 194, 195]. While CAR-T cell approaches to address stroma cells within the tumor microenvironment have been reported using targets such as fibroblast activation protein (FAP), no mono-specific CAR-T cell product with an intrinsic property to target cancer and stroma cells simultaneously has been reported [196].

Major concerns of cancer patients are the safety and efficacy of any novel treatment, which are evaluated in clinical trials. To facilitate the transition from preclinical to clinical testing, all constructs shown in this thesis are equipped with the tEGFR selection marker, which can be used to eradicate CAR-T cells in case of severe side effects, providing an additional safety measure [143]. Additionally, the tyrosine kinase inhibitor dasatinib has recently been described as a novel tool to transiently inactivate CAR-T cells to control acute side-effects [150]. Furthermore, therapeutic interventions need to be affordable, which can commonly be achieved by economies of scale. In this context, minicircle-based Sleeping Beauty transposition has recently been described as a novel approach to produce CAR-T cell products for clinical application [197]. In addition, the biomedical industry has started to establish production facilities for the generation of clinical-grade CAR-T cell products. While some companies have focused on their own cell products, others have developed commercially available closed systems which allow for on-site production.

Collectively, this study shows that ROR2 is a suitable target for CAR-T cell therapy, meeting the EBMT target selection criteria, and ROR2-specific CAR-T cells have been shown to clear the benchmarks for clinical translation.

References

1. Rosenberg, S.A., et al., *Use of tumor-infiltrating lymphocytes and interleukin-2 in the immunotherapy of patients with metastatic melanoma. A preliminary report.* N Engl J Med, 1988. **319**(25): p. 1676-80.
2. Sadelain, M., I. Rivière, and S. Riddell, *Therapeutic T cell engineering.* Nature, 2017. **545**(7655): p. 423-431.
3. Davila, M.L., et al., *Chimeric antigen receptors for the adoptive T cell therapy of hematologic malignancies.* International Journal of Hematology, 2014. **99**(4): p. 361-371.
4. Safarzadeh Kozani, P., et al., *Strategies for Dodging the Obstacles in CAR T Cell Therapy.* Front Oncol, 2021. **11**: p. 627549.
5. Hudecek, M., et al., *The B-cell tumor-associated antigen ROR1 can be targeted with T cells modified to express a ROR1-specific chimeric antigen receptor.* Blood, 2010. **116**(22): p. 4532-4541.
6. Park, S., et al., *Micromolar affinity CAR T cells to ICAM-1 achieves rapid tumor elimination while avoiding systemic toxicity.* Scientific Reports, 2017. **7**(1): p. 14366.
7. Rajabzadeh, A., et al., *A VHH-Based Anti-MUC1 Chimeric Antigen Receptor for Specific Retargeting of Human Primary T Cells to MUC1-Positive Cancer Cells.* Cell J, 2021. **22**(4): p. 502-513.
8. Hammill, J.A., et al., *Designed ankyrin repeat proteins are effective targeting elements for chimeric antigen receptors.* Journal for ImmunoTherapy of Cancer, 2015. **3**(1): p. 55.
9. Hudecek, M., et al., *Receptor affinity and extracellular domain modifications affect tumor recognition by ROR1-specific chimeric antigen receptor T cells.* Clin Cancer Res, 2013. **19**(12): p. 3153-64.
10. Alabanza, L., et al., *Function of Novel Anti-CD19 Chimeric Antigen Receptors with Human Variable Regions Is Affected by Hinge and Transmembrane Domains.* Mol Ther, 2017. **25**(11): p. 2452-2465.
11. Majzner, R.G., et al., *Tuning the Antigen Density Requirement for CAR T-cell Activity.* Cancer Discov, 2020. **10**(5): p. 702-723.
12. Heitzeneder, S., et al., *GPC2-CAR T cells tuned for low antigen density mediate potent activity against neuroblastoma without toxicity.* Cancer Cell, 2022. **40**(1): p. 53-69.e9.
13. Guedan, S., et al., *Enhancing CAR T cell persistence through ICOS and 4-1BB costimulation.* JCI Insight, 2018. **3**(1).
14. Kawalekar, O.U., et al., *Distinct Signaling of Coreceptors Regulates Specific Metabolism Pathways and Impacts Memory Development in CAR T Cells.* Immunity, 2016. **44**(2): p. 380-90.

15. Chmielewski, M. and H. Abken, *CAR T cells transform to trucks: chimeric antigen receptor-redirected T cells engineered to deliver inducible IL-12 modulate the tumour stroma to combat cancer.* Cancer Immunol Immunother, 2012. **61**(8): p. 1269-77.

16. Rafiq, S., et al., *Targeted delivery of a PD-1-blocking scFv by CAR-T cells enhances anti-tumor efficacy in vivo.* Nat Biotechnol, 2018. **36**(9): p. 847-856.

17. Caruana, I., et al., *Heparanase promotes tumor infiltration and antitumor activity of CAR-redirected T lymphocytes.* Nat Med, 2015. **21**(5): p. 524-9.

18. Davenport, A.J., et al., *Chimeric antigen receptor T cells form nonclassical and potent immune synapses driving rapid cytotoxicity.* Proc Natl Acad Sci U S A, 2018. **115**(9): p. E2068-e2076.

19. Gudipati, V., et al., *Inefficient CAR-proximal signaling blunts antigen sensitivity.* Nat Immunol, 2020. **21**(8): p. 848-856.

20. Salter, A.I., et al., *Comparative analysis of TCR and CAR signaling informs CAR designs with superior antigen sensitivity and in vivo function.* Sci Signal, 2021. **14**(697).

21. Chen, X., et al., *Rational Tuning of CAR Tonic Signaling Yields Superior T-Cell Therapy for Cancer.* bioRxiv, 2020: p. 2020.10.01.322990.

22. Eyquem, J., et al., *Targeting a CAR to the TRAC locus with CRISPR/Cas9 enhances tumour rejection.* Nature, 2017. **543**(7643): p. 113-117.

23. Feucht, J., et al., *Calibration of CAR activation potential directs alternative T cell fates and therapeutic potency.* Nat Med, 2019. **25**(1): p. 82-88.

24. Lynn, R.C., et al., *c-Jun overexpression in CAR T cells induces exhaustion resistance.* Nature, 2019. **576**(7786): p. 293-300.

25. Sykulev, Y., et al., *Evidence that a single peptide-MHC complex on a target cell can elicit a cytolytic T cell response.* Immunity, 1996. **4**(6): p. 565-71.

26. Nerreter, T., et al., *Super-resolution microscopy reveals ultra-low CD19 expression on myeloma cells that triggers elimination by CD19 CAR-T.* Nat Commun, 2019. **10**(1): p. 3137.

27. Caruso, H.G., et al., *Tuning Sensitivity of CAR to EGFR Density Limits Recognition of Normal Tissue While Maintaining Potent Antitumor Activity.* Cancer Res, 2015. **75**(17): p. 3505-18.

28. Liu, X., et al., *Affinity-Tuned ErbB2 or EGFR Chimeric Antigen Receptor T Cells Exhibit an Increased Therapeutic Index against Tumors in Mice.* Cancer Res, 2015. **75**(17): p. 3596-607.

29. Majzner, R.G., et al., *Tuning the Antigen Density Requirement for CAR T-cell Activity.* Cancer Discovery, 2020. **10**(5): p. 702-723.

30. Schmid, D.A., et al., *Evidence for a TCR affinity threshold delimiting maximal CD8 T cell function.* J Immunol, 2010. **184**(9): p. 4936-46.

31. Maus, M.V., et al., *An MHC-restricted antibody-based chimeric antigen receptor requires TCR-like affinity to maintain antigen specificity.* Mol Ther Oncolytics, 2016. **3**: p. 1-9.

32. Eisen, H.N., *Affinity enhancement of antibodies: how low-affinity antibodies produced early in immune responses are followed by high-affinity antibodies later and in memory B-cell responses.* Cancer Immunol Res, 2014. **2**(5): p. 381-92.

33. Rader, C., *Selection of human Fab libraries by phage display.* Methods Mol Biol, 2012. **901**: p. 81-99.

34. Weber, J., H. Peng, and C. Rader, *From rabbit antibody repertoires to rabbit monoclonal antibodies.* Exp Mol Med, 2017. **49**(3): p. e305.

35. Zahnd, C., P. Amstutz, and A. Plückthun, *Ribosome display: selecting and evolving proteins in vitro that specifically bind to a target.* Nature Methods, 2007. **4**(3): p. 269-279.

36. FDA. *Approved Cellular and Gene Therapy Products*. [Website] 2022 09.07.2022; Available from: https://www.fda.gov/vaccines-blood-biologics/cellular-gene-therapy-products/approved-cellular-and-gene-therapy-products.

37. ClinicalTrials.gov. *Current CAR-T cell trials*. [Website] 2022 09.07.22; Available from: https://clinicaltrials.gov/ct2/results?term=%22CAR+T%22+OR+%22CAR-T%22&recrs=b&recrs=a&recrs=f&recrs=d&age_v=&gndr=&type=&rslt=&Search=Apply.

38. NHI-NCI. *CAR T Cells: Engineering Patients' Immune Cells to Treat Their Cancers* [Website] 2022 22.04.2022; Available from: https://www.cancer.gov/about-cancer/treatment/research/car-t-cells.

39. Albinger, N., J. Hartmann, and E. Ullrich, *Current status and perspective of CAR-T and CAR-NK cell therapy trials in Germany.* Gene Therapy, 2021. **28**(9): p. 513-527.

40. Giavridis, T., et al., *CAR T cell–induced cytokine release syndrome is mediated by macrophages and abated by IL-1 blockade.* Nature Medicine, 2018. **24**(6): p. 731-738.

41. Riegler, L.L., G.P. Jones, and D.W. Lee, *Current approaches in the grading and management of cytokine release syndrome after chimeric antigen receptor T-cell therapy.* Ther Clin Risk Manag, 2019. **15**: p. 323-335.

42. Hill, J.A., et al., *CAR-T - and a side order of IgG, to go? - Immunoglobulin replacement in patients receiving CAR-T cell therapy.* Blood Rev, 2019. **38**: p. 100596.

43. Morgan, R.A., et al., *Case report of a serious adverse event following the administration of T cells transduced with a chimeric antigen receptor recognizing ERBB2.* Mol Ther, 2010. **18**(4): p. 843-51.

44. Lamers, C.H., et al., *Treatment of metastatic renal cell carcinoma with CAIX CAR-engineered T cells: clinical evaluation and management of on-target toxicity.* Mol Ther, 2013. **21**(4): p. 904-12.

45. Srivastava, S., et al., *Logic-Gated ROR1 Chimeric Antigen Receptor Expression Rescues T Cell-Mediated Toxicity to Normal Tissues and Enables Selective Tumor Targeting.* Cancer Cell, 2019. **35**(3): p. 489-503.e8.

46. Hudson, K., et al., *The Extrinsic and Intrinsic Roles of PD-L1 and Its Receptor PD-1: Implications for Immunotherapy Treatment.* Frontiers in Immunology, 2020. **11**.

47. Larson, R.C., et al., *CAR T cell killing requires the IFNγR pathway in solid but not liquid tumours.* Nature, 2022. **604**(7906): p. 563-570.

48. Rabilloud, T., et al., *Single-cell profiling identifies pre-existing CD19-negative subclones in a B-ALL patient with CD19-negative relapse after CAR-T therapy.* Nature Communications, 2021. **12**(1): p. 865.

49. Ruella, M. and M.V. Maus, *Catch me if you can: Leukemia Escape after CD19-Directed T Cell Immunotherapies.* Comput Struct Biotechnol J, 2016. **14**: p. 357-362.

50. Ruella, M., et al., *Induction of resistance to chimeric antigen receptor T cell therapy by transduction of a single leukemic B cell.* Nature medicine, 2018. **24**(10): p. 1499-1503.

51. Sotillo, E., et al., *Convergence of Acquired Mutations and Alternative Splicing of CD19 Enables Resistance to CART-19 Immunotherapy.* Cancer discovery, 2015. **5**(12): p. 1282-1295.

52. Samur, M.K., et al., *Biallelic loss of BCMA as a resistance mechanism to CAR T cell therapy in a patient with multiple myeloma.* Nature Communications, 2021. **12**(1): p. 868.

53. Pont, M.J., et al., *γ-Secretase inhibition increases efficacy of BCMA-specific chimeric antigen receptor T cells in multiple myeloma.* Blood, 2019. **134**(19): p. 1585-1597.

54. Liu, D., J. Zhao, and Y. Song, *Engineering switchable and programmable universal CARs for CAR T therapy.* Journal of Hematology & Oncology, 2019. **12**(1): p. 69.

55. Qi, J., et al., *Chemically Programmable and Switchable CAR-T Therapy.* Angew Chem Int Ed Engl, 2020. **59**(29): p. 12178-12185.

56. Shah, N.N., et al., *Multi Targeted CAR-T Cell Therapies for B-Cell Malignancies.* Frontiers in oncology, 2019. **9**: p. 146-146.

57. Cho, J.H., J.J. Collins, and W.W. Wong, *Universal Chimeric Antigen Receptors for Multiplexed and Logical Control of T Cell Responses.* Cell, 2018. **173**(6): p. 1426-1438.e11.

58. Maus, M.V., et al., *T cells expressing chimeric antigen receptors can cause anaphylaxis in humans.* Cancer Immunol Res, 2013. **1**(1): p. 26-31.

59. Gorovits, B. and E. Koren, *Immunogenicity of Chimeric Antigen Receptor T-Cell Therapeutics.* BioDrugs, 2019. **33**(3): p. 275-284.

60. Melenhorst, J.J., et al., *Decade-long leukaemia remissions with persistence of CD4+ CAR T cells.* Nature, 2022. **602**(7897): p. 503-509.

61. Turtle, C.J., et al., *Immunotherapy of non-Hodgkin's lymphoma with a defined ratio of CD8+ and CD4+ CD19-specific chimeric antigen receptor-modified T cells.* Sci Transl Med, 2016. **8**(355): p. 355ra116.

62. Goydel, R.S., et al., *Affinity maturation, humanization, and co-crystallization of a rabbit anti-human ROR2 monoclonal antibody for therapeutic applications.* The Journal of biological chemistry, 2020. **295**(18): p. 5995-6006.

63. Qian, L., et al., *The novel anti-CD19 chimeric antigen receptors with humanized scFv (single-chain variable fragment) trigger leukemia cell killing.* Cellular Immunology, 2016. **304-305**: p. 49-54.

64. Harding, F.A., et al., *The immunogenicity of humanized and fully human antibodies: residual immunogenicity resides in the CDR regions.* MAbs, 2010. **2**(3): p. 256-65.

65. Falkenburg, E.C.M.a.J.H.F. *What Defines a Good Tumour Antigen?* [Website] 2022 21.06.2022; Available from: https://link.springer.com/book/10.1007/978-3-030-94353-0.

66. Wallstabe, L., et al., *ROR1-CAR T cells are effective against lung and breast cancer in advanced microphysiologic 3D tumor models.* JCI Insight, 2019. **4**(18).

67. Frenquelli, M., et al., *The WNT receptor ROR2 drives the interaction of multiple myeloma cells with the microenvironment through AKT activation.* Leukemia, 2020. **34**(1): p. 257-270.

68. Bayerlová, M., et al., *Ror2 Signaling and Its Relevance in Breast Cancer Progression.* Frontiers in oncology, 2017. **7**: p. 135-135.

69. Rasmussen, N.R., et al., *Expression of Ror2 mediates invasive phenotypes in renal cell carcinoma.* PloS one, 2014. **9**(12): p. e116101-e116101.

70. Al-Shawi, R., et al., *Expression of the Ror1 and Ror2 receptor tyrosine kinase genes during mouse development.* Dev Genes Evol, 2001. **211**(4): p. 161-71.

71. DeChiara, T.M., et al., *Ror2, encoding a receptor-like tyrosine kinase, is required for cartilage and growth plate development.* Nat Genet, 2000. **24**(3): p. 271-4.

72. Matsuda, T., et al., *Expression of the receptor tyrosine kinase genes, Ror1 and Ror2, during mouse development.* Mech Dev, 2001. **105**(1-2): p. 153-6.

73. Yoda, A., I. Oishi, and Y. Minami, *Expression and Function of the Ror-Family Receptor Tyrosine Kinases During Development: Lessons from Genetic Analyses of Nematodes, Mice, and Humans.* Journal of Receptors and Signal Transduction, 2003. **23**(1): p. 1-15.

74. Morioka, K., et al., *Orphan receptor tyrosine kinase ROR2 as a potential therapeutic target for osteosarcoma.* Cancer Sci, 2009. **100**(7): p. 1227-33.

75. Billiard, J., et al., *The orphan receptor tyrosine kinase Ror2 modulates canonical Wnt signaling in osteoblastic cells.* Mol Endocrinol, 2005. **19**(1): p. 90-101.

76. Cha, J., et al., *Appropriate crypt formation in the uterus for embryo homing and implantation requires Wnt5a-ROR signaling.* Cell Rep, 2014. **8**(2): p. 382-92.

77. Forrester, W.C., *The Ror receptor tyrosine kinase family.* Cell Mol Life Sci, 2002. **59**(1): p. 83-96.

78. Oishi, I., et al., *The receptor tyrosine kinase Ror2 is involved in non-canonical Wnt5a/JNK signalling pathway.* Genes Cells, 2003. **8**(7): p. 645-54.

79. Green, J.L., S.G. Kuntz, and P.W. Sternberg, *Ror receptor tyrosine kinases: orphans no more.* Trends Cell Biol, 2008. **18**(11): p. 536-44.

80. Minami, Y., et al., *Ror-family receptor tyrosine kinases in noncanonical Wnt signaling: their implications in developmental morphogenesis and human diseases.* Dev Dyn, 2010. **239**(1): p. 1-15.

81. Consortium, T.U., *UniProt: the universal protein knowledgebase in 2021.* Nucleic Acids Research, 2020. **49**(D1): p. D480-D489.

82. UniProt. *UniProtKB Tyrosine-protein kinase transmembrane receptor ROR2*. [Database] 2022 19.07.2022; Available from: https://www.uniprot.org/uniprot/Q01974#entry_information.

83. Afzal, A.R., et al., *Recessive Robinow syndrome, allelic to dominant brachydactyly type B, is caused by mutation of ROR2.* Nat Genet, 2000. **25**(4): p. 419-22.

84. Schwabe, G.C., et al., *Ror2 knockout mouse as a model for the developmental pathology of autosomal recessive Robinow syndrome.* Dev Dyn, 2004. **229**(2): p. 400-10.

85. Dyba, T., et al., *The European cancer burden in 2020: Incidence and mortality estimates for 40 countries and 25 major cancers.* Eur J Cancer, 2021. **157**: p. 308-347.

86. Lu, C., et al., *Over-expression of ROR2 and Wnt5a cooperatively correlates with unfavorable prognosis in patients with non-small cell lung cancer.* Oncotarget, 2015. **6**(28): p. 24912-21.

87. Mei, H., et al., *High expression of ROR2 in cancer cell correlates with unfavorable prognosis in colorectal cancer.* Biochem Biophys Res Commun, 2014. **453**(4): p. 703-9.

88. Huang, J., et al., *High ROR2 expression in tumor cells and stroma is correlated with poor prognosis in pancreatic ductal adenocarcinoma.* Scientific reports, 2015. **5**: p. 12991-12991.

89. Nema, R., P. Patel, and A. Kumar, *Prognostic Role of Receptor Tyrosine Kinase-Like Orphan Receptors in Intestinal-Type Gastric Cancer.* Asian Pac J Cancer Prev, 2021. **22**(7): p. 2125-2134.

90. Henry, C., et al., *Targeting the ROR1 and ROR2 receptors in epithelial ovarian cancer inhibits cell migration and invasion.* Oncotarget, 2015. **6**(37): p. 40310-26.

91. Kim, Y., et al., *Wnt5a, Ryk and Ror2 expression in glioblastoma subgroups.* Pathol Res Pract, 2015. **211**(12): p. 963-72.

92. Castro, M.V., et al., *ROR2 has a protective role in melanoma by inhibiting Akt activity, cell-cycle progression, and proliferation.* J Biomed Sci, 2021. **28**(1): p. 76.

93. Chen, L., et al., *Higher expression level of tyrosine kinase-like orphan receptor 2 and Wnt member 5a in papillary thyroid carcinoma is associated with poor prognosis.* Oncol Lett, 2017. **14**(5): p. 5966-5972.

94. Ma, S.S., et al., *Validation of specificity of antibodies for immunohistochemistry: the case of ROR2.* Virchows Arch, 2017. **470**(1): p. 99-108.

95. Peng, H., et al., *Mining Naïve Rabbit Antibody Repertoires by Phage Display for Monoclonal Antibodies of Therapeutic Utility.* J Mol Biol, 2017. **429**(19): p. 2954-2973.

96. Waldmeier, L., et al., *Transpo-mAb display: Transposition-mediated B cell display and functional screening of full-length IgG antibody libraries.* MAbs, 2016. **8**(4): p. 726-40.

97. Sharp, L.L., et al., *Abstract 833: Anti-tumor efficacy of BA3021, a novel Conditionally Active Biologic (CAB) anti-ROR2 ADC.* Cancer Research, 2018. **78**(13_Supplement): p. 833-833.

98. Rebagay, G., et al., *ROR1 and ROR2 in Human Malignancies: Potentials for Targeted Therapy.* Front Oncol, 2012. **2**: p. 34.

99. Siegel, R.L., et al., *Cancer Statistics, 2021.* CA Cancer J Clin, 2021. **71**(1): p. 7-33.

100. Gkolfinopoulos, S., A. Psyrri, and A. Bamias, *Clear-cell renal cell carcinoma - A comprehensive review of agents used in the contemporary management of advanced/metastatic disease.* Oncol Rev, 2021. **15**(1): p. 530.

101. Escudier, B., et al., *Renal cell carcinoma: ESMO Clinical Practice Guidelines for diagnosis, treatment and follow-up†.* Ann Oncol, 2019. **30**(5): p. 706-720.

102. Rini, B.I., S.C. Campbell, and B. Escudier, *Renal cell carcinoma.* The Lancet, 2009. **373**(9669): p. 1119-1132.

103. Liu, K., et al., *Papillary renal cell carcinoma: a clinicopathological and whole-genome exon sequencing study.* Int J Clin Exp Pathol, 2015. **8**(7): p. 8311-35.

104. Sánchez-Gastaldo, A., et al., *Systemic treatment of renal cell cancer: A comprehensive review.* Cancer Treat Rev, 2017. **60**: p. 77-89.

105. Motzer, R.J. and P. Russo, *Systemic therapy for renal cell carcinoma.* J Urol, 2000. **163**(2): p. 408-17.

106. Xu, Y., et al., *Current status of antigen-specific T-cell immunotherapy for advanced renal-cell carcinoma.* Hum Vaccin Immunother, 2021. **17**(7): p. 1882-1896.

107. Bumpus, H.C., *The Apparent Disappearance of Pulmonary Metastasis in a Case of Hypernephroma Following Nephrectomy¹.* Journal of Urology, 1928. **20**(2): p. 185-192.

108. Janiszewska, A.D., S. Poletajew, and A. Wasiutyński, *Spontaneous regression of renal cell carcinoma.* Contemp Oncol (Pozn), 2013. **17**(2): p. 123-7.

109. Gastl, G., et al., *Major histocompatibility complex class I and class II expression in renal cell carcinoma and modulation by interferon gamma.* J Urol, 1996. **155**(1): p. 361-7.

110. Chevrier, S., et al., *An Immune Atlas of Clear Cell Renal Cell Carcinoma.* Cell, 2017. **169**(4): p. 736-749.e18.

111. Rooney, M.S., et al., *Molecular and genetic properties of tumors associated with local immune cytolytic activity.* Cell, 2015. **160**(1-2): p. 48-61.

112. Neidhart, J.A., et al., *Interferon-α Therapy of Renal Cancer1.* Cancer Research, 1984. **44**(9): p. 4140-4143.

113. Motzer, R.J., et al., *Effect of cytokine therapy on survival for patients with advanced renal cell carcinoma.* J Clin Oncol, 2000. **18**(9): p. 1928-35.

114. Motzer, R.J., et al., *Interferon-alfa as a comparative treatment for clinical trials of new therapies against advanced renal cell carcinoma.* J Clin Oncol, 2002. **20**(1): p. 289-96.

115. Belldegrun, A.S., et al., *Cancer-specific survival outcomes among patients treated during the cytokine era of kidney cancer (1989-2005): a benchmark for emerging targeted cancer therapies.* Cancer, 2008. **113**(9): p. 2457-63.

116. Schendel, D.J., et al., *Tumor-specific lysis of human renal cell carcinomas by tumor-infiltrating lymphocytes. I. HLA-A2-restricted recognition of autologous and allogeneic tumor lines.* J Immunol, 1993. **151**(8): p. 4209-20.

117. Bregni, M., F. Ciceri, and J. Peccatori, *Allogeneic Stem Cell Transplantation for Metastatic Renal Cell Cancer (RCC).* J Cancer, 2011. **2**: p. 347-9.

118. Motzer, R.J., et al., *Nivolumab plus Ipilimumab versus Sunitinib in Advanced Renal-Cell Carcinoma.* N Engl J Med, 2018. **378**(14): p. 1277-1290.

119. Oosterwijk, E., et al., *Monoclonal antibody G 250 recognizes a determinant present in renal-cell carcinoma and absent from normal kidney.* Int J Cancer, 1986. **38**(4): p. 489-94.

120. Adam, P.J., et al., *CD70 (TNFSF7) is expressed at high prevalence in renal cell carcinomas and is rapidly internalised on antibody binding.* British Journal of Cancer, 2006. **95**(3): p. 298-306.

121. Jilaveanu, L.B., et al., *CD70 expression patterns in renal cell carcinoma.* Human pathology, 2012. **43**(9): p. 1394-1399.

122. Borst, J., J. Hendriks, and Y. Xiao, *CD27 and CD70 in T cell and B cell activation.* Curr Opin Immunol, 2005. **17**(3): p. 275-81.

123. Prasad, K.V., et al., *CD27, a member of the tumor necrosis factor receptor family, induces apoptosis and binds to Siva, a proapoptotic protein.* Proc Natl Acad Sci U S A, 1997. **94**(12): p. 6346-51.

124. Rajkumar, S.V., *Updated Diagnostic Criteria and Staging System for Multiple Myeloma.* Am Soc Clin Oncol Educ Book, 2016. **35**: p. e418-23.

125. Chawla, S.S., et al., *Clinical course and prognosis of non-secretory multiple myeloma.* Eur J Haematol, 2015. **95**(1): p. 57-64.

126. Rodríguez-Lobato, L.G., et al., *CAR T-Cells in Multiple Myeloma: State of the Art and Future Directions.* Front Oncol, 2020. **10**: p. 1243.

127. Fonseca, R., et al., *Trends in overall survival and costs of multiple myeloma, 2000-2014.* Leukemia, 2017. **31**(9): p. 1915-1921.

128. Kawano, Y., et al., *Multiple Myeloma and the Immune Microenvironment.* Curr Cancer Drug Targets, 2017. **17**(9): p. 806-818.

129. Rajkumar, S.V. and S. Kumar, *Multiple Myeloma: Diagnosis and Treatment.* Mayo Clin Proc, 2016. **91**(1): p. 101-19.

130. Russell, S.J. and S.V. Rajkumar, *Multiple myeloma and the road to personalised medicine.* Lancet Oncol, 2011. **12**(7): p. 617-9.

131. Kumar, A., et al., *Management of multiple myeloma: a systematic review and critical appraisal of published studies.* Lancet Oncol, 2003. **4**(5): p. 293-304.

132. van de Donk, N. and S.Z. Usmani, *CD38 Antibodies in Multiple Myeloma: Mechanisms of Action and Modes of Resistance.* Front Immunol, 2018. **9**: p. 2134.

133. Pazina, T., et al., *The anti-SLAMF7 antibody elotuzumab mediates NK cell activation through both CD16-dependent and -independent mechanisms.* Oncoimmunology, 2017. **6**(9): p. e1339853.

134. McMillan, A., D. Warcel, and R. Popat, *Antibody-drug conjugates for multiple myeloma.* Expert Opin Biol Ther, 2021. **21**(7): p. 889-901.

135. Kleber, M., I. Ntanasis-Stathopoulos, and E. Terpos, *BCMA in Multiple Myeloma-A Promising Key to Therapy.* J Clin Med, 2021. **10**(18).

136. Raje, N., et al., *Anti-BCMA CAR T-Cell Therapy bb2121 in Relapsed or Refractory Multiple Myeloma.* N Engl J Med, 2019. **380**(18): p. 1726-1737.

137. Da Vià, M.C., et al., *Homozygous BCMA gene deletion in response to anti-BCMA CAR T cells in a patient with multiple myeloma.* Nat Med, 2021. **27**(4): p. 616-619.

138. Gogishvili, T., et al., *SLAMF7-CAR T cells eliminate myeloma and confer selective fratricide of SLAMF7(+) normal lymphocytes.* Blood, 2017. **130**(26): p. 2838-2847.

139. Caraux, A., et al., *Circulating human B and plasma cells. Age-associated changes in counts and detailed characterization of circulating normal CD138- and CD138+ plasma cells.* Haematologica, 2010. **95**(6): p. 1016-20.

140. Sandoval-Montes, C. and L. Santos-Argumedo, *CD38 is expressed selectively during the activation of a subset of mature T cells with reduced proliferation but improved potential to produce cytokines.* J Leukoc Biol, 2005. **77**(4): p. 513-21.

141. Bankhead, P., et al., *QuPath: Open source software for digital pathology image analysis.* Scientific Reports, 2017. **7**(1): p. 16878.

142. Hudecek, M., et al., *The nonsignaling extracellular spacer domain of chimeric antigen receptors is decisive for in vivo antitumor activity.* Cancer Immunol Res, 2015. **3**(2): p. 125-35.

143. Wang, X., et al., *A transgene-encoded cell surface polypeptide for selection, in vivo tracking, and ablation of engineered cells.* Blood, 2011. **118**(5): p. 1255-63.

144. Pfaffl, M.W., *A new mathematical model for relative quantification in real-time RT-PCR.* Nucleic Acids Res, 2001. **29**(9): p. e45.

145. Livak, K.J. and T.D. Schmittgen, *Analysis of relative gene expression data using real-time quantitative PCR and the 2(-Delta Delta C(T)) Method.* Methods, 2001. **25**(4): p. 402-8.

146. Riddell, S.R. and P.D. Greenberg, *The use of anti-CD3 and anti-CD28 monoclonal antibodies to clone and expand human antigen-specific T cells.* J Immunol Methods, 1990. **128**(2): p. 189-201.

147. Brown, C.E., et al., *Biophotonic cytotoxicity assay for high-throughput screening of cytolytic killing.* J Immunol Methods, 2005. **297**(1-2): p. 39-52.

148. Roederer, M., *Interpretation of cellular proliferation data: avoid the panglossian.* Cytometry A, 2011. **79**(2): p. 95-101.

149. Joshi, S., A.R. Singh, and D.L. Durden, *Pan-PI-3 kinase inhibitor SF1126 shows antitumor and antiangiogenic activity in renal cell carcinoma.* Cancer Chemother Pharmacol, 2015. **75**(3): p. 595-608.

150. Mestermann, K., et al., *The tyrosine kinase inhibitor dasatinib acts as a pharmacologic on/off switch for CAR T cells.* Sci Transl Med, 2019. **11**(499).

151. Miyakawa, Y., et al., *Establishment of a new model of human multiple myeloma using NOD/SCID/gammac(null) (NOG) mice.* Biochem Biophys Res Commun, 2004. **313**(2): p. 258-62.

152. Fan, W.L., et al., *Leptin Is Associated with Poor Clinical Outcomes and Promotes Clear Cell Renal Cell Carcinoma Progression.* Biomolecules, 2021. **11**(3).

153. Wright, T.M. and W.K. Rathmell, *Identification of Ror2 as a hypoxia-inducible factor target in von Hippel-Lindau-associated renal cell carcinoma.* J Biol Chem, 2010. **285**(17): p. 12916-24.

154. Gry, M., et al., *Correlations between RNA and protein expression profiles in 23 human cell lines.* BMC Genomics, 2009. **10**(1): p. 365.

155. Wang, D., *Discrepancy between mRNA and protein abundance: insight from information retrieval process in computers.* Comput Biol Chem, 2008. **32**(6): p. 462-8.

156. Majzner, R.G., et al., *Low CD19 Antigen Density Diminishes Efficacy of CD19 CAR T Cells and Can be Overcome By Rational Redesign of CAR Signaling Domains.* Blood, 2018. **132**(Supplement 1): p. 963-963.

157. Walker, A.J., et al., *Tumor Antigen and Receptor Densities Regulate Efficacy of a Chimeric Antigen Receptor Targeting Anaplastic Lymphoma Kinase.* Mol Ther, 2017. **25**(9): p. 2189-2201.

158. Li, H., et al., *CAIX-specific CAR-T Cells and Sunitinib Show Synergistic Effects Against Metastatic Renal Cancer Models.* J Immunother, 2020. **43**(1): p. 16-28.

159. Amato, R.J., et al., *Vaccination of metastatic renal cancer patients with MVA-5T4: a randomized, double-blind, placebo-controlled phase III study.* Clin Cancer Res, 2010. **16**(22): p. 5539-47.

160. Elkord, E., et al., *An MVA-based vaccine targeting the oncofetal antigen 5T4 in patients undergoing surgical resection of colorectal cancer liver metastases.* J Immunother, 2008. **31**(9): p. 820-9.

161. Oudard, S., et al., *A phase II study of the cancer vaccine TG4010 alone and in combination with cytokines in patients with metastatic renal clear-cell carcinoma: clinical and immunological findings.* Cancer Immunol Immunother, 2011. **60**(2): p. 261-71.

162. Iiyama, T., et al., *WT1 (Wilms' tumor 1) peptide immunotherapy for renal cell carcinoma.* Microbiol Immunol, 2007. **51**(5): p. 519-30.

163. Ali, S.A., et al., *T cells expressing an anti-B-cell maturation antigen chimeric antigen receptor cause remissions of multiple myeloma.* Blood, 2016. **128**(13): p. 1688-700.

164. Drent, E., et al., *A Rational Strategy for Reducing On-Target Off-Tumor Effects of CD38-Chimeric Antigen Receptors by Affinity Optimization.* Mol Ther, 2017. **25**(8): p. 1946-1958.

165. Smith, E.L., et al., *GPRC5D is a target for the immunotherapy of multiple myeloma with rationally designed CAR T cells.* Sci Transl Med, 2019. **11**(485).

166. Prommersberger, S., et al., *CARAMBA: a first-in-human clinical trial with SLAMF7 CAR-T cells prepared by virus-free Sleeping Beauty gene transfer to treat multiple myeloma.* Gene Ther, 2021. **28**(9): p. 560-571.

167. Sanber, K., B. Savani, and T. Jain, *Graft-versus-host disease risk after chimeric antigen receptor T-cell therapy: the diametric opposition of T cells.* British Journal of Haematology, 2021. **195**(5): p. 660-668.

168. Linette, G.P., et al., *Cardiovascular toxicity and titin cross-reactivity of affinity-enhanced T cells in myeloma and melanoma.* Blood, 2013. **122**(6): p. 863-71.

169. Hombach, A., A.A. Hombach, and H. Abken, *Adoptive immunotherapy with genetically engineered T cells: modification of the IgG1 Fc 'spacer' domain in the extracellular moiety of chimeric antigen receptors avoids 'off-target' activation and unintended initiation of an innate immune response.* Gene Ther, 2010. **17**(10): p. 1206-13.

170. Bausch-Fluck, D., et al., *The in silico human surfaceome.* Proceedings of the National Academy of Sciences, 2018. **115**(46): p. E10988-E10997.

171. Greenbaum, U., et al., *Chimeric Antigen Receptor T-Cells in B-Acute Lymphoblastic Leukemia: State of the Art and Future Directions.* Frontiers in Oncology, 2020. **10**.

172. Maude, S.L., et al., *Chimeric antigen receptor T cells for sustained remissions in leukemia.* N Engl J Med, 2014. **371**(16): p. 1507-17.

173. Summers, C., et al., *Long Term Follow-up after SCRI-CAR19v1 Reveals Late Recurrences As Well As a Survival Advantage to Consolidation with HCT after CAR T Cell Induced Remission.* Blood, 2018. **132**(Supplement 1): p. 967-967.

174. Lara, E., et al., *Epigenetic repression of ROR2 has a Wnt-mediated, pro-tumourigenic role in colon cancer.* Mol Cancer, 2010. **9**: p. 170.

175. Saji, T., et al., *Critical role of the Ror-family of receptor tyrosine kinases in invasion and proliferation of malignant pleural mesothelioma cells.* Genes Cells, 2018. **23**(7): p. 606-613.

176. Yu, J., et al., *Wnt5a induces ROR1/ROR2 heterooligomerization to enhance leukemia chemotaxis and proliferation.* J Clin Invest, 2016. **126**(2): p. 585-98.

177. Gardner, R.A., et al., *Preemptive mitigation of CD19 CAR T-cell cytokine release syndrome without attenuation of antileukemic efficacy.* Blood, 2019. **134**(24): p. 2149-2158.

178. Gardner, R.A., et al., *Intent-to-treat leukemia remission by CD19 CAR T cells of defined formulation and dose in children and young adults.* Blood, 2017. **129**(25): p. 3322-3331.

179. Bougherara, H., et al., *Real-Time Imaging of Resident T Cells in Human Lung and Ovarian Carcinomas Reveals How Different Tumor Microenvironments Control T Lymphocyte Migration.* Front Immunol, 2015. **6**: p. 500.

180. Kerns, S.J., et al., *Human immunocompetent Organ-on-Chip platforms allow safety profiling of tumor-targeted T-cell bispecific antibodies.* eLife, 2021. **10**: p. e67106.

181. Roguska, M.A., et al., *Humanization of murine monoclonal antibodies through variable domain resurfacing.* Proc Natl Acad Sci U S A, 1994. **91**(3): p. 969-73.

182. Viganò, S., et al., *Functional Avidity: A Measure to Predict the Efficacy of Effector T Cells?* Clinical and Developmental Immunology, 2012. **2012**: p. 153863.

183. Potthoff, B., et al., *A cell-based immunogenicity assay to detect antibodies against chimeric antigen receptor expressed by tisagenlecleucel.* Journal of Immunological Methods, 2020. **476**: p. 112692.

184. Henry, C.E., et al., *ROR1 and ROR2 play distinct and opposing roles in endometrial cancer.* Gynecol Oncol, 2018. **148**(3): p. 576-584.

185. Li, H., et al., *Targeting brain lesions of non-small cell lung cancer by enhancing CCL2-mediated CAR-T cell migration.* Nat Commun, 2022. **13**(1): p. 2154.

186. Ataide, M.A., et al., *BATF3 programs CD8(+) T cell memory.* Nat Immunol, 2020. **21**(11): p. 1397-1407.

187. Garcia-Guerrero, E., et al., *Panobinostat induces CD38 upregulation and augments the antimyeloma efficacy of daratumumab.* Blood, 2017. **129**(25): p. 3386-3388.

188. Jetani, H., et al., *CAR T-cells targeting FLT3 have potent activity against FLT3(-)ITD(+) AML and act synergistically with the FLT3-inhibitor crenolanib.* Leukemia, 2018. **32**(5): p. 1168-1179.

189. Gardner, T.J., et al., *Engineering CAR-T cells to activate small-molecule drugs in situ.* Nat Chem Biol, 2022. **18**(2): p. 216-225.

190. Debebe, Z. and W.K. Rathmell, *Ror2 as a therapeutic target in cancer.* Pharmacol Ther, 2015. **150**: p. 143-8.

191. Dave, H., et al., *ROR1 and ROR2-novel targets for neuroblastoma.* Pediatr Hematol Oncol, 2019. **36**(6): p. 352-364.

192. Morsut, L., et al., *Engineering Customized Cell Sensing and Response Behaviors Using Synthetic Notch Receptors.* Cell, 2016. **164**(4): p. 780-91.

193. Roybal, K.T., et al., *Precision Tumor Recognition by T Cells With Combinatorial Antigen-Sensing Circuits.* Cell, 2016. **164**(4): p. 770-9.

194. Apte, M.V., et al., *Desmoplastic reaction in pancreatic cancer: role of pancreatic stellate cells.* Pancreas, 2004. **29**(3): p. 179-87.

195. Labiche, A., et al., *Stromal compartment as a survival prognostic factor in advanced ovarian carcinoma.* Int J Gynecol Cancer, 2010. **20**(1): p. 28-33.

196. Bughda, R., et al., *Fibroblast Activation Protein (FAP)-Targeted CAR-T Cells: Launching an Attack on Tumor Stroma.* Immunotargets Ther, 2021. **10**: p. 313-323.

197. Monjezi, R., et al., *Enhanced CAR T-cell engineering using non-viral Sleeping Beauty transposition from minicircle vectors.* Leukemia, 2017. **31**(1): p. 186-194.

List of figures

List of tables

List of abbreviations

Abbreviation	Explanation
°C	centigrade
µg	microgram
µl	microliter
µM	micromole
7-AAD	7-Aminoactinomycin
Akt	Akt serine/threonine kinase
ANOVA	analysis of variance
ASCT	autologous stem cell transplantation
ATCC	American Type Culture Collection
B-CLL	B-cell chronic lymphocytic leukemia
BCMA	B-cell maturation antigen
BLI	bioluminescence imaging
BSA	bovine serum albumin
CAA	cancer-associated antigen
CAIX	carbonic anhydrase IX
CAR	chimeric antigen receptor
ccRCC	clear cell renal cell carcinoma
CD	cluster of differentiation
cDMEM	complete Dulbecco's modified Eagle's medium
cDNA	complementary deoxyribonucleic acid
CFSE	Carboxyfluoresceinsuccinimidylester
ChRCC	chromophobe renal cell carcinoma
cRPMI	complete Roswell Park Memorial Institute medium
CSA	cancer specific (neo-) antigen

C_t	cycle threshold (qPCR parameter)
CTL	T cell medium
DAB	3,3’ Diaminobenzidine
DEPC	diethyl pyrocarbonate
dMFI	median fluorescence intensity difference
DMSO	dimethyl sulfoxide
DNA	deoxyribonucleic acid
DPBS	Dulbecco's phosphate buffered saline
EBMT	European Society for Blood and Marrow Transplantation
ECL	enhanced chemiluminescence
EDTA	Ethylenediaminetetraacetic acid
EGFR	epidermal growth factor receptor
ELISA	enzyme-linked immunosorbent assay
FACS	fluorescence activated cell sorting
FBS	fetal bovine serum
FDA	Food and Drug Administration (US)
ffLuc	firefly luciferase
ffLuc-eGFP	firefly luciferase - enhanced green fluorescent protein fusion
FITC	fluorescein isothiocyanate
FMC63	CD19-specific antibody clone FMC63
FMO	fluorescence minus one
g	gram
GAPDH	glyceraldehyde 3-phosphate dehydrogenase
GM-CSF	granulocyte-macrophage colony-stimulating factor
h	hour/hours
Her2	receptor tyrosine-protein kinase erbB-2

HIER	heat-induced epitope retrieval
HLA	human leukocyte antigen
hROR2	human ROR2
HTLV	human T-cell lymphotropic virus
hX3.12.5	humanized version of the X3.12 binder
hX3.12.6	humanized version of the X3.12 binder
ICAM-1	intercellular adhesion molecule 1
IFNγ	interferon gamma
IgG	immunoglobulin G
IHC	immunohistochemistry
IL-2	Interleukin-2
IL-6	Interleukin-6
K_D	equilibrium dissociation constant
kg	kilogram
l	liter
LAG3	lymphocyte activation gene 3 protein
LAT	linker for activation of T cells
M	mole
mAb	monoclonal antibody
MACS	magnetic-activated cell sorting
MFI	median fluorescence intensity
MFI-FC	median fluorescence intensity fold change
MGUS	monoclonal gammopathy of undetermined significance
MHC	major histocompatibility complex
ml	milliliter
MM	multiple myeloma

mM	millimole
mROR2	murine ROR2
mTOR	mammalian target of rapamycin
NaCl	sodium chloride
ng	nanogram
nM	nanomole
NSG	NOD.Cg-Prkdc^{scid} Il2rg^{tm1Wjl}/SzJ
PE	phycoerythrin
PD-1	programmed cell death protein 1
PI3K	phosphoinositide 3-kinase
pRCC	papillary renal cell carcinoma
PVDF	polyvinylidene fluoride
qPCR	real-time polymerase chain reaction
RCC	renal cell carcinoma
rhIL-2	recombinant human interleukin 2
RIPA	radioimmunoprecipitation assay buffer
RNA	ribonucleic acid
ROR1	receptor tyrosine kinase-like orphan receptor 1
ROR2	receptor tyrosine kinase-like orphan receptor 2
RTK	receptor tyrosine kinase
scFv	single-chain variable fragment
SD	standard deviation
SDS	sodium dodecyl sulfate
SEM	standard error of the mean
SLAMF7	signaling lymphocytic activation molecule family member 7
SMM	smoldering multiple myeloma

TBS	TRIS -buffered saline
TBS-T	TRIS -buffered saline -Tween 20
TCGA	The Cancer Genome Atlas
TCR	T cell receptor
tEGFR	truncated epidermal growth factor receptor
TIM3	hepatitis A virus cellular receptor 2
TM	transmembrane domain
u	unit
UTD	untransduced
VEGF	vascular endothelial growth factor
VEGFR	vascular endothelial growth factor receptor
V_H-V_L	variable heavy - variable light chain
WPRE	Woodchuck Hepatitis Virus Posttranscriptional Regulatory Element
x g	times gravitational force
X3.12	X3.12 binder (affinity matured version of XBR2-401)
XBR2-401	XBR2-401 binder (ROR2 specific binder)
ZAP-70	zeta-chain-associated protein kinase 70

Affidavit

I hereby confirm that my thesis entitled "*Development and preclinical assessment of ROR2-specific CAR-T cells for the treatment of clear cell renal cell carcinoma and multiple myeloma"* is the result of my own work. I did not receive any help or support from commercial consultants. All sources and / or materials applied are listed and specified in the thesis.

Furthermore, I confirm that this thesis has not yet been submitted as part of another examination process neither in identical nor in similar form.

Würzburg,

Place, Date Signature

Eidesstattliche Erklärung

Hiermit erkläre ich an Eides statt, die Dissertation *„Entwicklung und präklinische Evaluation ROR2-spezifischer CAR-T Zellen zur Behandlung des klarzelligen Nierenzellkarzinoms und des Multiplen Myeloms"* eigenständig, d.h. insbesondere selbständig und ohne Hilfe eines kommerziellen Promotionsberaters, angefertigt und keine anderen als die von mir angegebenen Quellen und Hilfsmittel verwendet zu haben.

Ich erkläre außerdem, dass die Dissertation weder in gleicher noch in ähnlicher Form bereits in einem anderen Prüfungsverfahren vorgelegen hat.

Würzburg,

Ort, Datum Unterschrift

Acknowledgements

First, I would like to express my sincere gratitude to my primary supervisor, Prof. Dr. Michael Hudecek for accepting me as a PhD candidate and for giving me the opportunity to work on this amazing project. His continuous support and our scientific discussions had a tremendous impact on this project and have shaped me as an aspiring scientist. He is a supervisor to whom I will always look up, because of his tremendous experience, willingness to share novel ideas and the inspiring environment he has created. I am also grateful for the opportunities to develop additional soft skills, and for the possibility to travel, meet fellow scientists and engage in scientific debates with like-minded people all over the world.

I would also like to thank PD Dr. Thomas Nerreter for continuously supporting me in conceptual aspects of my projects and for sharing his experience in laboratory techniques and experimental design with me.

Next, I would like to express my gratitude to Prof. Dr. Christoph Rader, who has been a mentor for me ever since I joined his team as a student intern in 2016. Christoph's ideas and feedback had (and still have) an enormous impact on me as a scientist and I will be forever thankful for his support.

Furthermore, I would also like to thank Prof. Dr. Thomas Herrmann and Prof. Dr. Herrmann Einsele for their support during my PhD. Their feedback with regards to immunological and clinical aspects of cellular therapy had a significant impact on my project development.

Finally, I am truly thankful for the support of all current and former members of the Hudecek-Lab. Our scientific discussions and the support I experienced from everybody on the team have left a profound impression on me and have shaped my perception of teamwork in a scientific environment. Thanks a lot, to everybody for the last five years: it has been an amazing and exiting journey with all of you.

Last but not least, I would like to thank my family and friends for their continuous encouragement – words cannot express how much your support means to me.

Curriculum Vitae